



HAL
open science

A Multi-Scale Strategy for the Probabilistic Modeling of Reinforced Concrete Structures

Christian Nader

► **To cite this version:**

Christian Nader. A Multi-Scale Strategy for the Probabilistic Modeling of Reinforced Concrete Structures. Mechanics of materials [physics.class-ph]. Université Paris-Est, 2017. English. NNT : 2017PESC1157 . tel-01630570

HAL Id: tel-01630570

<https://theses.hal.science/tel-01630570>

Submitted on 7 Nov 2017

HAL is a multi-disciplinary open access archive for the deposit and dissemination of scientific research documents, whether they are published or not. The documents may come from teaching and research institutions in France or abroad, or from public or private research centers.

L'archive ouverte pluridisciplinaire **HAL**, est destinée au dépôt et à la diffusion de documents scientifiques de niveau recherche, publiés ou non, émanant des établissements d'enseignement et de recherche français ou étrangers, des laboratoires publics ou privés.



A thesis submitted for the degree of
Doctor of Philosophy
Specialty: Materials and Structures

by

Christian NADER

Doctoral School: Sciences, Ingénierie et Environnement

A Multi-Scale Strategy for the Probabilistic Modeling of Reinforced Concrete Structures

Thesis defended on 21 April 2017 before the jury composed of:

Pr.	MASSICOTTE Bruno	Ecole Polytechnique de Montréal	Reviewer
Pr.	MILLARD Alain	CEA Saclay	Reviewer
Pr.	SELLIER Alain	INSA Toulouse	Examiner
Ing.	LABBE Pierre	EDF	Examiner
Dr.	ROSSI Pierre	IFSTTAR Paris	Thesis director



Institut français des sciences et technologies des transports, de l'aménagement et des réseaux
14-20 Bd. Newton / Cite Descartes, Champs sur Marne / F-77447 Marne la Vallée Cedex

“When you look at yourself from a universal standpoint, something inside always reminds or informs you that there are bigger and better things to worry about.”

Albert Einstein

Acknowledgments

The present work could not have been completed without the great support that I have received from many people over the past three years. I wish to offer my most heartfelt thanks to the following people, without whom, this dissertation would not exist.

To my director, Pierre Rossi. Thank you for the trust that you have given me by accepting to supervise this doctoral work. And thank you for the advice, support, and willingness that allowed me to pursue research on topics for which I am truly passionate. I sought in my work, and seek in life, to achieve the same drive and passion that you apply in your own research efforts.

To my mentor and supervisor, Jean-Louis Tailhan. You have been an ever present beacon of support, encouragement, and advice. Thank you for keeping your office door open and available these past years. The skills and ideas that you were willing to share with me and the time you dedicated to me ultimately allowed this thesis to find its way and come to completion.

To the examiners, Alain Millard and Bruno Massicotte, who have taken the time to review this manuscript carefully. I particularly appreciated their interest in my work, their meticulous critique and their enlightening remarks and feedback that have been absolutely invaluable.

To the members of the jury, Alain Sellier and Pierre Labbe, their remarks and questions were sources of reflection and enrichment.

To everyone at the LBA-Marseille, it was great sharing laboratory with all of you during the last three years. It was fantastic to have the opportunity to work a majority of my research in such a facility. What a cracking place to work!

And finally, to my family, for the love, support, and constant encouragement I have gotten over the years. In particular, my father, who taught me critical thinking and always believed in me, and my mom who nurtured my love for science since the very beginning. I try to live by your lessons every day.

UNIVERSITÉ PARIS-EST

Abstract

Doctoral School: Sciences, Ingénierie et Environnement

Specialty: Materials and Structures

Doctor of Philosophy

Current modeling approaches come short in terms of providing reliable information about the cracking process in large/complex reinforced concrete structures. However, this is an important issue for controlling the lifespan of structures, which is at the heart of the principal of sustainable development. In this work we introduce a new approach to model the cracking processes in large reinforced concrete structures, like dams or nuclear power plants. For these types of structures it is unreasonable, due to calculation time, to explicitly model the rebars and the steel-concrete bond. Nevertheless, access to data about the cracking process is imperative for structural analysis and diffusion problems. So in order to draw the information about cracking in the structure, without resorting to the use of local approaches, we developed a probabilistic macroscopic cracking model based on a multi-scale simulation strategy. The strategy is a sort of a multi-steps process that takes over the whole modelization of the structure in the framework of the finite element method, from meshing, to model creation, and parameter identification. The heart of the strategy is inspired from *regression (supervised learning) algorithms*: data at the local scale — the training data coupled with working knowledge of the mechanical problem — would shape the macroscopic model. The probabilistic macroscopic model identification is case-specific because it holds information about the local behavior, obtained in advance via numerical experimentation. This information is then projected to the macroscopic finite element scale via inverse analysis. Numerical experiments are performed using a validated cracking model for concrete and a bond model for the steel-concrete interface, allowing for a fine description of the cracking processes. Although the identification phase can be relatively time-consuming, the structural simulation is as a result, very time-efficient, leading to a sensitive reduction of the overall computational time, with no loss in information/accuracy of results on the macroscopic scale.

Key words: *Reinforced concrete structures; Cracking process; Finite Elements; Multi-Scale Modeling Strategy; Probabilistic Approach.*

UNIVERSITÉ PARIS-EST

Résumé

Doctoral School: Sciences, Ingénierie et Environnement

Specialty: Materials and Structures

Doctor of Philosophy

Il n'existe pas de nos jours une approche modélisatrice satisfaisante de la fissuration des structures en béton de grandes dimensions, capable d'apporter à la fois des informations sur son comportement global et local. Il s'agit pourtant d'un enjeu important pour la maîtrise de la durée de vie des structures, qui s'inscrit pleinement dans le cadre du développement durable. Nous introduisons ainsi une nouvelle approche pour modéliser le processus de fissuration dans les grandes structures en béton armé, comme les barrages ou les centrales nucléaires. Pour ces types de structures, il n'est pas raisonnable, en termes de temps de calcul, de modéliser explicitement les armatures et l'interface acier-béton. Néanmoins, l'accès aux données sur la fissuration est impératif pour les problèmes d'analyse structurelle et de diffusion. Nous avons donc développé un modèle de fissuration macroscopique probabiliste basé sur une stratégie de simulation multi-échelles afin d'obtenir de l'information sur la fissuration dans la structure, sans avoir besoin d'utiliser des approches locales. La stratégie est une sorte de processus multi-étapes qui reprend toute la modélisation de la structure dans le cadre de la méthode des éléments finis, du maillage, à la création de modèles et l'identification des paramètres. Le cœur de la stratégie est inspiré des *algorithmes de régression (apprentissage supervisé)*: les données à l'échelle locale — base de données d'apprentissage associées à la connaissance pratique du problème mécanique — aident à formuler le modèle macroscopique. L'identification des paramètres du modèle macroscopique probabiliste dépend du problème traité car ca contient des informations sur le comportement local, obtenues en avance à l'aide de l'expérimentation numérique. Cette information est ensuite projetée à l'échelle des éléments finis macroscopiques par analyse inverse. L'expérimentation numérique est réalisée avec un modèle validé de fissuration du béton et d'un modèle d'interface acier-béton, ce qui permet une description détaillée des processus de fissuration. Bien que la phase d'identification puisse être relativement longue, le calcul structurel est ainsi très efficace en termes de temps de calcul, conduisant à une réduction importante du temps de calcul global, sans perte d'information / précision sur résultats à l'échelle macroscopique.

Mots clés: *Structures en béton armé; Processus de fissuration; Éléments finis; Stratégie multi-échelles de modélisation; Approche probabiliste.*

Contents

Acknowledgments	iii
Abstract	iv
Résumé	v
List of Figures	ix
List of Tables	xi
1 Introduction	1
1.1 Problematic	1
1.2 Objectives and Methodology	2
2 Bibliography	5
2.1 Modeling of Concrete	5
2.1.1 Cracking of Concrete: Basic Modeling Concepts	6
2.1.1.1 Literature	7
2.1.2 Probabilistic Cracking of Concrete	9
2.1.2.1 Explicit Cracking Model (Contact Elements)	10
2.1.2.2 Semi-Explicit Cracking Model (Macroscopic Elements)	11
2.2 Reinforcing Steel	16
2.3 Modeling of Reinforced Concrete	18
2.3.1 Local Scale Approach: Bond Between Concrete and Reinforcing Steel	20
2.3.1.1 Steel-Concrete Interface Model	21
2.4 Macroscopic Scale Approach	24
2.4.1 Multi-scale Constitutive Modeling and Homogenization Techniques	24
2.4.2 FEM Macro Elements	26
2.5 Conclusion	28
3 Numerical Strategy for Developing a Probabilistic Model for Reinforced Concrete Structures	29
3.1 Objectives and Philosophy	29
3.2 Reinforced Concrete Macro Element	31
3.2.1 “Best” Partitioning	32

3.3	Supervised Learning	34
3.3.1	Choice of Training Data	35
3.3.2	Choice of Learning Algorithm	36
3.3.2.1	Probabilistic Macro Model for Reinforced Concrete Elements . .	37
3.3.2.2	Maximum Likelihood Approach for Parameters Identification . .	38
3.4	Optimization Scheme	40
3.4.1	Choosing the Objective Function	40
3.4.2	Response Surface Methodology	42
3.4.2.1	Design and Analysis of a Four-Factor Experiment	42
3.5	Implementation	44
4	Validation	46
4.1	Reinforced Slab-Beam (2D)	46
4.1.1	Dimensions and Loading Conditions	46
4.1.1.1	Materials Characteristics	47
4.1.2	Local and Macro Meshes	48
4.1.3	Tie-Beam Numerical Tests	50
4.1.4	2D Macroscopic Model	51
4.1.4.1	Philosophy	51
4.1.4.2	Constitutive Law	52
4.1.5	Parameters Identification	55
4.1.6	Rundown of the Strategy	56
4.1.7	Results	58
4.1.7.1	Numerical Tie-Beams	58
4.1.7.2	Numerical Slab-Beam	60
4.1.8	Discussion	65
4.2	Reinforced D.C.B. (3D)	66
4.2.1	Dimensions and Loading Conditions	66
4.2.1.1	Materials Characteristics	68
4.2.1.2	Experimental Results	69
4.2.2	Numerical Simulation Using Local Models	70
4.2.3	D.C.B. Macro Mesh: Three Types of Macro-Elements	74
4.2.4	Tie-Beam Numerical Tests	76
4.2.5	3D Macroscopic Model	77
4.2.5.1	Philosophy	78
4.2.5.2	Constitutive Law	79
4.2.6	Parameters Identification	82
4.2.7	Results	84
4.2.7.1	Numerical Tie-Beams	84
4.2.7.2	Numerical D.C.B.	87
4.2.8	Discussion	92
4.3	Reflections on the Macro Model Design	93
5	Conclusions and Prospects	95
5.1	Conclusions	95
5.2	Prospects	97

List of Figures

2.1	Fracture modes and material failure types	7
2.2	Probabilistic explicit cracking model for concrete	11
2.3	Cracking process in quasi-brittle materials [Huespe and Oliver, 2011]	12
2.4	The probabilistic semi-explicit cracking model [Rastiello, 2013]	14
2.5	Crack opening calculation according to the semi-explicit cracking model [Rastiello, 2013]	15
2.6	Reinforcing steel stress-strain behavior	16
2.7	Pull-out test setup [Häussler-Combe, 2014]	18
2.8	Simple bond model	20
2.9	Steel-concrete interface behavior, $2D$ elements	22
2.10	Mohr-Coulomb friction after failure of the steel-concrete interface	23
2.11	Length scales for most metal materials	25
2.12	Macro-element in the macroscopic structure representing a mesoscale window containing the microstructure information [Markovic and Ibrahimbegovic, 2004]	27
3.1	Different ways for partitioning a reinforced concrete block into macro-elements	31
3.2	Macro-element complexity with respect to its constitution	32
3.3	Design of a tie-beam test for each direction parallel to the steel bars in case the macro element represents multi-directional reinforcements	36
3.4	Local/macro tie-beam numerical tests global results comparison given a set of macro-model parameters	37
3.5	Reinforced concrete macro model	38
3.6	Pairing of micro and local curves with respect to minimum area outlined by the two load-displacement curves	41
3.7	Line sweep algorithm trying to find the intersections between two sets of line segments	41
3.8	Pareto plot	43
3.9	Visualization of RSM for a model with 2 parameters a and b	44
4.1	Slab-beam dimensions and loading conditions	47
4.2	Longitudinal section, reinforcement plan for reinforced slab beams	47
4.3	Cross section, reinforcement plan for reinforced steel beam slabs	48
4.4	Slab-beam $2D$ meshes	49
4.5	The chosen macro-element of reinforced concrete	49
4.6	A cross-sectional view of what the macro element represents as a volume	50
4.7	Tie-beam $2D$ mesh	50
4.8	Numerical tie-beam: local approach, load-displacement curves	51

4.9	Probabilistic piece-wise linear model for macro elements of reinforced concrete, reinforced slab-beam case study	54
4.10	Multi-scale modeling strategy.	57
4.11	Numerical tie-beam: Load-displacement curves	58
4.12	Numerical tie-beam: Total number of cracks	59
4.13	Numerical tie-beam: Total cracks opening	59
4.14	Numerical slab-beam: Load-deflection curves	60
4.15	Numerical slab-beam: Cracking pattern	61
4.16	Numerical slab-beam: Total number of cracks (for cracks with width $> 20 \mu\text{m}$) .	61
4.17	Numerical slab-beam: Total number of cracks (for cracks with width $> 200 \mu\text{m}$) .	62
4.18	Numerical slab-beam: Total crack openings	62
4.19	Numerical slab-beam: Largest crack width	63
4.20	Numerical slab-beam: Cracking profile	64
4.21	Double Cantilever Beam: Geometrical characteristics	67
4.22	Double Cantilever Beam: Position of the reinforcements	67
4.23	Double Cantilever Beam: Application of load P , prestress F , and measurement of displacement	68
4.24	Double Cantilever Beam: Experimental load-displacement curve [Rossi, 1986] . .	69
4.25	Concrete block under tension. Elements in the mesh are in the same size range of those used in the D.C.B. local approach calculations	71
4.26	Numerical tie-beam: Microscopic approach, $2D$ mesh	72
4.27	Double Cantilever Beam: Local approach, $2D$ mesh	73
4.28	Double Cantilever Beam: Local approach, load displacement curves	73
4.29	Double Cantilever Beam: $3D$ macroscopic mesh	74
4.30	Three representations of the macroscopic element of reinforced concrete in the D.C.B.	75
4.31	$2D$ look at the three macroscopic D.C.B.s in the XY plane	76
4.32	Tie-beam numerical experiments: micro/macro meshes	77
4.33	Probabilistic piece-wise linear model for macro elements of reinforced concrete, D.C.B. case study	82
4.34	Numerical tie-beam, ERC5 : Load-displacement curves	84
4.35	Numerical tie-beam, ERC5 : Cracking pattern	85
4.36	Numerical tie-beam, ERC10 : Load-displacement curves	85
4.37	Numerical tie-beam, ERC10 : Cracking pattern	86
4.38	Numerical tie-beam, ERC20 : Load-displacement curves	86
4.39	Numerical tie-beam, ERC20 : Cracking pattern	87
4.40	Numerical D.C.B, ERC5 : Load-displacement curves	88
4.41	Numerical D.C.B, ERC10 : Load-displacement curves	88
4.42	Numerical D.C.B, ERC20 : Load-displacement curves	89
4.43	Numerical D.C.B: Cracking pattern	89
4.44	Numerical D.C.B: Crack width measurements at three different heights in the beam	90
4.45	Numerical D.C.B, ERC5 : Cracking profile	90
4.46	Numerical D.C.B, ERC10 : Cracking profile	91
4.47	Numerical D.C.B, ERC20 : Cracking profile	91

List of Tables

4.1	Composition of concrete used (per m^3), reinforced slab-beam case study	48
4.2	Local models parameters, reinforced slab-beam case study	49
4.3	Macroscopic model parameters	56
4.4	Numerical slab-beam: Computation time	63
4.5	Composition of concrete used (per m^3), D.C.B. case study	69
4.6	Local models parameters, D.C.B. case study	72
4.7	Macro model parameters for each type of ERC	83
4.8	3D Numerical D.C.B.: Computation time	91
4.9	2D Numerical D.C.B.: Computation time	92

To my wonderful parents . . .

Chapter 1

Introduction

1.1 Problematic

Reinforced concrete is a complex, composite material that is used in the construction of almost all of modern structures (dams, buildings, bridges...). Indeed, without reinforced concrete, modern structures as we know them would not exist. Furthermore, designing and implementing efficient reinforced concrete components is key to creating the optimal structure. Small changes in design can have a significant impact on material costs, ultimate strength and even the end use of the structure. Nevertheless, to this day, reinforced concrete structures are usually designed according to empirical rules and regulations (or recommendations) based on simplistic and outdated (usually linear) models. The compound problem in these models is the mechanics of members consisting of two materials, where one of the materials, concrete, behaves differently in tension than in compression, and may be considered to be either elastic or inelastic, if it is not neglected entirely. In contrast, many structures are designed to contain liquids (water or liquefied gas tanks) or gases (nuclear containment buildings). In this context, a concrete structure must provide structural functions that go beyond that of simple resistance. Here the cracking of reinforced concrete plays a dominant role in the durability, watertightness, and even the safety of the structure. Current numerical tools at the disposal of engineers are limited and do not allow for quantitative predictions concerning the influence of cracking on the evolution of these characteristics during the lifetime of the structure. Despite the emergence of the finite element method, which has made model simulation of nonlinear structural behavior computationally possible, some limitations are impediments to the wide use of this analytical tool. Inadequate material modeling of concrete is most often one of the major factors in limiting the capabilities of this method. Thus considerable effort has been expended in recent years in understanding concrete. Then there is the case of reinforced concrete which is on a whole different level of complexity due to the concrete/rebar interaction. And whenever the problem

of cracking in reinforced concrete structures is addressed, the solutions presented always involve local scale type of simulations which are very expensive and therefore rendered ineffective when dealing with large or complex structures.

For the past decade, the French Institute for Transport Science and Technology, and Network Development, IFSTTAR, has been developing tools for the probabilistic modeling of the nonlinear behavior of concrete structures, taking into account the scale effects which is a characteristic of heterogeneous materials. These tools are progressively enriched by taking into account various mechanisms (deferred behavior, thermo-hydro-mechanical coupling, etc.). Overall, they all share the same multi-scale modeling strategy that allows to consider these phenomena on the scale of the concrete material as well as that of structural elements (beams, slabs, etc.). However, in order to simulate large structures (urban constructions), we still need to take into account, in the context of this multi-scale approach, the role of active and passive reinforcements, which will be integrated into a macro-element using a local/macro strategy combining information at different scales.

1.2 Objectives and Methodology

The final objective of this thesis is to develop an approach that allows efficient simulation of the cracking process in large/complex structures of civil engineering.

To achieve this, a multi-scale strategy for the probabilistic modeling of reinforced concrete structures is proposed. It consists of two main aspects:

1. The development, in the framework of the finite element method, of macro-elements integrating the non-linear behavior of reinforced concrete, as well as implementing a methodology to identify their behavior (via numerical experimentation).
2. The implementation of a multi-scale strategy for simulating civil engineering structures using the reinforced concrete macro-elements.

In literature, multi-scale approaches are divided into two families:

Subdomain decomposition: decomposition into sub-structures and subdomains which ensure the continuity in displacement fields [Ladevèze *et al.*, 2010].

Sub-structuring: finely meshed elements are integrated in the algorithm, then the displacement fields obtained on the fine mesh are extrapolated to the main macro element nodes via Lagrange multipliers [Darby *et al.*, 2001].

In our case, we will seek to identify the behavior of predefined macro elements in our structure, independently of the rest of the structure, and then inject this law into the final

calculation. Advantages of this approach is that the numerical implementation of the model is simple compared to other approaches, since it does not require specially devised experiments in order to determine any model parameters. On the other hand, parameters identification can seem to be a long and difficult task.

Here, the multi-scale notion refers to several things:

- Material models: it is necessary to have at our disposal a set of models adapted to different scales of calculation and crack representation.
- Numerical simulation strategy: we should implement a numerical system that allows for the global modeling of the structure using information from a lower scale description of the physical phenomena.
- Adapt digital tools to handle complex and costly computations (parallel computing or sub-structuring).

In this context, the first part of my thesis will consist of a bibliographic study focused on the following two axes:

- The probabilistic modeling of the cracking process in concrete. These models, based on a fine analysis of the physical processes at the origin of the fracture, take into account the heterogeneous nature of the material and its high sensitivity to scale effects. Different models, developed at different scales, allow the characterization of micro and macro-cracking of structural concrete. Two families of models are represented here, the *probabilistic explicit cracking model* for concrete (with contact elements) [Rossi and Richer, 1987; Rossi and Wu, 1992; Tailhan *et al.*, 2010], and the *semi-explicit cracking model* (volume elements) [Rastiello, 2013], which operates on a larger scale like that of a structural element.
- The modeling of the reinforcing steel and the steel-concrete interaction. Research into the behavior of the steel-concrete interface and its modeling is a specialty of IFSTTAR. When taken into account, we realize that this steel-concrete interface has a significant impact on the cracking process in reinforced concrete. And understanding the mechanisms behind interface degradation is key to understanding the cracking processes in reinforced concrete. The focus here will be on the *steel-concrete interface model* developed at IFSTTAR [Phan *et al.*, 2013b,a, 2015].

Afterwards, we will introduce the multi-scale strategy which is more of a multi-steps process that allows the development and implementation of simple probabilistic models for reinforced concrete macro elements, integrated into the global structure, that accurately predicts the global behavior as well as the cracking process in the structure.

And finally, two validation examples are considered: the reinforced slab-beam, and the double cantilever beam. Each case is different in the sense of how the cracking process takes place in the structure, as well as differences in the numerical implementation of the strategy, which should give us a wider understanding of the strengths and limitations of the proposed strategy under different situations.

Chapter 2

Bibliography

2.1 Modeling of Concrete

Modern structural engineering relies heavily on numerical simulation, so the need for realistic material models is ever present, and the complex behavior of concrete requires special consideration. Concrete can generally be regarded as a composite material made of cement, aggregates, and water. After chemical hardening the material consists of a mortar matrix including randomly distributed aggregates. While the stress-strain relation (under tension/compression) of both the mortar and the aggregate material (sand, gravel) is more or less linear up to the peak strength and brittle in the post-peak branch, concrete as a composite material shows pronounced nonlinear behavior even at low loading levels. This difference in the stress-strain behavior of the components and that of the composite material is caused by cracking at the microscopic level. After reaching the peak load, a descending branch can be observed in concrete under displacement control. Furthermore, the failure initiation criterion in concrete exhibits asymmetry with respect to tension and compression. The failure of concrete is governed by different processes of degradation inside the cement-aggregate composite. Experiments by Hurlbut [1985] show the development of highly localized tensile cracks that result in the brittle failure of concrete under uniaxial tension. Under uniaxial compression we observe a brittle softening behavior that transitions into a ductile rupture regime with little or no degradation in strength [Hurlbut, 1985; Smith, 1987]. Concrete subjected to high triaxial compression stresses fails by compaction of micro-pores [Bažant *et al.*, 1986].

The rapid development of effective mathematical algorithms and the increased availability of powerful computing resources over the past decades have facilitated the development of realistic constitutive material models. The Finite Element Method (FEM) as well as the highly sophisticated constitutive models have become an indispensable tool in structural engineering

for the prediction of the service load, as well as the ultimate load and the corresponding failure mechanism.

Because of the large number of constitutive models for concrete only a broad and general overview of the main classes of constitutive theories, with special attention to those which can provide a basis for modeling of damage and fracture will be given. Attention is restricted to time-independent models for monotonic loading.

2.1.1 Cracking of Concrete: Basic Modeling Concepts

The formation of cracks is a characteristic property of concrete, reinforced concrete and reinforced concrete structures. Cracks are unavoidable due to the relatively low tensile strength of concrete. The formation of cracks changes the stiffness relations, thus causing the redistribution of stresses and internal forces in a structure. The width of the crack must also be limited to ensure the durability and visual integrity of a structure.

Fracture mechanics is the main field in which we study crack formation. Linear elastic fracture mechanics (LEFM) at its core. The LEFM analyzes given cracks in homogeneous elastic bodies, the cracks being surfaces or planes in 3D bodies, or curves or lines in 2D bodies defining internal limits allowing discontinuities of displacements. LEFM distinguishes three basic fracture modes, Figure 2.1a, that can be analytically treated within the framework of elasticity:

- Mode I: Opening caused by tensile stresses normal to the crack plane
- Mode II: Sliding caused by shear stresses parallel to the crack plane but normal to the front of the crack plane
- Mode III: Tearing caused by shear stresses parallel to the crack plane and parallel to the front of the crack plane

Material failure type is a subcategory of fracture modes. We distinguish: brittle failure, quasi-brittle failure and ductile failure. We consider the uniaxial stress-strain relations (the behavior before reaching the strength is assumed as elastic) to simplify the discussion, Figure 2.1b.

- Brittle fracture: describes a sudden drop of stress after reaching critical strength. The internal elastic energy is transformed to form the new fracture surfaces.
- Quasi-brittle fracture: After reaching critical strength we observe decreasing stress. The internal energy is transformed into process zone (or crack band) creation. This type of failure is typical for concrete.

- Ductile fracture: describes yielding and hardening, i.e., with a slightly increasing stress after the strain passes the point of yielding. Yielding and hardening go on for a relatively long range of strain before localization starts ending with rupture. The internal energy is predominantly transformed into crystalline sliding. This is typical for metals.

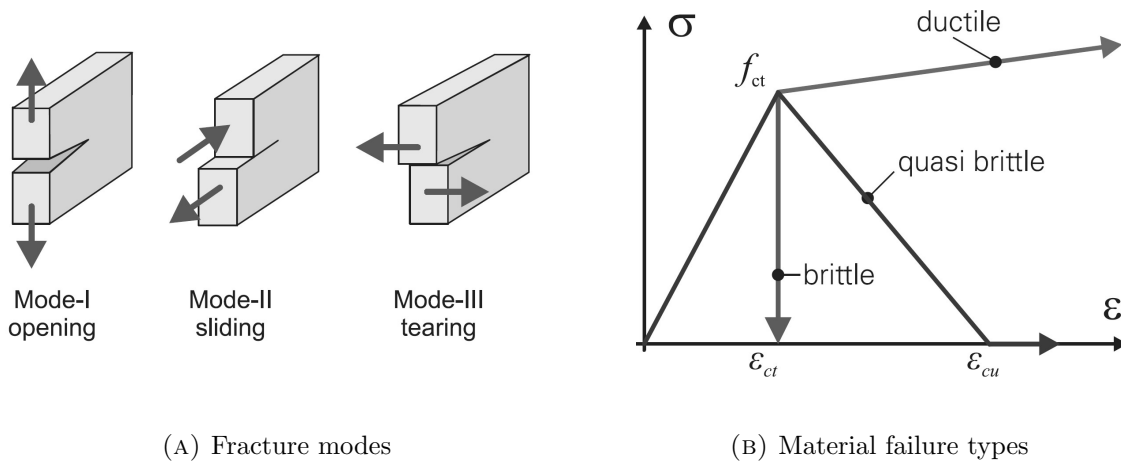


FIGURE 2.1: Fracture modes and material failure types

The application of LEFM is limited to cases of fragile/brittle failure. In the case of quasi-fragile failure LEFM is no longer directly applicable due to the formation of a process zone or a crack band ending in a macrocrack [Bažant and Oh, 1983]. Continuous mechanics is not appropriate for a detailed microscopic (spatial dimensions of micrometers) or even mesoscopic (spatial dimensions of millimeters) description of the complex mechanisms during the formation of the crack band. In addition, the macroscale point of view requires the homogenization of the crack band.

2.1.1.1 Literature

There exists numerous approaches in the literature to describe the cracking of concrete (from initiation to the propagation of cracks). Broadly speaking, they can be classified into two groups according to their implicit or explicit method to treat the kinematic discontinuity associated with the crack:

- In models developed in the context of continuum mechanics (*damage models* [Mazars, 1984; Pijaudier-Cabot and Bažant, 1987; Frémond and Nedjar, 1995], *plasticity* [Feenstra and De Borst, 1995], *diffuse crack* [Rashid, 1968; Cope *et al.*, 1980; De Borst and Nauta, 1985]) the crack is represented implicitly by a regular field of inelastic deformations through the use of more or less complex constitutive laws.

- In explicit models, the crack is explicitly represented by a discontinuity of displacement at the interfaces between the finite elements or integrated in the formulation of the finite element itself (methods based on the *partition of unity method* [Babuska and Melenk, 1995; Melenk and Babuška, 1996], *XFEM* [Dolbow and Belytschko, 1999; Moës and Belytschko, 2002], *EFEM* [Simo and Oliver, 1994; Oliver, 1996; Armero and Garikipati, 1996]).

An important aspect in the response of concrete structures is its sensibility to scale effects. Scale effect is the change in response when the spatial dimensions are set to a larger or smaller scale while geometry and all other characteristics are conserved, it is a quintessential problem of any physical theory. The classical theory suggests a continuous three-dimensional generalization of the model of the weakest link which is the cause of failure of a chain of links of random resistances, which means that heterogeneity is one of the major causes of scale effects in materials. The ability of a cracking model to take into account these scale effects in concrete is therefore necessary.

There already exists a vast literature on this subject. From the first considerations of Galilei [1632], to Weibull's theory of the weakest link [Weibull, 1951], up to Bažant's recent energetic theories [Bažant and Raftshol, 1982; Bažant and Planas, 1997], and geometric theories (Carpinteri's fractal theory [Carpinteri, 1994; Carpinteri *et al.*, 1995]), among others. The physical representation and mathematical validity of the various formulations is still the subject of heated discussions [Bažant and Yavari, 2005; Carpinteri *et al.*, 2007; Saouma and Fava, 2006; Bažant and Yavari, 2007; Carpinteri and Puzzi, 2009].

Several experimental investigations [Rossi *et al.*, 1992b, 1994b] led to the realization that these phenomena can be adequately described, taking into account the heterogeneity of concrete (which is at the origin of the scale effects) in the context of a probabilistic approach. Heterogeneity is an intrinsic property of concrete that induces scale/volume effects. Therefore, the local mechanical characteristics (i.e. Young's modulus E , the tensile strength f_t , ...) are subject to random variations that depend on the volume of the stressed material. The cracking process is mainly driven by the interactions between the random defects in the cement paste and the internal stress gradients. The presence of defects significantly influences the quality of the cement paste, a good indicator of which may be the compressive strength f_c . The heterogeneity of the material can be characterized by the ratio of the stressed volume V of material over the volume of the largest aggregate V_g . In general, the weight of this heterogeneity is all the more important as the ratio V/V_g gets smaller. From scale effect laws, mean values and standard deviations of material characteristics for different concretes were obtained experimentally by Rossi *et al.* [1994a].

2.1.2 Probabilistic Cracking of Concrete

In the context of macroscopic approaches, several authors propose that heterogeneity be taken into account by applying statistical distributions on the local material characteristics (for example, the tensile strength). Material properties are therefore considered as random variables, distributed spatially according to different levels of correlation. The use of correlation fields proved to be a numerically efficient method when dealing with the cracking of quasi-brittle materials [Colliat *et al.*, 2007; Vořechovský, 2007; Bruggi *et al.*, 2008; Yang and Xu, 2008; Su *et al.*, 2010; Ibrahimbegovic *et al.*, 2011; Syroka-Korol *et al.*, 2013; Sellier and Millard, 2014]. It requires however the introduction of a spatial correlation length, which only adds to the problem.

As was shown by Rossi *et al.* [1992a], if we assume an equivalence between the finite elements of the mesh and the volumes of heterogeneous material, the use of uncorrelated random fields makes it possible to achieve a consistent representation of the scale effects. Original models based on these concepts have been proposed according to two typologies of formulation:

1. “Explicit” cracking models [Rossi and Wu, 1992; Rossi *et al.*, 1996; Tailhan *et al.*, 2012].
2. “Semi-explicit” cracking [Tailhan *et al.*, 2010; Rastiello *et al.*, 2015].

The main difference between the two approaches is how we numerically process the kinematic discontinuity.

In the first case, the cracks are explicitly represented by zero-thickness interface elements positioned between the elastic solid elements (representing the uncracked concrete). The tensile strength of the interface elements is randomly distributed following a Weibull distribution [Weibull, 1951] over all elements, and depends on the total volume of the elements that are in contact with the interface. The propagation of cracks is recognized as the creation of elementary rupture planes that appear randomly and can coalesce to create macro-cracks.

In the second case, the energy associated with the crack is integrated in the formulation of the volume element according to a Rashid-type approach [Rashid, 1968]. In the case of local elastic-fragile behavior, when the maximum tensile stress of the concrete is reached at the center of gravity of the element, the stiffness of the element is set to zero. In a sense, a “hole” appears in the mesh. The tensile strength is distributed randomly on all the elements in the mesh. The parameters of the probability distribution function (again, a Weibull one) used are functions of the ratio of the volume of the finite element over the volume of the largest aggregate, as well as the compressive strength of the concrete. This approach is called “semi-explicit” in the sense that a discrete vision of the crack is preserved (i.e. the material properties are distributed discretely in the mesh, cracking is treated element by element), but the elementary cracking is taken into account through its energetic effect.

Next we shall present the local cracking models for concrete used in this study in more depth since they constitute, as we will later see, the backbone of the new proposed multi-scale approach.

2.1.2.1 Explicit Cracking Model (Contact Elements)

The model was first developed at IFSTTAR (formerly LCPC) by Rossi and Richer [1987]; Rossi and Wu [1992] and improved by Tailhan *et al.* [2010]. It describes the behavior of concrete via its two main characteristics: heterogeneity, and sensitivity to scale effects [Rossi *et al.*, 1994b]. The physical basis of the model can be summarized as follow:

1. The heterogeneity of concrete is due to its composition. The local mechanical characteristics (Young's modulus E , the tensile strength f_t , the shear strength τ_c) are randomly distributed
2. The scale effects are a consequence of the heterogeneity of the material. The mechanical response directly depends on the volume of material that is stressed.
3. The cracking process is piloted by defects in the cement paste, the heterogeneity of the material, and the development of tensile stress gradients.

In order to account for these physical evidences, the model is developed in the framework of the finite element method, each element representing a given volume of (heterogeneous) material. Previous works [Rossi *et al.*, 1994b, 1996] have shown that it is possible to establish a link between the tensile strength f_t or Youngs modulus E and the volume of the stressed concrete element. An experimental scale effect law was then established for the tensile strength mean and standard deviation $[m(f_t); s(f_t)]$ as functions of easily measurable quantities such as the volume of the specimen V_s and the volume of the coarsest aggregate V_g (which is representative of the degree of heterogeneity of the concrete used) and the compressive strength of concrete f_c (an indicator of the quality of the cement paste).

$$m(f_t) = F_\alpha\left(\frac{V_s}{V_g}, f_c\right) \quad (2.1)$$

$$s(f_t) = F_\beta\left(\frac{V_s}{V_g}, f_c\right) \quad (2.2)$$

The shear strength is also distributed randomly on all elements using a probability distribution function with a mean value that is independent of the mesh size and is assumed equal to the half of the average compressive strength of the concrete (a fair first approximation in the absence of more detailed research about this subject), and its deviation depends on the element size, and is the same (for elements of same size) as that of the tensile strength.

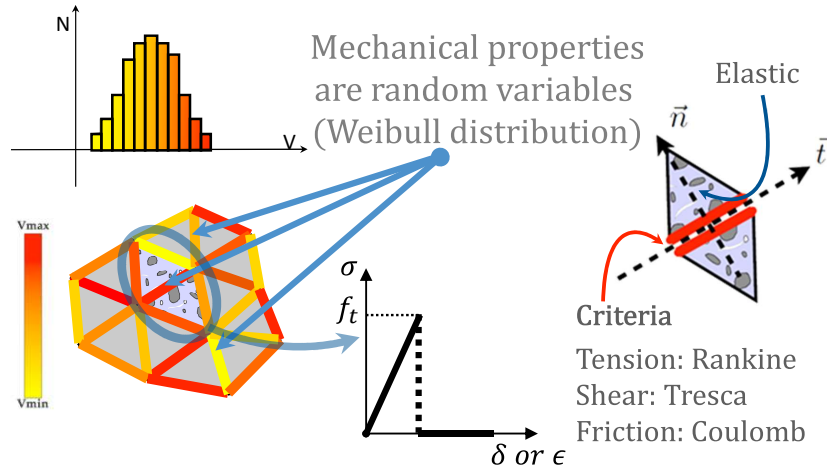


FIGURE 2.2: Probabilistic explicit cracking model for concrete

The cracks are explicitly represented by interface elements of zero thickness. These elements connect volume elements representing un-cracked plain concrete. Failure criteria of Rankin in tension and Tresca in shear are used. As far as tensile or shear stresses remain lower than their critical values, the interface element ensures the continuity of displacements between the nodes of the two neighboring volume elements. The material cell gathering these two volume elements and the interface element remains therefore elastic. Once one of the preceding failure criteria is reached, the interface element fails and an elementary crack is created. Its tensile and shear strengths as well as its normal and tangential stiffness values become equal to zero. In case of crack re-closure, the interface element recovers its normal stiffness and follows a classical Coulomb's law [Rossi *et al.*, 1996]. Note that in this model, the creation and the propagation of a crack is the result of the creation of elementary failure planes that can randomly appear and then coalesce to form the macroscopic cracks, Figure 2.2.

2.1.2.2 Semi-Explicit Cracking Model (Macroscopic Elements)

The process of crack creation and propagation is schematized in Figure 2.3. The creation and propagation of a network of microcracks around the crack tip induce a local non-linear behavior with energy dissipation.

When loading increases, the propagation of microcracks gives rise to an unstable process: some microcracks coalesce into one main macrocrack, while the others tend to reclose. Modeling this process using classical continuous approaches (damage mechanics, diffuse cracking, elasto-plasticity,...) turns out to be, in general, a very difficult task. Several problems of mathematical and numerical nature arise when constitutive laws are used to describe the softening behavior.

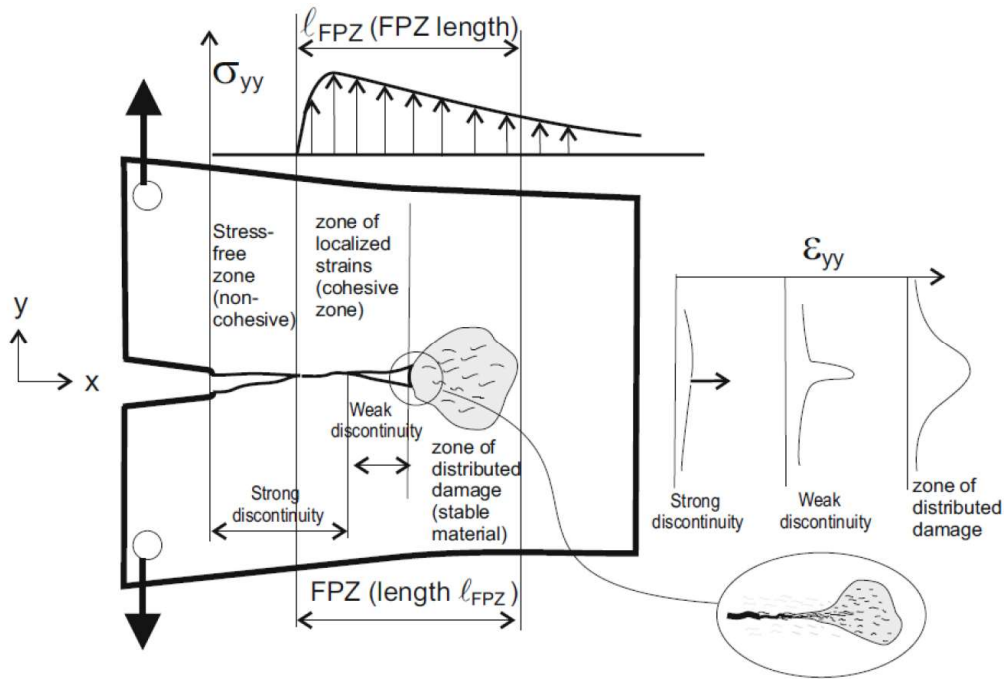


FIGURE 2.3: Cracking process in quasi-brittle materials [Huespe and Oliver, 2011]

From a mathematical point of view, we note the loss of ellipticity of equations of equilibrium and the loss of uniqueness of the solution. From a numerical point of view, these methods suffer from mesh sensitivity.

In this regard, one proposition is to use enriched continuous models (non-local damage, gradient type, Cosserat models). In these models, the microstructure of the material and the deformation process at the microscopic scale are taken into account by introducing new degrees of freedom: micro-rotations associated with micro-moments in Cosserat models [Cosserat *et al.*, 1909], or assuming that the stress state in a point in space is influenced by its spatial gradient [DE and De Vree, 1996; Peerlings *et al.*, 1998] or the stress/strain state in its vicinity (non-local models, [Pijaudier-Cabot and Bažant, 1987; Bažant and Jirásek, 2002; Giry *et al.*, 2011]). However, it is still necessary to include an internal characteristic length into the constitutive law (representative of the microstructural scale of the material). This characteristic length, which needs to be intrinsic to the material, does not in fact have a very clear physical explanation. For a given material, this length usually depends on the problem at hand (geometry of the structure, boundary conditions, etc...) [Toutlemond and Rossi, 1998].

From a numerical point of view, a simple and effective method for solving this problem consists in introducing, on the scale of the finite element, a dependence between the parameters of the constitutive law and the dimension of the element itself [Cedolin and Bažant, 1980; Pietruszczak and Mroz, 1981]. The use of a volume energy density g_f , linked to the surface energy of cracking G_f through a characteristic length of the element (or of the mesh), makes it possible to

regularize the solution and to recover the energy objectivity with respect to mesh size, ensuring a constant energy dissipation independent of spatial discretization. This method has the advantage of being rather simple to implement in a constitutive law without requiring heavy numerical calculations. Even in this case a series of mathematical, numerical and parameter identification problems arise. Mathematically this method does not preserve the well-posed equilibrium equations. Numerically simulated cracking is found to be dependent on the mesh morphology [Bažant and Jirásek, 2002]. Finally, the use of the cracking energy G_f as a material parameter is not clear because its experimental determination is highly dependent on the type of test, the geometry of the test piece used, and especially on the dimensions of the test specimen (i.e. it is subject to scale effects).

The model presented here does not deal with the propagation of cracks, at least not in the sense of fracture mechanics, but with the “random” creation of elementary cracks. A macrocrack is then the consequence of several elementary cracks. In other words, the rupture of successive elements can be considered, at a macroscopic level, as representative of the propagation of a macrocrack. The model is based on the following fundamental assumptions [Rossi *et al.*, 1994a; Tailhan *et al.*, 2010]:

1. The model is probabilistic. To describe the material heterogeneity, its mechanical properties must be randomly distributed on the finite element mesh (using uncorrelated fields).
2. We consider that a finite element is representative of a volume of heterogeneous material, and the element degree of heterogeneity is defined by the ratio of its volume V_e to the volume of the largest aggregate V_g
3. The physical mechanisms influencing the cracking process remain the same regardless of the scale of observation. We assume that it is possible to define macroscopic quantities independently of the size of the finite element. The mechanical behavior of the finite element depends on its size, and the behavior of each finite element is subject to random variations. Its mechanical properties are then a function of its own volume through the degree of heterogeneity $r_e = V_e/V_g$.

At the scale of the element, the model considers that the process of cracking can induce a certain dissipation of energy. The term “cracking process” refers here to the creation and propagation of a crack within the element itself. When the total amount of energy available to the element is consumed, it is therefore “cracked” and its rigidity drops to zero. An elasto-damaging model is a simple and efficient way of dissipating the energy locally (at the scale of the finite element). This dissipated energy being the consequence of the cracking process in the finite element, which is not explicitly represented here. In this approach, cracking only makes sense when the energy is completely dissipated: it is at this point that the element splits and a portion of a macro

crack is represented. Accordingly, the damage parameter will be used here only to dissipate energy and not to characterize the crack.

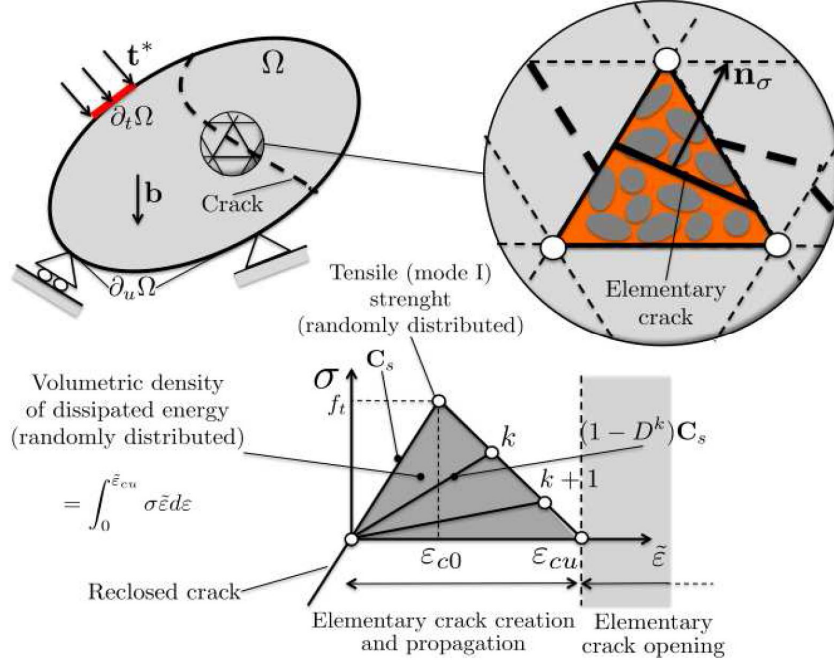


FIGURE 2.4: The probabilistic semi-explicit cracking model [Rastiello, 2013]

Numerically speaking, when the tensile strength f_t in a gauss point of the element is reached in the direction of the principal stress σ_1 , the damaged elastic tensor \mathbf{C}^s is calculated like so:

$$\mathbf{C}^s := (1 - D)\mathbf{C}^e \quad (2.3)$$

$$\boldsymbol{\sigma} = \mathbf{C}^s : \boldsymbol{\varepsilon} \quad (2.4)$$

where \mathbf{C}^e is the initial elastic tensor and $D \in [0, 1]$ is the damage variable. Its evolution is a function of the internal variable k according to a flow law

$$D = g(k) \quad (2.5)$$

The loading function $f = f(\tilde{\varepsilon}, k)$ rules over damage evolution, where $\tilde{\varepsilon}$ is a scalar function of the deformation field $\boldsymbol{\varepsilon}$. The function f and the rate of change of the variable k must satisfy the Kuhn-Tucker conditions:

$$f \leq 0, \quad \dot{k} \geq 0, \quad f\dot{k} = 0 \quad (2.6)$$

The f function chosen uses a bilinear formulation of the stress-strain relationship, Figure 2.4. Only when the rupture criterion is reached can the crack opening be calculated. This calculation is carried as a projection along the direction of the principal constraint (which continues to evolve

in line with the changes in the stress field in the material during loading) of nodal displacements, Figure 2.5. Concerning crack reclosure, we simply assume that the element completely regains its rigidity in compression when the calculated crack opening is zero once more.

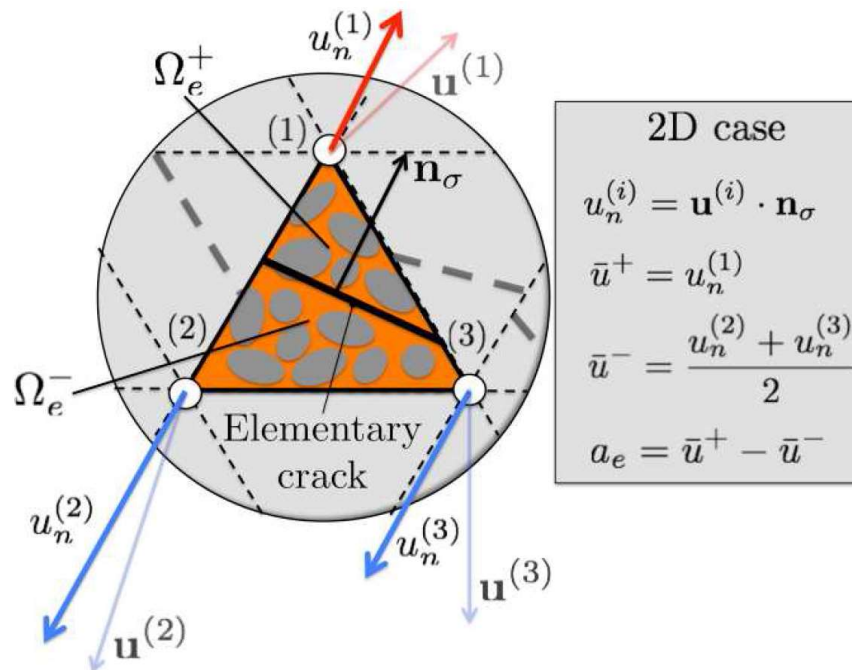
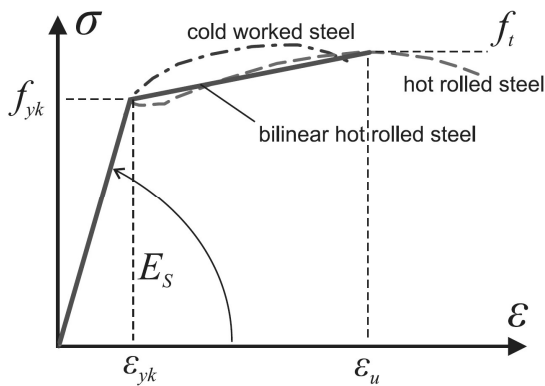


FIGURE 2.5: Crack opening calculation according to the semi-explicit cracking model [Rastiello, 2013]

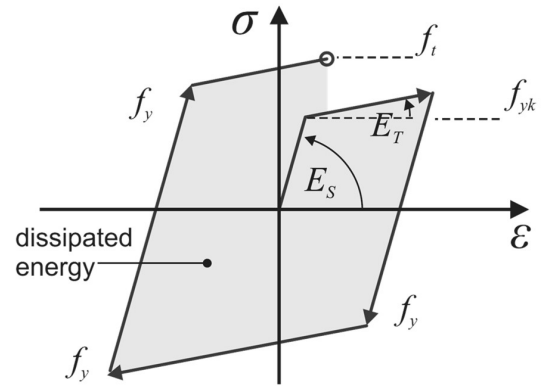
2.2 Reinforcing Steel

Reinforcing steel has to be considered as a second basic component beneath plain concrete. With spatial dimensions of millimeters, steel can be considered as a homogeneous material in contrast to concrete. Furthermore, steel has the same behavior under compression and tension. Experimental data in Figure 2.6a shows the typical uniaxial stress-strain relations. Characteristics of the stress-strain relation are:

1. An initial linear elastic part.
2. Transition zone with the initiation of yielding.
3. The yielding part with high strains and slightly increasing stresses.
4. A relatively short softening zone followed by failure.



(A) Uniaxial stress-strain behavior



(B) Cyclic behavior with hardening

FIGURE 2.6: Reinforcing steel stress-strain behavior

Aspects of these parts may vary with different types of steel. Relevant design properties of reinforcing steel are given in BSI [2004]; CEB-FIP [2010]. A bilinear approximation of uniaxial stress-strain relations is generally used for the design and computation of the steel reinforcements in reinforced concrete structures. It is characterized by the initial Young's modulus E_s , an initial yield stress f_{yk} , a failure stress f_t and a corresponding failure strain ϵ_u . Hardening occurs when $f_t > f_{yk}$ (i.e. the material gains strength). The yield strain and tangential material stiffness in the hardening range are given by:

$$\epsilon_y = \frac{f_{yk}}{E_s}, \quad E_T = \frac{f_t - f_{yk}}{\epsilon_u - \epsilon_y} \quad (2.7)$$

Nonlinear steel behavior is characterized by elastoplasticity. We can observe this nonlinear material behavior when we unload while in the yielding phase: *Plasticity* is characterized

by approximately the same material stiffness for initial elastic loading and unloading. Thus, plastic strains remain as permanent strains while unloading from yielding to zero stresses. This phenomenon is a result of the sliding of atomic planes in the crystal microstructure.

The cyclic behavior is schematically illustrated in Figure 2.6b. Unloading from a tensile regime may proceed to reloading the steel into the compressive regime while crossing a zero stress. After the maximum stress f_y is reached for tensile hardening the material is linear elastic during reloading until stress reaches $-f_y$ and plastic yielding continues with further hardening in the compressive range. The *isotropic hardening* cycle is presented in Figure 2.6b. Elastoplasticity allows for closed cycles of stress-strain behavior, i.e., a particular state of stress and strain $[\sigma, \varepsilon]$ in the hardening range can again be reached after a cycle. The area within such a cycle amounts to the specific internal *dissipated energy*. On the other hand, energy dissipation in a structure contributes to its *ductility*: its ability to deform while its internal forces retain their level.

2.3 Modeling of Reinforced Concrete

Reinforcements are often applied in concrete structures to help take over tensile forces, due to the limited tensile strength of concrete. An experimental setup to expose the transmission of forces between a rebar and the surrounding concrete is shown in Figure 2.7a: a single rebar is pulled out of a concrete block. The system is characterized by measures of the relative displacement of the rebar compared to the concrete block, and the forces created by the rebar tension and concrete block retention. Transmission of forces relies on three mechanisms:

1. Adhesion: a rigid connection of boundary layers of concrete and steel.
2. Friction: resistance to slip between the boundary surfaces of concrete and steel combined with lateral pressure.
3. Rebars usually have profiled surfaces with ribs or dents acting like consoles.

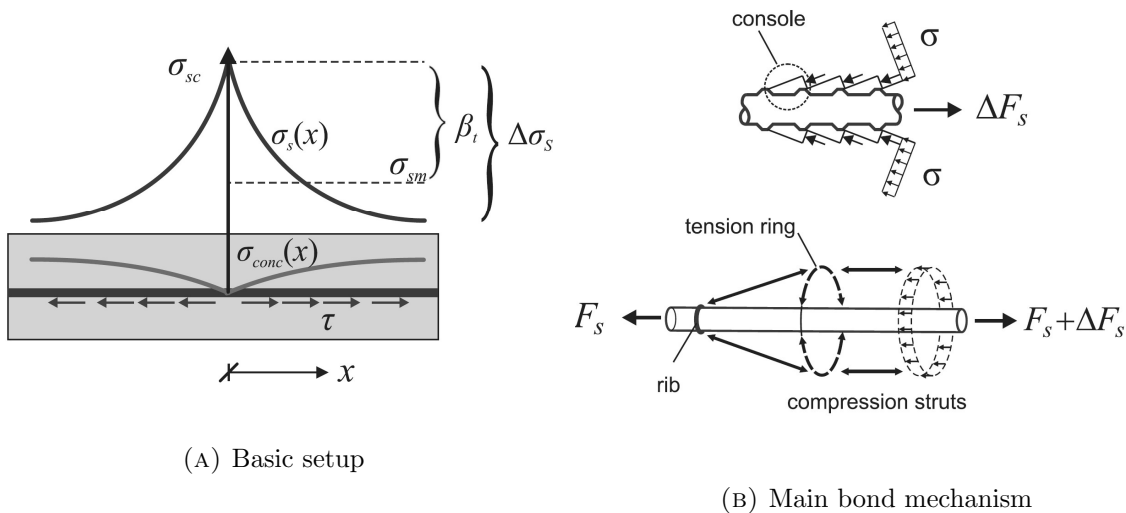


FIGURE 2.7: Pull-out test setup [Häussler-Combe, 2014]

This last-mentioned mechanism contributes the largest amount to the rebar force. Such an interaction, due to profiled surfaces, leads to a triaxial state of stresses in the surrounding concrete, Figure 2.7b. From a cross-section point of view, a system of skew concrete struts braces against the rebar ribs. These concrete struts form a cone in the spatial view. A circumferential tensile ring redirects the cone compression into a cylinder compression aligned with the rebar force. The tensile cylinder around the rebar is activated through tensile stresses within the concrete. Failure may occur with concrete splitting along the rebar when these tensile stresses exceed the limit tensile strength of concrete. This can be prevented by placing a lateral secondary reinforcement or through reducing tensile stresses by increasing the radial concrete cross section or by providing sufficient concrete cover, respectively.

In the scientific literature, models proposed to simulate reinforced concrete vary depending mainly on which scale of analysis they operate. In each case, one must consider the range of applications and prospects of the model, which are crucial criteria to avoid excessive or unsuitable computational burden or inappropriate results output. Such models can be classified as follows:

1. local models aimed at small structural elements, member joints or other local geometric singularities. A local modeling approach is applied involving sophisticated constitutive relations for concrete (damage models, smeared cracking, etc...), steel rebar (plasticity...), and the steelconcrete bond.
2. At the intermediate scale, a multilayer modeling method for RC structural elements (panels, slabs and walls,...) or multi-fibre modeling of RC members is often employed. Simplified constitutive relations of steel and concrete are used where the nonlinear behavior of bond might be merged with the steel reinforcement plastic behavior [Ngo and Scordelis, 1967; Guedes *et al.*, 1994; Spacone *et al.*, 1996].
3. At the macroscopic scale, *homogenized* RC models for structural elements (members, beams and columns,...), nonlinear models are often proposed. These models summarize the main aspects of the nonlinear response at the scale of the whole structure, and their parameters are calibrated with reference to experimental results and characteristic material data.

We can therefore identify two main typical formulations for constitutive models used in describing the behavior of reinforced concrete:

1. For local/intermediate scale models, the usual approach consists in developing a series of theoretical expressions idealizing each elementary phenomenon involved in the overall behavior and calibrated from a series of experimental data. The RC constitutive model is then built by adding/coupling these elementary mechanisms: concrete, steel rebars, and the interaction between these two.
2. For macroscopic RC models, a general framework would serve as a basis for developing the constitutive model in order to consistently formulate the state equations and evolution laws. Homogenization techniques or multi-scale analysis are typically used in order to transfer the physical variables and equations from the microscopic to the macroscopic scale [Andrieux *et al.*, 1986; Suquet, 1993; Perić *et al.*, 2011].

2.3.1 Local Scale Approach: Bond Between Concrete and Reinforcing Steel

The bond is a complex mechanical problem which requires the mesoscale view for a thorough understanding, whereby each rebar and concrete has to be considered as three-dimensional solids with nonlinear material behavior. A simplified macroscopic model is shown in Figure 2.8.

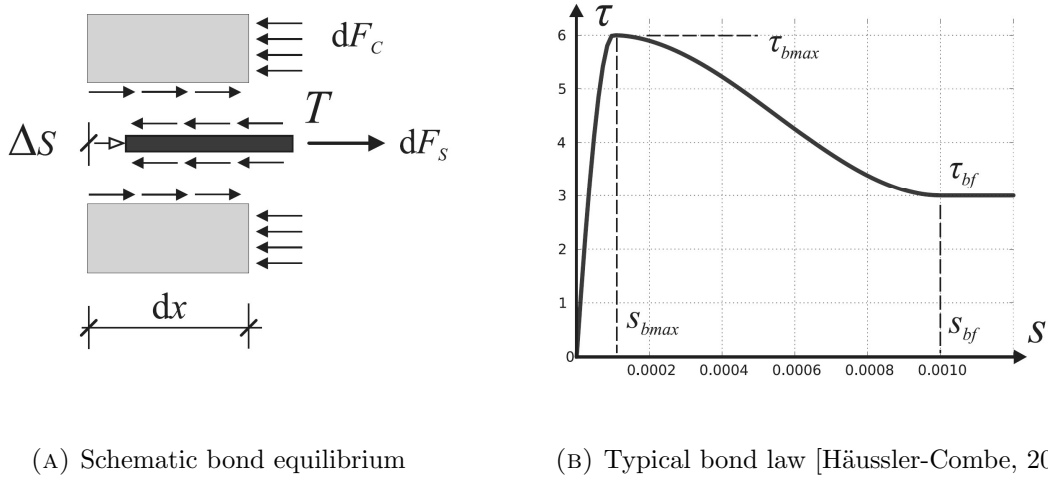


FIGURE 2.8: Simple bond model

Transmission forces between a simplified cylindrical rebar and the concrete body exposes a *bond force flow* T :

$$T = \frac{dF_s}{dx} = \frac{dF_c}{dx} \quad (2.8)$$

where F_s is the force applied on the rebar force and F_c the resulting force in the concrete body. The relative displacement between rebar and concrete is measured by a slip s . The notion of slip assumes the deformation of concrete in a cross section as approximately homogeneous beyond the immediate surroundings of the rebar and defines slip s as the difference between the longitudinal displacements of the outer concrete area and the center axis of the rebar, Figure 2.8a.

The force variable T and the kinematic variable s are connected by a *bond law*:

$$T = f_T(s) \quad (2.9)$$

If we assume that the rebar has a constant circumference U , then the bond stress is $\tau = T/U$, which leads to:

$$\tau = f_\tau(s) \quad (2.10)$$

Such a formulation is generally used as it is independent of specific geometric properties and may be considered as a special case of a material law [CEB-FIP, 2010]. A typical response from a bond law is shown in Figure 2.8b. Characteristics of the response curve are:

1. An initial elastic part with increasing nonlinear mechanisms due to nonlinear behavior of reinforced concrete (development of microcracks in the concrete body).
2. A high point, or range of maximum bond stress (related to the tensile strength of concrete), when τ_{max} is reached.
3. A softening part with increasing slip and decreasing bond stress due to softening in the tensile range of concrete (this is true as long as it is not a highly reinforced structure).
4. A final horizontal part with approximately constant bond stress τ_f and increasing slip due to the friction of sheared concrete consoles.

This particular law is composed of a quadratic, cubic and linear polynomial with continuous derivatives at the nodes which improves convergence when applying the Newton-Raphson method for nonlinear problem solving. The main parameters are values of τ_{bmax} , τ_{bf} and the corresponding slip values s_{bmax} , s_{bf} . These values have to be determined from experimental data.

2.3.1.1 Steel-Concrete Interface Model

A simple and robust model has been developed and validated at IFSTTAR [Phan *et al.*, 2013b,a, 2015]. It takes into account the nonlinear behavior of the concrete-rebar bond in the frame of damage mechanics. It can represent physical phenomena such as interface sliding, cracks appearance as well as the degradation process. The concrete-rebar bond is modeled as interface elements. Their role is to:

1. Ensure the displacement continuity between the concrete and the steel before the slip of the interface and before the cracking of the concrete, thus ensuring the transfer of stresses between steel and concrete.
2. Represent the macroscopic mechanical effect of the rebar at the ribs. In other words, it replaces the ribs in the mesh and insures their mechanical role.
3. Simulate a local failure between steel and concrete along the rebar resulting from a loss of the local adhesion due to shear cracking.
4. Simulate the local friction between the concrete and the steel after the interface failure.

The concrete-rebar bond is considered as a material zone that progressively degrades in shear (the tensile failure is neglected). Prior to total failure, stresses are continuously transmitted through the interface. A damage model approach is implemented that maintains a constant level of stress when the critical shear has been reached, Figure 2.9a. When the relative tangential

displacement between the concrete and the rebar exceeds a critical value, the interface element is declared broken. After failure, a Mohr-Coulomb type of friction behavior is maintained.

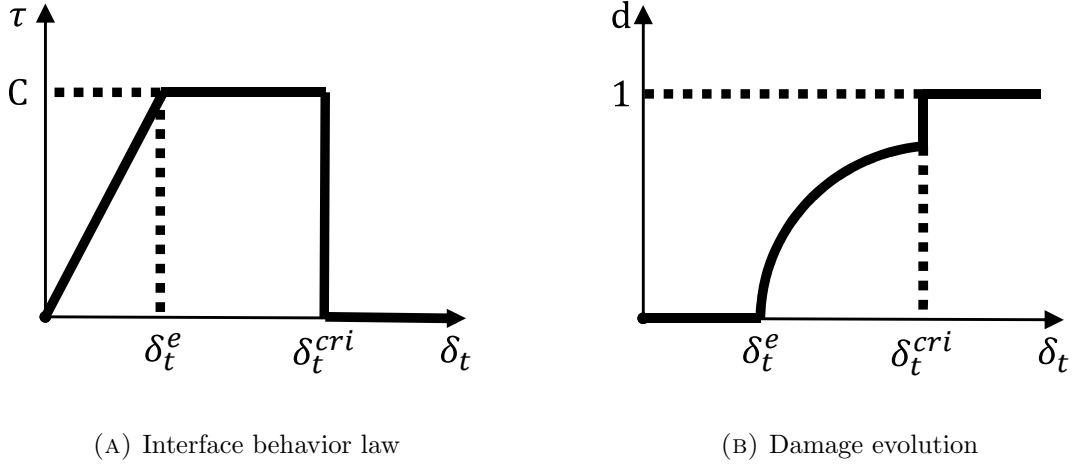


FIGURE 2.9: Steel-concrete interface behavior, 2D elements

The interface model is deterministic. This is a valid approximation because the cracking process around the rebar is governed by the presence of the ribs (and has little to do with the heterogeneity of concrete) [Rossi, 1993].

The 3D constitutive relations of the model are summarized as follows:

$$\begin{bmatrix} \sigma_n \\ \tau_1 \\ \tau_2 \end{bmatrix} = (1 - d) \begin{bmatrix} k_n & 0 & 0 \\ 0 & k_{t1} & 0 \\ 0 & 0 & k_{t2} \end{bmatrix} \times \begin{bmatrix} \delta_n \\ \delta_{t1} \\ \delta_{t2} \end{bmatrix} \quad (2.11)$$

Where σ_n is the normal stress, and τ_1, τ_2 are the tangential stresses in two directions, d is a damage parameter, δ_n, δ_{t1} and δ_{t2} are respectively the normal and tangential displacements, and k_n, k_{t1} and k_{t2} the normal and tangential stiffness values of the contact element. The values of k_n, k_{t1} and k_{t2} can be found in some commercial finite element codes like CESAR [Humbert *et al.*, 2005] or CODE ASTER [Proix *et al.*, 2000].

The damage evolution, Figure 2.9b, is given by:

$$\begin{cases} d = 0, & |\delta_t| \leq \delta_t^e \\ d = 1 - \frac{\delta_t^e}{|\delta_t|}, & \delta_t^e < |\delta_t| < \delta_t^cri \\ d = 1, & |\delta_t| \geq \delta_t^cri \end{cases} \quad (2.12)$$

Where $\delta_t^e = f(C, k_{t1}, k_{t2})$ is the threshold of tangential elastic displacement (C is the cohesion parameter), δ_t^cri is the critical tangential displacement ($\delta_t^cri > \delta_t^e$) and $|\delta_t| = f(\tau, k_{t1}, k_{t2})$ is the variable which drives damage evolution.

The evolution of the damage variable (a state variable) has to verify some conditions to satisfy the second law of thermodynamics:

$$\begin{cases} \dot{\delta} \geq 0 \\ d = \max(d_0, d) \end{cases} \quad (2.13)$$

Where d_0 is the initial damage state, and d is the actual damage state.

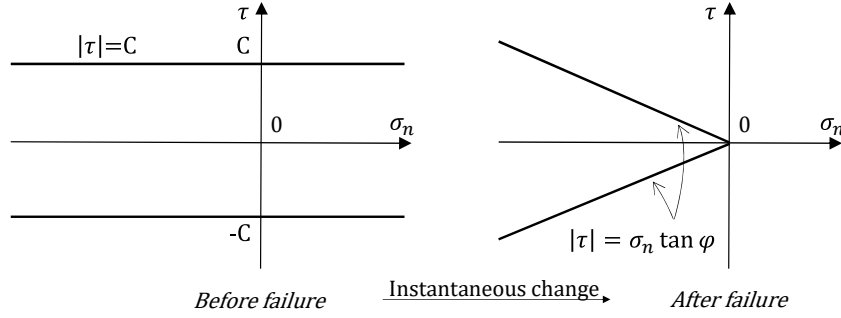


FIGURE 2.10: Mohr-Coulomb friction after failure of the steel-concrete interface

After failure, we switch to a friction behavior, Figure 2.10, with an associated flow rule. The yield criterion is given by:

$$f(\boldsymbol{\sigma}, \varphi) = |\tau| - \sigma_n \tan \varphi \quad (2.14)$$

And the associated flow rule:

$$\begin{cases} \dot{\mathbf{d}}^p = \lambda \frac{\partial g}{\partial \boldsymbol{\sigma}} \\ g(\boldsymbol{\sigma}, \psi) = |\tau| - \sigma_n \tan \psi \\ \psi = \varphi \end{cases} \quad (2.15)$$

Where $\dot{\mathbf{d}}^p$ is the evolution of the plastic relative displacement, λ the plastic multiplier, $g(\boldsymbol{\sigma}, \psi)$ the associated function, φ and ψ are respectively the friction and dilatancy angles. A value of 30 is selected for both φ and ψ (value from Rossi *et al.* [1996]).

Only the values of the maximum shear stress, C , and of the tangential critical relative displacement, δ_t^{cri} , have to be determined. This is done by numerical inverse analysis.

2.4 Macroscopic Scale Approach

The local scale approach often needs refined meshes and suffers from iterative procedures convergence issues, due to extreme non-linearity and singularities. Therefore, such an approach cannot be reasonably proposed for the analyses of a large structure. Hence the introduction of macroscopic continuous approach of the mechanics of reinforced concrete that assumes that the whole system of discrete variables (nonlinear steel behavior, steel concrete bond, concrete cracking,...) can be replaced by continuous field equations relating stress σ and strain ϵ on the macroscopic scale.

In macroscopic continuum theories, plasticity theory, continuum damage mechanics, and fracture mechanics offer a solid background to address the main features of RC behavior in a relatively compact form. On the macroscopic scale, concrete is often considered a homogeneous material. Microcracks within the material volume that conglomerate into macrocracks in a changing stress field are quantified on the macroscopic level in terms of internal state variables. More specifically, in isotropic damage mechanics, we consider that the microcracks are uniformly distributed within the material and their density is quantified generally by a damage tensor. The result of this process is manifested as degradation of material stiffness with damage mechanics describing the initiation and evolution of crack growth, whereas sliding along the crack edges is usually modeled using plasticity theory [Ragueneau *et al.*, 2000]. Consequently, damage and plasticity should be taken into account in combination to accurately describe the behavior of a quasi-brittle material like concrete [Richard and Ragueneau, 2013].

2.4.1 Multi-scale Constitutive Modeling and Homogenization Techniques

Homogenization techniques aim to predict the macroscopic behavior by means of the homogenization of the mesoscopic response of the simulated material region “MR” or the representative elementary volume “REV”. Reinforced concrete is then modeled by means of this control volume (REV, representative elementary volume) within a micromacro approach. In this multi-scale context, a justification of the modeling by means of an averaging homogenisation technique is chosen to deduce the overall behaviour of the RC section from local phenomena

In order to develop a macroscopic model, we still require a fairly good understanding of the mechanics and interactions that happens on the micro scale. The introduction of multi-scale theories has allowed the modeling of the dissipative behavior of solids. The general concept of multi-scale modeling extends from quantum mechanics and particle physics, molecular dynamics, and dislocation theory to macroscopic constitutive relations, Figure 2.11. It is now well accepted that classical theories in which the constitutive response is defined by a set of ordinary differential equations, possess stringent restrictions on the complexity of strain paths

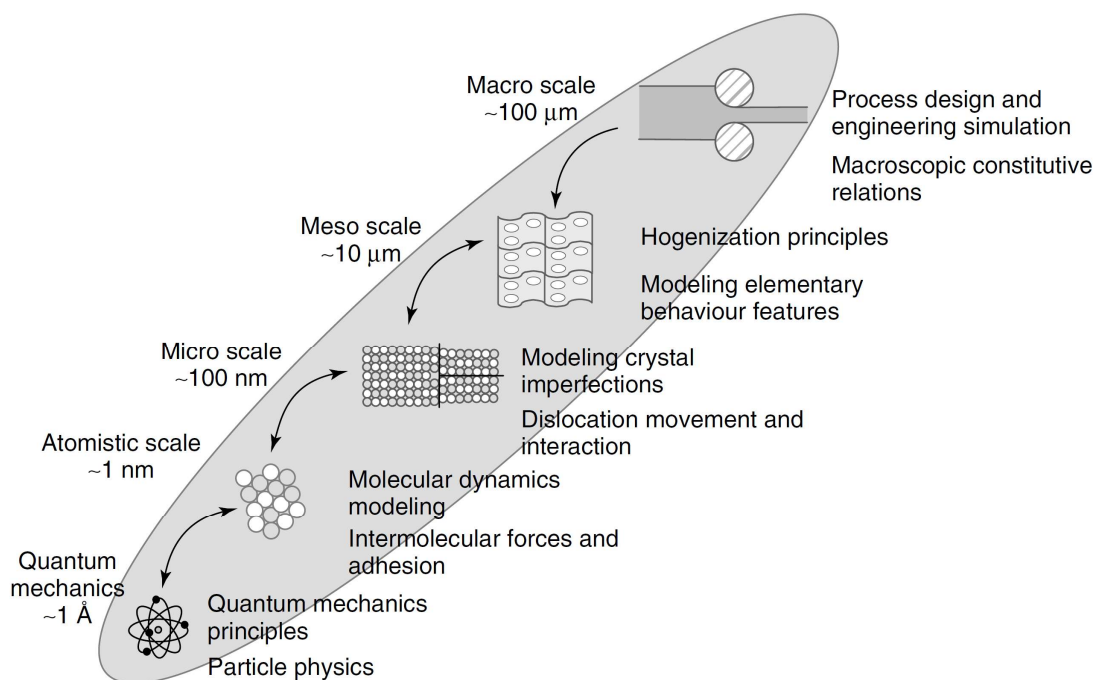


FIGURE 2.11: Length scales for most metal materials

for which reasonable predictions can be obtained. This is particularly true when more intricate phenomena on the microscale such as damaging, microcracking, or phase debonding happen. Furthermore, capturing details of the phenomenological effects of such mechanisms on the overall response of the material, requires the introduction of a great number of internal state variables and the identification and definition of their corresponding evolution laws with the associated material parameters. This is by no means easily accomplished. Hence the adoption of multi-scale theories, where the macroscopic stress and strain tensors are defined as volume averages of their microscopic counterparts over the materials representative elementary volume (REV). The foundations for this family of constitutive theories were laid by Nguyen *et al.* [1983]. Such theories are particularly attractive for the description of complex constitutive response by means of finite element approximations due to their suitability for implementation within a nonlinear finite element framework. Complex macroscopic response can be obtained by averaging over a discretized finite element containing a relatively accurate representation of the morphology of the microstructure and whose constituents are modeled by simple phenomenological constitutive theories, with possible added nonlinear phase interaction laws. Multi-scale approaches are usually implemented as follows:

1. Determination of the material parameters of an assumed canonical macroscopic constitutive model by fitting the homogenized response produced by finite element solutions of a single REV under defined boundary conditions [Terada *et al.*, 2008; Speirs *et al.*, 2008].

2. Development of new macroscopic constitutive laws capable of capturing the homogenized response of a discretized finite element REV [Pellegrino *et al.*, 1999; Michel *et al.*, 1999; Giusti *et al.*, 2009].
3. Fully coupled two-scale finite element analyses where the macroscopic equilibrium problem is solved simultaneously with one REV equilibrium problem for each Gauss quadrature point of the macroscopic mesh. The constitutive law at each Gauss point is defined by the homogenized response of the corresponding discretized REV [Miehe *et al.*, 1999; Terada and Kikuchi, 2001; Matsui *et al.*, 2004; Kouznetsova *et al.*, 2004].

The main advantage of the multi-scale approach lies in the (relatively) low computing times required to compute the solution of macroscopic boundary value problems involving only conventional (macroscopic) constitutive models compared to those of similar simulations based on the fully coupled (local) approach. Hence, preference should be given to macroscopic multi-scale models whenever it is possible to describe the homogenized behavior of the microstructure by means of an existing macroscopic model with acceptable accuracy. There exist however some drawbacks with this approach:

1. The set of macroscopic parameters that minimize information loss may not be unique and the selection procedure needs to be sufficiently robust.
2. The behavior of the constituents of the REV needs to be known and appropriate models need to be selected together with their corresponding material parameters. This can often be a problem as, in many realistic situations, it is not possible or practical to test the behavior of the individual constituents of a composite material.

2.4.2 FEM Macro Elements

The finite element method (FEM) is widely known for its flexibility in analyzing arbitrarily shaped domain geometries and inhomogeneous materials. However, it requires long computational time, especially in multiscale problems. One of the approaches proposed to overcome this inconvenience was the use of macro-elements. For FEM problems where local fine grids are necessary, it is suggested to use special macro-elements. Each macro-element captures the mechanical behavior of its entire region and has the form of a generalized rigidity matrix. It describes the relationship between stress and strain fields on the boundary of the macro-element. The macro-elements are represented by a reduced order model, described by a significantly smaller number of unknowns (equal to the number of boundary nodes), thus improving overall simulation speed, Figure 2.12.

A macro-element, in the framework of the finite element method, is used to describe a finite element suitable for modeling a domain with minimum discretization [Parsons *et al.*, 1985].

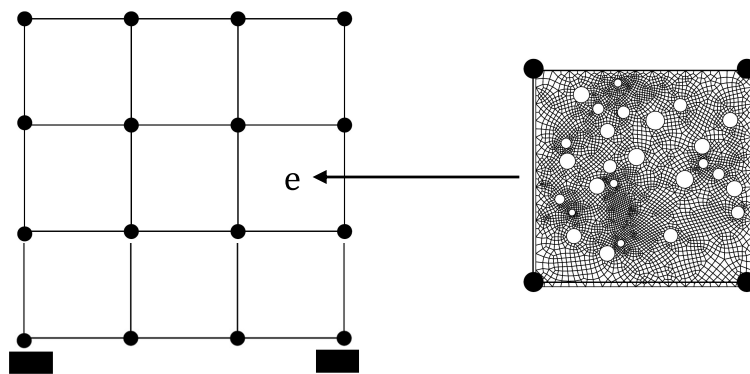


FIGURE 2.12: Macro-element in the macroscopic structure representing a mesoscale window containing the microstructure information [Markovic and Ibrahimbegovic, 2004]

The subdomains of very fine mesh are separated from the global domain as so called macro-elements that undergo model reduction. The macro-elements of reduced order are described by a significantly smaller number of unknowns, thus improving overall simulation speed.

The macro element encompasses internal nodes and sub-elements; they constitute the prerequisite for the determination of the residual vector and the tangent stiffness matrix. The element response (the state of stress and strain) will be projected onto the external nodes, and related to the rest of the domain via these nodes only, hence the “Model Order Reduction”. In order to evaluate the stresses, the averaged deformation gradient has to be determined. The averaged deformation gradient makes use of the averaged gradient of the shape functions in the initial configuration of each sub-element. One way to determine the average gradient is via standard numerical integration on Gauss points in each sub-element. Alternatively, the evaluation of the integral for the averaged deformation gradient can be performed analytically using the kinematics of an enhanced strain element [Hill, 1963; Bornert *et al.*, 2001].

Since the proposed technique is intended for the simulation of multiscale FEM problems, one of the main issues is to connect the nodes from the two regions: coarse and refined. One way is to expand the stress/strain fields on the boundary of the macro-element using polynomials in order to provide transition between meshes of different density.

If the computational domain contains many identical small areas, then the same fine mesh and corresponding FEM matrices can be used for each subdomain. This requires an equal number of nodes on each macro-element border, which can be forced during mesh generation. Therefore, only one reduction is required for all of the macro-elements. This process is called macro-element cloning and provides considerable saving of simulation time and memory.

2.5 Conclusion

There exist nowadays many techniques to model the cracking in reinforced concrete. From the micro (dents, notches: direct link), to local (bond), to the macroscopic scale (homogenized reinforced concrete structural elements), different models are used in order to extract information on the scale on which they were designed to operate on. For large structures, a handful of approaches are considered, usually consisting of a macroscopic approach of some sort or a multi-scale modeling. But the calculations remain relatively expensive in terms of time and memory whenever we want access to local information like crack opening, crack spacing, number of cracks, etc. . . It seems that there is no escape from going through some sort of local scale calculation that enables the extraction of the information on that scale. We recently began noticing the emergence of studies aimed at answering that very problematic [Combescuré *et al.*, 2013; Huguet *et al.*, 2014; Andriotis *et al.*, 2015; Sun *et al.*, 2015]. Nonetheless, no macro model or multi-scale approach has yet been decently successful at reducing the calculation costs compared to the information loss endured by forsaking the local-scale computation.

In the next section we will introduce a new multi-scale modeling strategy based “learning” by means of intelligent numerical experimentation. Following the strategy, we create probabilistic macroscopic models that implicitly integrates the rebar, the concrete, and the steel-concrete bond, and yields accurate predictions about the cracking process in the reinforced concrete structure.

Some local models aforementioned will play a crucial role in the unfolding of the multi-scale strategy, notably the *probabilistic explicit cracking model* and the *semi-explicit cracking model* for concrete, Sections 2.1.2.1 and 2.1.2.2, and the steel-concrete interface model, Section 2.3.1.1.

Chapter 3

Numerical Strategy for Developing a Probabilistic Model for Reinforced Concrete Structures

3.1 Objectives and Philosophy

The problem we are facing is the modeling of the cracking processes in large reinforced concrete structures. In order to compute the solution to such a problem with reasonable calculation time, we clearly cannot use a local approach by explicitly modeling the steel bars in the large structure. We will instead turn to a multi-scale strategy that will allow us, using intelligently designed numerical experimentation, to implicitly incorporate the reinforced concrete into macro-elements that faithfully predict the behavior on the macroscopic scale, while retaining most information on the local scale, without the need for explicit representation of local aspects of the structure. Simply stated, the objective is to solve a problem on the macroscopic scale, that depends on interactions and behaviors on the local scale.

The idea is to replace a complex reinforced concrete “block” in the given structure with a macro-element of the same size and dimensions. A macro-model paired with this macro-element will be “trained” to predict the behavior of such an element at time $t + 1$, as well as the transfer of stresses to adjacent elements, given the stress/strain field at time t . This is possible since we are in the framework of the finite element method.

Therefore, in order to use the multi-scale strategy in the modeling of reinforced concrete structures, one has to perform the following steps:

1. Define the different groups of macro-elements stemming from an optimal partitioning of the structure.
2. Design a numerical experiment for each family of macro-elements. These tests will provide information about the cracking process of the reinforced concrete element.
3. Run selected numerical experiments using a validated local approach with local models to describe the concrete, the steel and the steel/concrete interface. As a result, information about the global behavior and the cracking process of the reinforced concrete element will be available for further analysis.
4. Use a supervised learning method to draw information about the cracking process of the reinforced concrete elements on the data gathered from the numerical experimentation phase. This would help customize a macro-model for each type of macro-element in the structure.
5. Run the structural simulation using the macroscopic discretization that yields the macro-elements using the corresponding macro-models.

Our reasoning is such that by scaling up to a macroscopic level type of calculation, a substantial gain in time/memory cost is achieved, but in doing so, a loss in accuracy and access to some information specially on the local scale is inevitable. We hope that by using statistical learning we would be able to infer/recover information about the cracking process (fracture opening, profile, etc.) otherwise inaccessible without performing a full scale calculation.

3.2 Reinforced Concrete Macro Element

The first thing to realize is that almost any reinforced concrete volume can be partitioned into one or many groups of identical sub-blocks or “elements” of reinforced concrete, Figure 3.1.

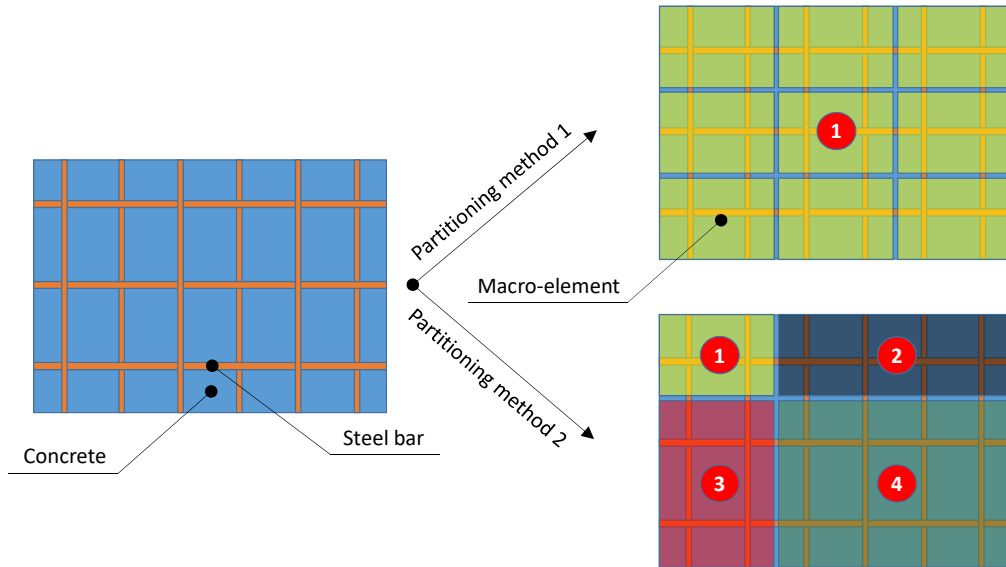


FIGURE 3.1: Different ways for partitioning a reinforced concrete block into macro-elements

In statistical terms this is called “sampling”, or grouping items with respect to certain attributes. Here we sample elements of reinforced concrete from within a structure with respect to their dimensions and constitution (concrete used and rebars type, number and orientation).

There are 3 limitations to keep in mind while choosing a method of partitioning: *element size*, *element complexity* and *element regularity*.

Element size is a measure of how fine or coarse the partitioning is. A very fine partition is no different than an explicit representation of the local scale. So we might be tempted to go for a really coarse partition, but there actually exists an upper limit to how big the elements can get, and that is because an elastic simulation of the structure using the finite element partition/mesh would still have to yield the correct kinematic field.

Element complexity is a measure of the number of model parameters needed in order to fully describe an element. For instance, a steel bar, and its interface with surrounding concrete, introduces additional non-linearities in the element in the direction parallel to it. So the behavior of a reinforced concrete element is more difficult to represent than that of a plain concrete element, hence it is of higher complexity, Figure 3.2.

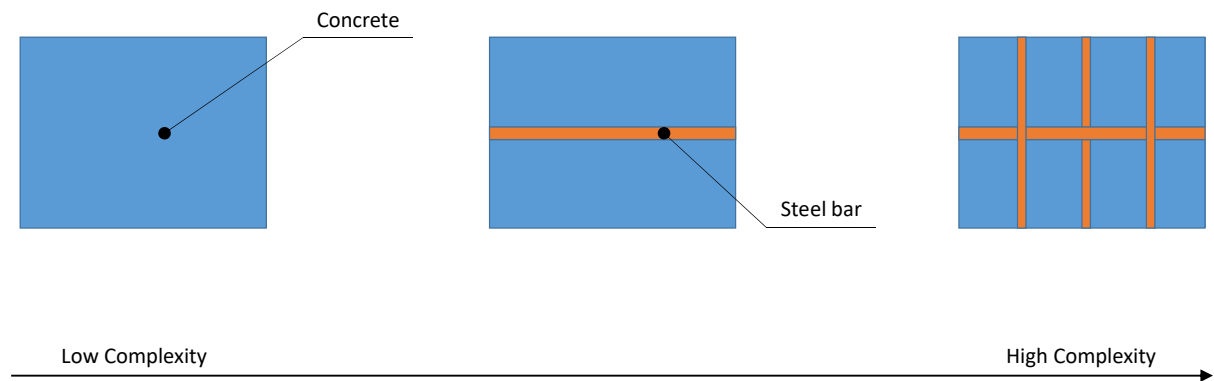


FIGURE 3.2: Macro-element complexity with respect to its constitution

Element regularity is a measure of the number of groups of distinct elements resulting from the partition. Macro-elements in a symmetrical structure will be highly regular, which in turn means less behaviors to describe.

With fine partitioning, we are more likely to end up with fewer distinct groups of low complexity elements, but a high number of total elements. On the other hand, a sampling of low complexity elements will result in a higher density of elements, as well as more distinct groups. And if we go for element uniformity we will be grounded with high complexity elements.

Evidently, to save on calculation time, the optimal combination would be a mesh of relatively large, simple and identical elements. But such a partitioning is rarely, if ever, possible. So it is a problem of compromise between the 3 factors. Additionally, it is not clear beforehand which of these factors will have the most influence on calculation time, so we need a sensible approach to help us choose the best partitioning possible.

3.2.1 “Best” Partitioning

A safe approach to follow would be to start by figuring out the largest dimensions that an element can take in a certain structure. An elastic simulation of the given structure is performed, taking into account the boundary conditions of the problem. 2D or 3D (as required) “volume elements” are used without describing any reinforcements. This step will determine the coarsest finite element mesh of the structure that would still yield the correct kinematic field. This will set an upper limit on the size of the macro element.

Once we have a range of possible element sizes, all that is left is to find a compromise between complexity and uniformity. But unfortunately there is no simple answer to that question.

As we will see later as the strategy unfolds, is that for every element “type” (or group), we will conceive and run test simulations using the local models. This is how we will describe how it will behave in the structure. These simulations make up most of the incompressible time in the unfolding of the strategy, and both element complexity and element uniformity affect this cost. With more complexity, the cost in time of individual tests will rise. But if we favor simple element design we will end up with more groups, and more behaviors to describe, which means more test simulations to run.

Likewise, the macro model for a complex element will most likely carry more parameters that will need identification. This should also figure in the time cost balance. The full factorial experiments for parameters identification are of $\mathcal{O}(2^n)$ time complexity, where n is the number of parameters in a single macro-model. Hence, when it comes to the time cost of parameter identification, we should favor a less complex design, even if it means more macro-models to describe.

3.3 Supervised Learning

In the field of machine learning, supervised learning is a task for inferring a function from a set of training data. The training data is usually a set of N measurements $\{(x_1, y_1), \dots, (x_i, y_i), \dots, (x_N, y_N)\}$, from which we construct prediction rules for the function. The (x_i, y_i) pair consists of an input x_i (classically the *independent variables*) of the i^{th} example and its measured output y_i (classically the *dependent variables*). Outputs can vary in nature: *qualitative* or *quantitative*. And so follows the type of algorithm used: *classification* or *regression*.

We will only be looking at regression supervised learning since our output data is always of quantitative, continuous nature.

Let $X \in \mathfrak{R}^p$ denote a real value input vector of size p , and $Y \in \mathfrak{R}$ a real value output variable, with joint distribution $Pr(X, Y)$. The objective here is to define a function $f(X)$ for predicting Y given X . We define a *loss function* $L(Y, f(X))$ for penalizing errors in prediction. A common loss function is the *squared error loss*:

$$L(Y, f(X)) = (Y - f(X))^2 \tag{3.1}$$

A criterion for choosing f would be the expected prediction error, $EPE(f)$:

$$EPE(f) = E(Y - f(X))^2 \tag{3.2}$$

$$= \int [y - f(x)]^2 Pr(dx, dy) \tag{3.3}$$

And by conditioning on X , we get

$$EPE(f) = E_X E_{Y|X}([Y - f(X)]^2 | X) \tag{3.4}$$

and that is all that we need in order to minimize EPE for every $X = x$:

$$f(x) = \operatorname{argmin}_c E_{Y|X}((Y - c)^2 | X = x) \tag{3.5}$$

The solution to this is

$$f(x) = E(Y | X = x) \tag{3.6}$$

the conditional expectation, also known as the *regression function*. So this is telling us that, when measured by the average squared error, the best predictor of Y at point $X = x$ is the conditional mean.

Now we assume that the regression function $f(x)$ is approximately linear in its arguments:

$$f(x) \approx x^T \beta \tag{3.7}$$

Plugging this into (3.2) and differentiating, we can solve for β :

$$\beta = [E(XX^T)]^{-1}E(XY) \quad (3.8)$$

Note that the famous least squares solution of the linear regression problem (which we will not be developing here) amounts to replacing the expectation in (3.8) by averages over the training data.

Although we will not be using the rigid linear model, nor the squared error loss (the L_2 loss function), the principal idea for developing a model in the frame of supervised learning remains similar to what we have just seen. As we will see later in Section 3.3.2, we will use a clever loss function, well tailored for our needs, to capture not only the conditional mean of an output, but also the variance.

3.3.1 Choice of Training Data

To solve a given problem of supervised learning the first thing to do is to determine the type of training examples. Before doing anything else, we should decide what kind of data is to be used as a training set. In the case of spam email for example, all we need is a bunch of emails that are classed respectively as spam and non-spam. In the case of reinforced concrete structures however, the problem is a bit more complicated.

The difficulty lies in describing the behavior of reinforced concrete in the direction of the reinforcement. More specifically, the tensile strength and the residual stiffness after cracking and before the yielding of the steel. In other words, the cracking process in the direction of the steel bars.

Knowing that cracking is almost always caused by tension stresses, a strong assumption is therefore made, which states that the macro element behaves only in tension in the considered direction(s) of reinforcement(s). Furthermore, it would be conceptually difficult for a plain macro element to host multiple cracks. Thus we made the assumption that only one macro-crack (which can actually represent one macroscopic crack in the element or multiple microscopic ones) can appear in each macro element, and it is oriented perpendicularly to the reinforcements in the direction in which it was detected. With this strong assumption we can manage to easily identify a broken element in the structure, as well as gather information about crack opening on the element level. Additionally, by linking broken macro-elements we can restore the path of a fracture on the structural level.

As a consequence, a suitable test to simulate the cracking process in a certain macro element would be a tie-beam under tension. The tie-beam consists of a succession of the reinforced

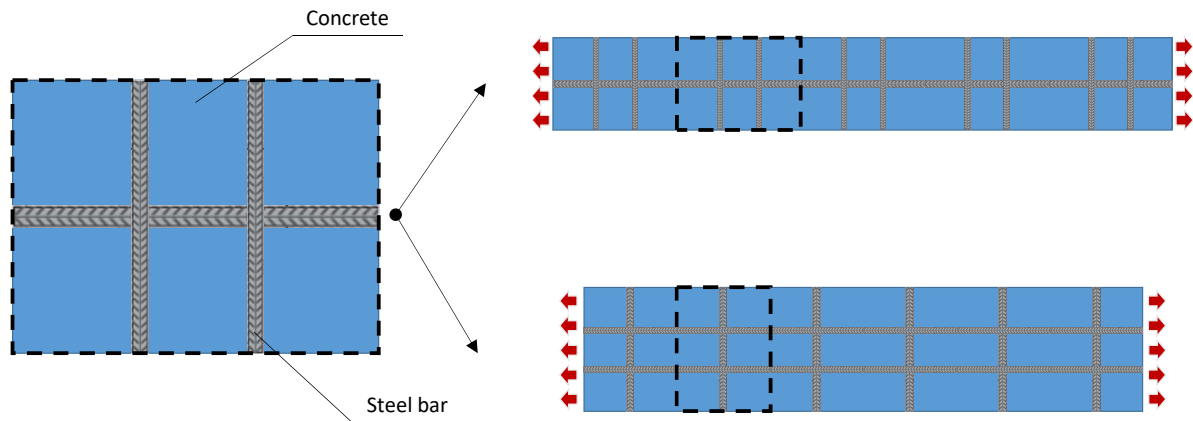


FIGURE 3.3: Design of a tie-beam test for each direction parallel to the steel bars in case the macro element represents multi-directional reinforcements

concrete elements that are represented by the macro-element. It should be long enough to get a representative cracking pattern for such an element, Figure 3.3.

Numerical simulations on the tie-beams are run to get information about cracking and global responses. To that end, we use validated local models: a probabilistic explicit cracking model for concrete and an interface element model for the steel-concrete bond.

3.3.2 Choice of Learning Algorithm

We have gathered a training set that is representative of the real-world use of the function. Now we need to determine the input feature representation of the learned function. What that means is that we need to choose what features of the training data to learn from.

The tie-beam tests yield information about the global behavior, but also the cracking pattern, number, opening and spacing of micro and macro fractures in the beam. The micro fracture information is useless because the macro-element is limited to one macro-crack. Likewise, the macro cracking pattern would be a complicated feature to implement in a learned function. The best we can do is learn the global behavior of the tie-beam, by fitting a model for the macro-elements. If a certain macro-model yields the correct global behavior then we know we are on the right track, and we can check for similarities in the macro-cracking pattern.

The peculiarities of the problem make it so that simple parametric¹ models are well suited for the purpose of analyzing our data and inferring the predictive function. Therefore a simple piece-wise linear model with model parameters $\{b_1, \dots, b_k\}$ can act as a macro-model for the

¹During training, the parametric model “absorbs” the information from the training data into the parameters; afterwards, the data can be discarded.

macro-element. And a macro tie-beam test should be able to perform well on the training set given the correct model parameters, Figure 3.4.

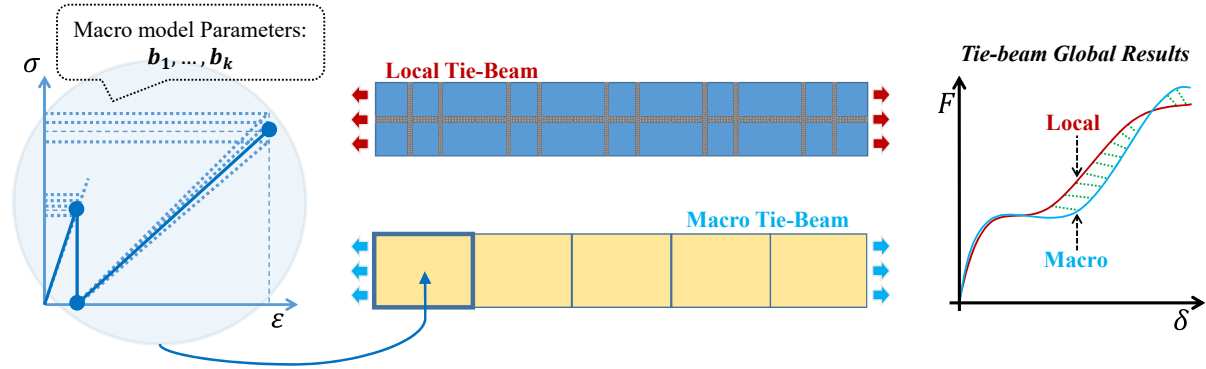


FIGURE 3.4: Local/macro tie-beam numerical tests global results comparison given a set of macro-model parameters

Finally, the cracking process of reinforced concrete is a probabilistic phenomenon due to the heterogeneity of the material. Therefore, the model unknowns $\{b_1, \dots, b_i, \dots, b_k\}$ will each have a parametric model θ_i that needs to be identified. For some model parameter $Z := [b_1; \dots; b_k]$, and its probability distribution function g ,

$$Z \sim g_\theta(z) \quad (3.9)$$

where θ is the parametric model for Z . As an example, let g be the *log-normal distribution*, then

$$\theta = (\mu, \sigma^2) \quad (3.10)$$

and

$$g_\theta(z) = \frac{1}{z\sigma\sqrt{2\pi}} \exp\left(-\frac{(\ln z - \mu)^2}{2\sigma^2}\right) \quad (3.11)$$

With this simple model-based² approach, we are certain to get the correct global behavior of the tie-beam, and if our hypothesis is correct, this should be enough to closely predict the macro-cracking behavior of the same element in a real structure, as we will see in the validation section, Chapter 4.

3.3.2.1 Probabilistic Macro Model for Reinforced Concrete Elements

A model-based macro model is introduced that will act on the specific finite elements representing reinforced concrete volumes in a given structure. The model main objective is to provide information on macrocracks and the cracking process: openings, distribution...

²We specify a model for the regression function.

The idea behind the model is simple and builds on three main hypothesis:

- The model variables are defined according to a learned probability distribution function.
- A macro model and its parameters are unique in a sense that they are associated to a specific type of macro element.
- Only one macro crack can be accounted for in the macro element which will be represented implicitly.

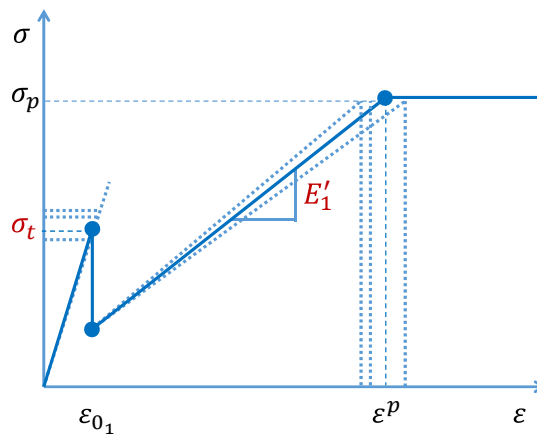


FIGURE 3.5: Reinforced concrete macro model

The physical phenomena represented in the macro model, Figure 3.5, are:

- The brittle failure of the concrete matrix when the tensile strength σ_t of the element is reached.
- Steel intervention: stiffness recovery by the reinforcements and the phenomenon of tension stiffening, represented by E'_1 .
- Plastic behavior of the rebars and the whole element when the ultimate tensile strength of the steel σ_p is reached.

3.3.2.2 Maximum Likelihood Approach for Parameters Identification

A suitable analytical representation of the problem of identifying the parametric model is the maximum likelihood approach.

Given data, the likelihood function (simply likelihood) is a function of the parameters of a statistical model.

Let Z be a set of N parameters:

$$Z_i \sim g_\theta(z_i) \tag{3.12}$$

Where g_θ is the model for Z (in our case g is the log-normal distribution function), and θ is the parametric model of Z (θ is the unknown in our problem). We can then write the likelihood function as follows:

$$L(\theta; Z) = \prod_{i=1}^N g_\theta(z_i) \tag{3.13}$$

This is true as long as the parameters are independent. Unfortunately, in our case the parameters are very dependent of one another, therefore this should be replaced by the joint probability of all the variables. If all parameters are normally distributed, the likelihood function becomes:

$$L(\theta; Z) = \frac{1}{(2\pi)^{N/2} \sqrt{\det(\text{Cov}(z_1, \dots, z_N))}} \exp \left(-\frac{1}{2} \begin{bmatrix} z_1 - \nu_1 \\ \vdots \\ z_N - \nu_N \end{bmatrix} \text{Cov}^{-1} \begin{bmatrix} z_1 - \nu_1 \\ \vdots \\ z_N - \nu_N \end{bmatrix}^T \right) \tag{3.14}$$

So in a sense, the likelihood function is the probability of getting the observed data under the model g_θ . More specifically, it's the probability that the testing data and the training data are alike.

Therefore, in order to determine θ all we need to do is to maximize the likelihood. In practice, the algebra is often more convenient when working with the logarithm of the likelihood function, the log-likelihood (for independent variables):

$$l(\theta; Z) = \sum_{i=1}^N l(\theta; z_i) \tag{3.15}$$

Where $l(\theta; z_i) = \log g_\theta(z_i)$ is a log-likelihood component. To solve this, we define the score function:

$$\dot{l}(\theta; Z) = \sum_{i=1}^N \dot{l}(\theta; z_i) \tag{3.16}$$

Where

$$\dot{l}(\theta; z_i) = \frac{\partial l(\theta; z_i)}{\partial \theta} \tag{3.17}$$

Finally we solve for $\hat{\theta}$:

$$\dot{l}(\hat{\theta}; Z) = 0 \tag{3.18}$$

Next we will present a simple and efficient numerical method to identify the model parameters.

3.4 Optimization Scheme

Given the state of the problem, there exists no analytical solution capable of finding the correct set of parameters for the macro-element model. So we will use a numerical strategy to fit the macro-model parameters to get an accurate macro tie-beam global response.

A standard form for the optimization problem is the minimization of a real valued function f , also called the *objective function*. This is a parallel to the notion of a *loss function* introduced in Section 3.3.

3.4.1 Choosing the Objective Function

Common loss functions like $L_1 = E|Y - f(X)|$ or $L_2 = E(Y - f(X))^2$ could work up to a certain point. We know that the predicted solution for the L_2 loss function is the conditional mean. And that of the L_1 function is the median. So we can choose between two different measures of location. Nonetheless, neither can give us information about variance.

To do that, we have to find a special function that will allow us to find the set of model parameters that not only reproduce the expected output, but capture its variability as well.

The idea is not to minimize the error point-wise, but on the whole scale, by minimizing the surface between the two tie-beams load-displacement curves. Furthermore, since we are using probabilistic modeling to allow for a statistical analysis of the structural behavior, we are gonna have multiple local and macro tie-beam load-displacement curves.

Let N be the total number of local tie-beam numerical experiments that represent the real-world behavior of that tie-beam. Consequently, we will run N macro tie-beam simulations with starting model parameters. For each pair of local/macro curves, we compute the area of the complex, self-intersecting polygon outlined by the two curves.

Let the curves from the local tie-beam tests be denoted as $[l_1, \dots, l_n]$, and those from the macro tie-beam tests as $[m_1, \dots, m_n]$. Let the area outlined by two curves be noted as $A_{ij}(l_i, m_j)$. Therefore, the total number of combinations of different areas to compute is N^2 . In order to capture the true mean and variance we apply a sorting algorithm that would check, at each iteration, for the absolute minimum value of A_{ij} , store it, and remove l_i and m_j from the set of curves and start again, Figure 3.6. Until we end up with a vector of size N of increasing area values. The mean value of the elements in this vector constitutes the objective function, while also conditioning on a low CV^3 (standard deviation / mean) ratio.

³We chose $CV \leq 1$. This fair assumption means we only have to minimize the mean and verify that the standard deviation is acceptable.

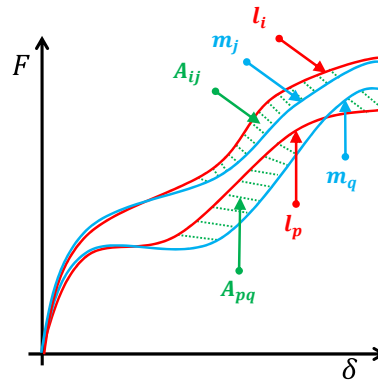


FIGURE 3.6: Pairing of micro and local curves with respect to minimum area outlined by the two load-displacement curves

The outline of two such curves actually forms a complex, highly irregular, self-intersecting polygon. In order to compute its surface area we used the Bentley-Ottmann algorithm. because each curve is nothing more than a set of line segments, we apply a sweep line approach, in which a vertical line moves from left to right across the plane, intersecting with the input line segments in a sequence as it moves. All intersections between the two curves are noted and a node (vertex) is added. In the end we will have a set of ordered polygons which areas are easily computed, Figure 3.7.

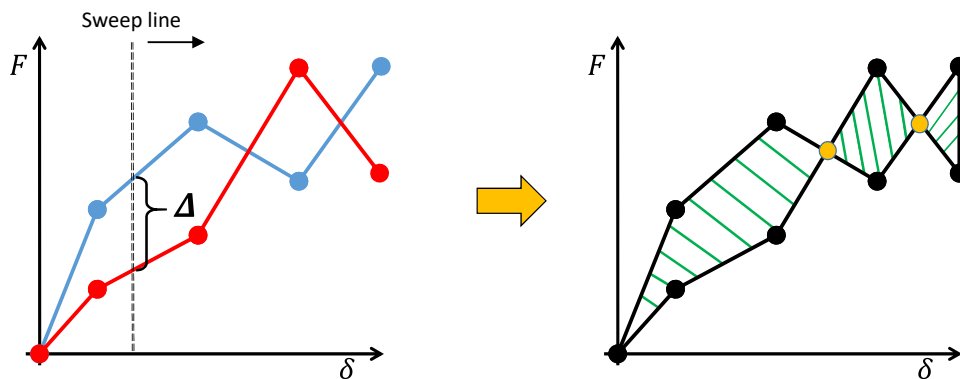


FIGURE 3.7: Line sweep algorithm trying to find the intersections between two sets of line segments

3.4.2 Response Surface Methodology

Now what is left is to fit the model parameters by minimizing the objective function presented in Section 3.4.1. The optimization tool most suited for this problem is the *Response Surface Methodology* or RSM. RSM is a way to explore the effect of operating conditions (the factors/-parameters) on the response variable. Here the response variable is non other than the objective function f . As we map out the unknown response surface of f , we move the process as close as possible towards an optimum, taking into account any constraints of the problem. In this case, a constraint that we might want to impose on the process is the minimum/maximum number of macro-cracks in the macro tie-beam at any time.

For an in-depth look on how to implement the response surface methodology for a problem case similar to ours, please refer to the example presented in Section 3.4.2.1.

The parameters yielded by the RSM will be implemented in the corresponding macro-model to be used for the macroscopic structural calculation.

3.4.2.1 Design and Analysis of a Four-Factor Experiment

Suppose for example that the model contains 2 unknown random variables each described by a log-normal probability density function. In the real setting, the first variable might be the tensile strength of the reinforced concrete element in the direction of reinforcements, and the second variable would be the post-cracking residual stiffness.

Then the parametric model $\theta_i = (\mu_i, \sigma_i^2)$, for $i \in [1, 2]$ of each variable is what constitute the model's actual parameters

What RSM does, is it takes 2 extreme values for each parameter, and a middle value. We scale the values for each parameter to a $[-1, 0, 1]$ segment. Thus creating a hypercube in the 4 dimensional euclidean space. We then compute the value of the objective function f at each vertex and at the center. This is a full factorial experiment of the order 2^n where n is the number of parameters (4 in this scenario). We can now fit a linear model through our data to predict how a change in the parameters would affect the objective function. The linear model is a polynomial function of $(\mu_1, \sigma_1, \mu_2, \sigma_2)$ of the form

$$\hat{y} = b_0 + b_1\mu_1 + b_2\sigma_1 + b_3\mu_2 + b_4\sigma_2 + b_5\mu_1\sigma_1 + \dots + b_{16}\mu_1\sigma_1\mu_2\sigma_2 \quad (3.19)$$

where \hat{y} is a prediction of the real value of f for any values of the input parameters. Although it becomes less reliable the further we get from the initial input parameters. It is in the end but an approximation of a complex function by a linear model. Nonetheless, this model will prove itself useful when we're looking to minimize f . All we need to do is to evolve the parameters

in the direction of steepest ascent, that which reduces \hat{y} , and then repeat. This “direction” is a 4 dimensional vector that can be computed from the coefficients of the linear model by taking partial derivatives of the model function (we could choose to ignore terms with small coefficients like most interaction terms). Let V_m be the minimization vector, then:

$$V_m = \begin{pmatrix} \frac{\partial \hat{y}}{\partial \mu_1} \\ \frac{\partial \hat{y}}{\partial \sigma_1} \\ \frac{\partial \hat{y}}{\partial \mu_2} \\ \frac{\partial \hat{y}}{\partial \sigma_2} \end{pmatrix} \tag{3.20}$$

One way to visualize the effect of factors on the response variable is with a Pareto plot.

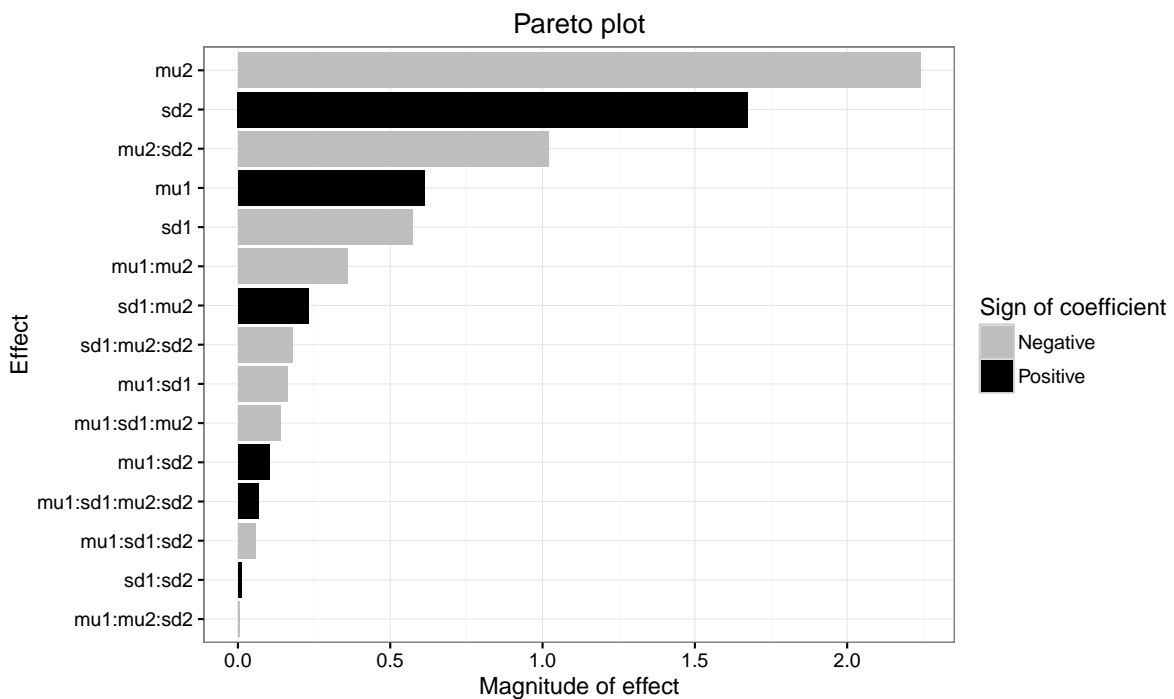


FIGURE 3.8: Pareto plot

Figure 3.8 is an example of a Pareto plot of a 4 variables linear model. We can see that in order to minimize \hat{y} and therefore f , we should mainly increase μ_2 , and next in order, decrease σ_2 and μ_1 and increase σ_1 .

Multiple iterations might be necessary before we accept the value of f . At the end of this step, the parameters that minimize f are the ones we input into the model for the final calculations.

Figure 3.9 is a visual representation of the RSM iterations in the case of a two-factor full factorial experiment.

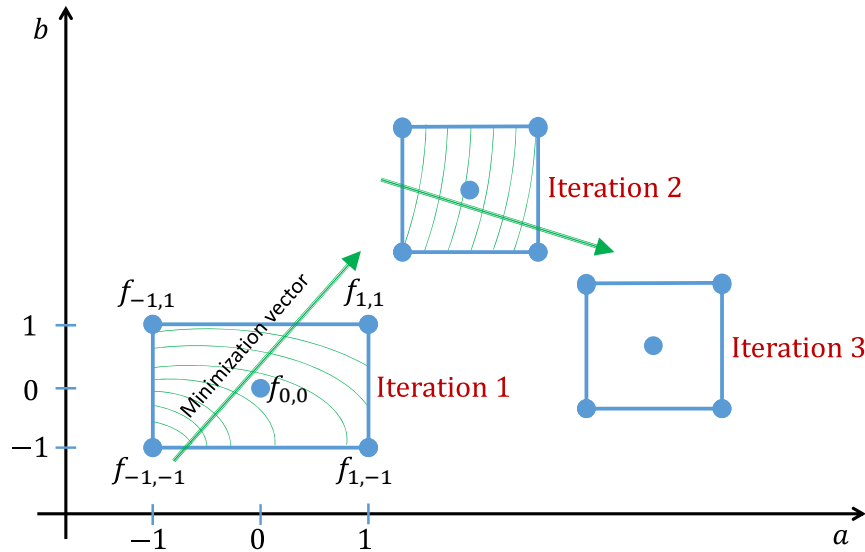


FIGURE 3.9: Visualization of RSM for a model with 2 parameters a and b

3.5 Implementation

To implement the *Multi-Scale Modeling Strategy*, one can proceed as follows:

1. Start by defining a mesh suitable for a local-scale calculation of the structure at hand (explicitly modeling the steel bar and the steel/concrete interface). This will help define the optimal macroscopic mesh of the structure.
2. Partition the structure, thus defining a set of macro-elements of reinforced concrete characterized by their dimensions and the layout of steel bars contained in it. This step carries on a big impact on the total calculation costs of the methodology. Therefore, many aspects have to be taken into account while considering a certain partitioning method. A sensible procedure was developed in order to assure an optimal running time, Section 3.2.
3. Numerical experimentation phase: for each type of macro-element, and in every direction of reinforcements, define a characteristic tie-beam numerical test, Section 3.3.1. Numerical simulations on the tie-beams are run to get information about cracking and global responses. To that end, we use validated local models: a probabilistic explicit cracking model for concrete and an interface element model for steel-concrete bond.
4. Results from the tie-beam simulations (along with some working knowledge) will help us infer, by inverse analysis, the cracking behavior of the different macro elements in the structure, Section 3.4.

5. Run the final calculations on the macroscopic discretization of the structure using the corresponding macro-models.

In the next chapter we will discuss 2 validation examples of the strategy and show how to apply different approaches to different structural problems. We will be putting the strategy through scrutinizing evaluation to test the rigor of its outcome.

Chapter 4

Validation

4.1 Reinforced Slab-Beam (2D)

As a first validation example we chose an interesting structural problem from a study that was conducted in part at our laboratory. Three slab-beam test designs part of an experimental campaign meant to study the effect of different types of steel bars (12 mm high adherence round bars, flat bars of the same section area) on the loading capacity and the cracking profile of reinforced concrete. Subsequently, a numerical study was conducted on the same slab-beams as a validation of the *probabilistic explicit cracking model for concrete* and the *steel-concrete bond model* [Phan, 2012; Phan *et al.*, 2013a, 2015].

We have at our disposal the necessary data in order to validate our approach , as well as the numerical tools needed for the numerical experimentation phase of our strategy (the parameters for the local models used).

In this section we will go through a full implementation of the multi-scale strategy, summarized in 3.5, and we will compare the accuracy of our results and calculation costs with that of existing numerical simulations.

4.1.1 Dimensions and Loading Conditions

The structural element concerned is a reinforced slab-beam submitted to three-point bending: 3.3 m long (3 m between supports), 0.8 m wide, and 0.16 m thick (an element must have a thickness $\leq 1/5$ of its width to be considered a slab), Figure 4.1. Experimental tests of the slab-beam were carried out in the laboratory of Civil Engineering at Polytech Clermont-Ferrand [MATIERE®, 2011].

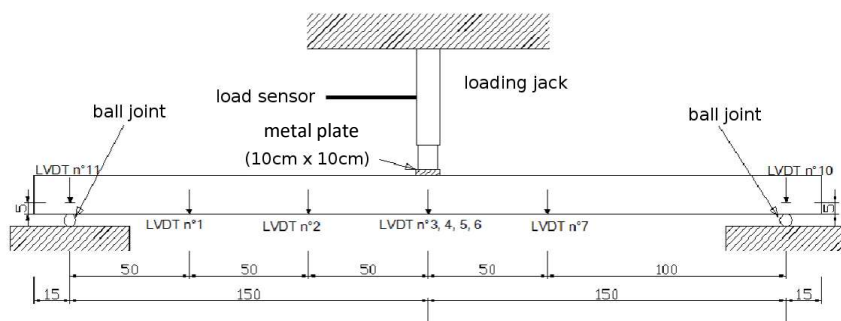


FIGURE 4.1: Slab-beam dimensions and loading conditions

We will only be looking at the case of the slab-beam reinforced with high adherence round rebars, 12 mm in diameter. Detailed layout of the reinforcements in the slab-beam can be found in Figures 4.2 and 4.3.

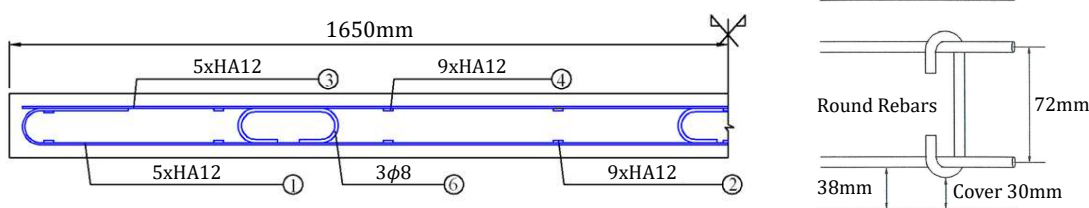


FIGURE 4.2: Longitudinal section, reinforcement plan for reinforced slab beams

4.1.1.1 Materials Characteristics

- **Concrete**

The composition used in these tests is detailed in Table 4.1. Conventional tests for mechanical characterization (compression, splitting) yield the following average values:

- Average compression strength: $f_c = 55$ MPa
- Average tensile strength: $f_t = 3.7$ MPa
- Young modulus: $E_c = 35\,000$ MPa

- **Steel**

Below are the mechanical characteristics of the steel used:

- Round HA Φ 12: $R_e = 640$ MPa, $R_u = 720$ MPa, $E_s = 200\,000$ MPa

It is worth noting that the proposed slab-beam is not the best suited candidate to validate the macroscopic model: its thickness and the type of loading prompt the creation of numerous,

Components	Weight in kg
Sand 0/4	743
Gravel 4/10	340
Gravel 10/16	752
Cement CEMI 52.5 PMES	400
Superplasticizer	2.6
Water	165
Total	2402.6

TABLE 4.1: Composition of concrete used (per m^3), reinforced slab-beam case study

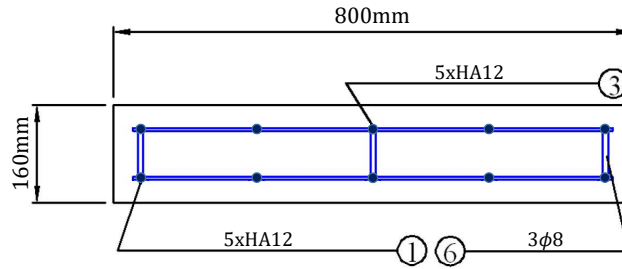


FIGURE 4.3: Cross section, reinforcement plan for reinforced steel beam slabs

thinner macro-cracks; the macro model, on the other hand, favors more localized and wider ones. Nevertheless, this extreme case is interesting (specially because of all the available data) for evaluating the applications, potentials, and limitations of the proposed Multi-Scale Modeling Strategy.

4.1.2 Local and Macro Meshes

The numerical simulations will be carried out in 2D under plane stresses condition. First we need to define the appropriate mesh if we were to simulate the slab-beam using a local approach, Figure 4.4a.

The local models used for the calculations are: the *probabilistic explicit cracking model for concrete*, Section 2.1.2.1, and the *steel-concrete bond model*, Section 2.3.1.1. The behavior of round steels is modeled by a Von-Mises elastoplastic model with isotropic hardening. Concerning the steel-concrete interface, the values of the parameters were determined from parametric studies carried out on tie-beam tests. The material characteristics as well as other parameters for both local models, Table 4.2, are already available to us from the study mentioned above [Phan, 2012].

The local models were validated on experimental data from the slab-beam. Therefore, we will use these simulations as a baseline to validate our multi-scale strategy both in the accuracy of its results and calculation costs.

Model/Material	Parameters	Symbol	Values	Unit
Cracking of concrete	Compressive strength	f_c	55	MPa
	Young modulus	E_c	35000	MPa
	Aggregate diameter	D_g	0.016	m
Steel-concrete interface	Cohesion	C	25	MPa
	Critical tangent displacement	δ_t^{cri}	15	10^{-6} m
Steel bar	Young modulus	E_s	200000	MPa
	Elastic limit	R_e	640	MPa
	Ultimate limit	R_u	720	MPa
	Nonlinear hardening modulus	H_s	$\frac{1815}{\log(\sigma)+322}$	MPa

TABLE 4.2: Local models parameters, reinforced slab-beam case study

The resulting macro mesh is generated such that the steel bar, the steel-concrete interface, and the surrounding concrete is replaced with macro-elements that exhibit the behavior of reinforced concrete ($Q4$ elements). The remaining volume in the slab-beam consists of plain concrete and so it will be simulated with the probabilistic explicit cracking model (triangular elements), Figure 4.4b.

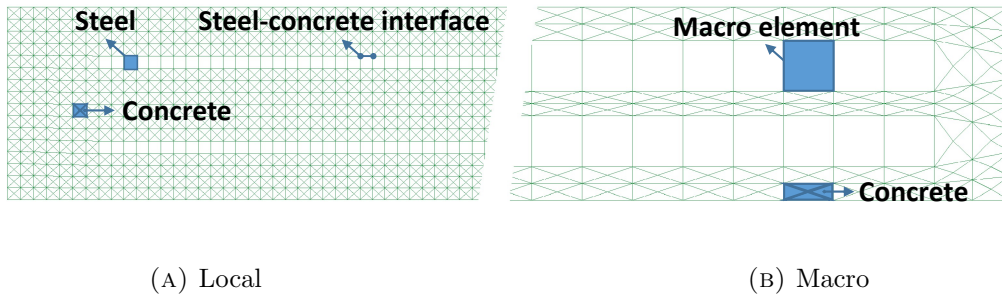


FIGURE 4.4: Slab-beam 2D meshes

Dimensions of the macro-element and what it represents in terms of reinforced concrete in the locally meshed structure are shown in Figure 4.5.

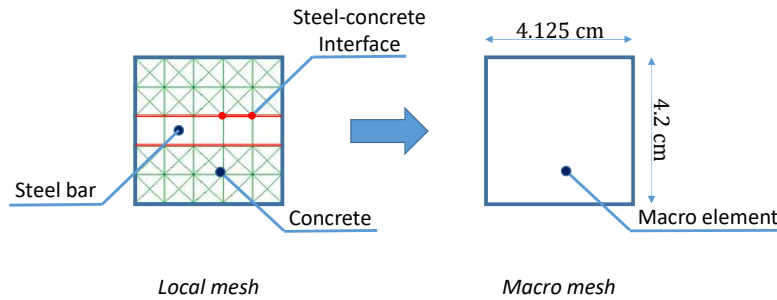


FIGURE 4.5: The chosen macro-element of reinforced concrete

For the interface model proposed, it is necessary to specify the width of the steel-concrete interface which corresponds to the depth of the element in the direction perpendicular to the modeling plane. Round steel is modeled by an equivalent square section of side equal to $a = \sqrt{\pi r^2} = r\sqrt{\pi}$. Knowing that the surface of adhesion is the product of the perimeter of the round steel ($p = 2\pi r$) and the length of aperture, the width of the interface element must be equal to half the perimeter, Figure 4.6.

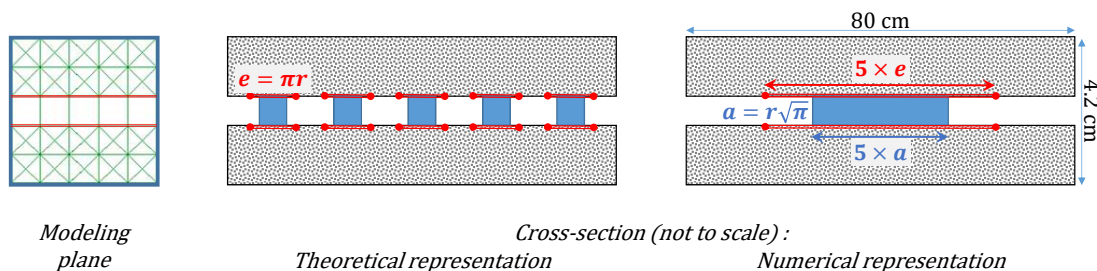


FIGURE 4.6: A cross-sectional view of what the macro element represents as a volume

4.1.3 Tie-Beam Numerical Tests

Now that we have the dimensions and composition of the macro-elements, it is easy to design the numerical tie-beam tests. As mentioned before in section 3.3, we assume that the macro-element behaves only in tension in the considered direction of reinforcements, allowing the development of only one macro-crack perpendicular to the rebars.

Following this logic, a simple tie-beam test consisting of a succession of macro-elements is sufficient to describe the cracking behavior of that element. The meshes for the local tie-beam, and its equivalent macroscopic tie-beam are shown in Figure 4.7.

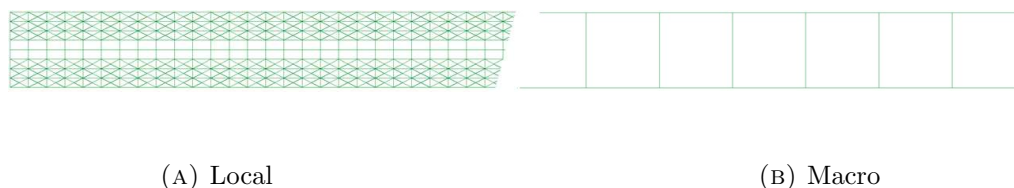


FIGURE 4.7: Tie-beam 2D mesh

In the frame of the Monte Carlo method, 10 randomly sampled results of the local tie-beam numerical tests are considered. The numerical tests are run, using the local models described in Section 2.1.2.1 and 2.3.1.1 (the explicit probabilistic cracking model for concrete, and the

steel-concrete bond model). As specified back in 3.3.1, the set of global force/displacement results from the local tie-beam numerical tensile tests will act as our training data, Figure 4.8.

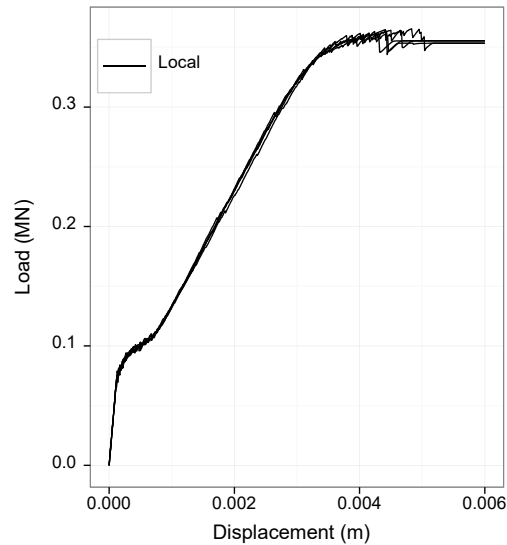


FIGURE 4.8: Numerical tie-beam: local approach, load-displacement curves

4.1.4 2D Macroscopic Model

Due to the nature of the multi-scale strategy, the macro model acting on the macro-element requires an intelligent design so it is suited, to the best degree possible, to the structure and the boundary conditions of the problem at hand.

Additionally, the model is required to have the following features:

- The ability to get information on macro-cracks spacing and openings in a large reinforced concrete structure.
- A probabilistic modeling to allow for a statistical analysis of the structural behavior via a Monte Carlo approach (reliability analysis of the structure).

In this section we will discuss the design of the macro model in the case of the reinforced concrete slab-beam structural element.

4.1.4.1 Philosophy

To achieve our objectives, and still save on calculation time, the model has to be simple. Therefore, some strong assumptions are made:

1. At the structural scale, the concrete part of the macro-element breaks in a brittle way. Therefore, we assume that the composite element have an elastic perfectly brittle behavior. Failure criteria in tension and in shear are considered (the criterion for shear is only relevant when compression stress fields are involved). These criteria are applied at the center of gravity of the macro-element.
2. Once the matrix is broken, the stresses in the element plunge to zero—a reasonable approximation at the scale of structural elements. Then, immediately after, the rebars intervene mechanically. This requires a new evaluation of the coefficients of the stiffness matrix of the macro-element in the direction parallel to the rebars. The new values of these coefficients are associated with the stiffness of the rebars and the phenomenon of tension stiffening¹.
3. The macroscopic model will account for the plastic behavior of the rebars: when the linear elastic stress limit of the steel is reached at the center of gravity of the macro-element, its behavior would be represented by an elastic-perfectly-plastic model. We chose, for simplicity, to simulate this behavior with a damage model (we disregard permanent deformations due to the yield of the rebars). This simplification is only possible if monotonically increasing loads are involved, which is the case in this example.

The validation example is treated in $2D$ plane stresses condition, the mathematical relations of the mechanical aspects of the model are developed next in that same framework.

4.1.4.2 Constitutive Law

The macro element is a volume element that represents both a given volume of concrete and steel rebars, part of the structural reinforcement. For such an element, a fixed orthogonal reference frame is locally defined with direction $\mathbf{1}$ as that of the principal reinforcement. Next, in agreement with homogenization techniques, we consider that the element consists of a smeared orthotropic material. Thus the elastic $2D$ plane stress constitutive law is:

$$\boldsymbol{\sigma} = \mathbf{H} \times \boldsymbol{\varepsilon} \quad (4.1)$$

$$\begin{bmatrix} \sigma_{11} \\ \sigma_{22} \\ 0 \\ \sigma_{12} \end{bmatrix} = \frac{1}{1 - \nu_{12} \times \nu_{21}} \begin{bmatrix} E_1 & \nu_{21}E_2 & 0 & 0 \\ \nu_{12}E_1 & E_2 & 0 & 0 \\ 0 & 0 & 0 & 0 \\ 0 & 0 & 0 & G \end{bmatrix} \times \begin{bmatrix} \varepsilon_{11} \\ \varepsilon_{22} \\ \varepsilon_{33} \\ 2\varepsilon_{12} \end{bmatrix} \quad (4.2)$$

Approximating the elastic coefficients of the orthotropic stiffness matrix \mathbf{H} :

¹Tension stiffening results from the contribution of concrete between cracks to load bearing. This leads to a larger stiffness of a cracked reinforced concrete element compared to the corresponding rebar stiffness.

- E_1 : Young modulus in the direction of the rebars; calculated as a result of the average Young modulus of both the concrete and the rebars according to the rule of mixture.
- E_2 : Young modulus of the concrete. Since we only got steel bars in direction **1** we assume that the young modulus in direction **2** can be simply approximated with that of the concrete.
- ν_{12} : Poisson ratio of the concrete.
- $\nu_{21} = \frac{E_2}{E_1}\nu_{12}$ (to ensure that \mathbf{H} is symmetric)
- G : Shear modulus; takes into consideration the presence of the steel bars in the volume of the element with respect to the rule of mixture.

The elastic behavior of this composite material is defined fairly intuitively, but the difficulty lies in the cracking mode of the element, and its behavior thereafter.

According to the preceding assumptions, failure criteria are applied in tension (Rankine) or in shear (Tresca) when the corresponding strengths are reached. As a consequence, a sudden drop of the stresses to zero is permitted. From this state of stress and strain, stresses are immediately picked up by a reduced elastic matrix representing the remaining contribution of the steel bars, plus residual friction with the surrounding cracked concrete. Some terms of the initial elastic constitutive relation (4.4) are then affected by a reduction coefficient β (that could also be viewed as the result of an initial anisotropic constant damage):

$$\boldsymbol{\sigma} = \mathbf{H}' \times \boldsymbol{\varepsilon}' \quad (4.3)$$

$$\begin{bmatrix} \sigma_{11} \\ \sigma_{22} \\ 0 \\ \sigma_{12} \end{bmatrix} = \frac{1}{1 - \nu_{12} \times \nu_{21}} \begin{bmatrix} \beta E_1 & \nu_{21} \beta E_2 & 0 & 0 \\ \nu_{12} \beta E_1 & E_2 & 0 & 0 \\ 0 & 0 & 0 & 0 \\ 0 & 0 & 0 & G \end{bmatrix} \times \begin{bmatrix} \varepsilon'_{11} \\ \varepsilon'_{22} \\ \varepsilon'_{33} \\ 2\varepsilon'_{12} \end{bmatrix} \quad (4.4)$$

With

$$\boldsymbol{\varepsilon}' = \boldsymbol{\varepsilon} - \boldsymbol{\varepsilon}_0 \quad (4.5)$$

Where $\boldsymbol{\varepsilon}_0$ is the state of strain after the sudden drop of stresses (i.e. after the brittle failure of the concrete). This behavior is held until the (predetermined) yield limit of the steel is reached. To represent the plastic behavior of the reinforcements we chose a damage model type of behavior for the simplicity of its implementation. Once the stresses in the element reach the yield limit of the steel, the behavior of the element will be represented as follows:

$$\boldsymbol{\sigma} = (1 - D) \times \mathbf{H}' \times \boldsymbol{\varepsilon}' \quad (4.6)$$

Where D is a damage variable. Similarly to the damage model for the concrete-rebar bond in Section 2.3.1.1, D is considered a state variable, thus its evolution has to verify the following conditions:

$$\begin{cases} \dot{D} \geq 0 \\ D = \max(D_0, D) \end{cases} \quad (4.7)$$

Where D_0 is the initial damage state, and D is the current damage state. The initial damage threshold D_0 is reached when the maximum axial stress (in the direction of the reinforcement) is equal to the yielding stress σ^p . The damage evolution is then given by the following relations:

$$\begin{cases} D(\tilde{\varepsilon}) = 0, & \tilde{\varepsilon} \leq \varepsilon_{01} + \frac{\sigma^p}{E'_1} \\ D(\tilde{\varepsilon}) = 1 - \frac{\sigma^p}{E'_1 \tilde{\varepsilon}}, & \tilde{\varepsilon} > \varepsilon_{01} + \frac{\sigma^p}{E'_1} \end{cases} \quad (4.8)$$

Where $\tilde{\varepsilon} = \langle \varepsilon_1 \rangle_+$ ($\langle \cdot \rangle_+$ is the positive part of (\cdot))

Figure 4.9 summarizes how the model treats pre and post cracking behavior in the direction of the reinforcements.

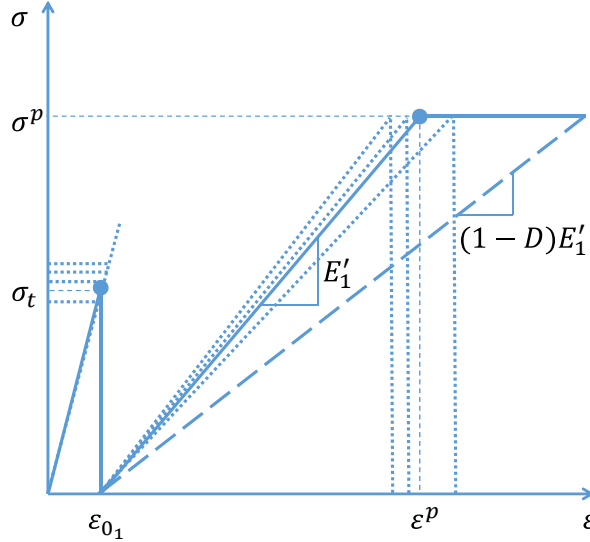


FIGURE 4.9: Probabilistic piece-wise linear model for macro elements of reinforced concrete, reinforced slab-beam case study

Finally, one might question whether or not the model we just described is too “rigid”. In fact, since the cracking process in our macro element is governed mainly by the steel bars (5 rebars in the element thickness), we affixed a structural behavior on the element (stresses in the element plunge to zero right after the tensile limit is reached). Basic statistics tells us that we might not be able to exactly fit our training data (the richer the model the better is its capacity

to fit a certain response). But this is the only way to avoid the real problem of over-fitting the data. It is possible to devise a rich macro element that would perfectly fit the results of the local tie-beam tests (the training data), but this would not guarantee the correct result on the global structure or any other structural problem for that matter. This is why we hard-coded the shape of the macro model so that it mirrors the reinforced concrete element in its specific structural setting.

4.1.5 Parameters Identification

At this stage, the model still carries two unknown parameters:

- σ_t^{cri} , the tensile strength of the uncracked element
- $E'_1 = \beta E_1$, the residual stiffness in direction **1**. It represents the stiffness of the elastic steel bars in this direction, plus friction with the cracked concrete matrix.

All the parameters concerned are continuous and lower bounded by zero. Therefore, one can argue that the *log-normal* distribution function is best suited to model them.

The mean shear modulus G is assumed to be equal to the half of the compression strength of concrete, and its standard deviation equal to that of the tensile strength of the uncracked element (a reasonable assumption since G is directly proportional to shear strength which in turn is linked to the maximum tensile strength of the material).

We now have a probabilistic piece-wise linear model with two main variables. Both variables will have a *log-normal* distribution, therefore it is the parametric model of each variable that will constitute the parameters that needs identification:

$$z := [\sigma_t^{cri}, E'_1] \quad (4.9)$$

$$z_i \sim g_\theta(z) \quad (4.10)$$

Where θ is the parametric model for Z and Z has a *log-normal* distribution with mean μ and variance σ^2 . Hence:

$$\theta = (\mu, \sigma^2) \quad (4.11)$$

$$g_\theta(z) = \frac{1}{z\sigma\sqrt{2\pi}} \exp^{-\frac{(\ln z - \mu)^2}{2\sigma^2}} \quad (4.12)$$

Numerical macroscopic tie-beam tests are run, where macro elements behave according to the macro model with a predetermined shape and starting model parameters. The resulting force-displacement curves from the numerical experimentation on the macroscopic tie-beams are

then fitted to that of the equivalent local tie-beam tests (the training data, see Section 4.1.3). The best fit will determine the correct parameters for both distribution functions. Consequently, this classifies the methodology as an optimization problem. The optimization tool used to solve our problem is the Response Surface Method (RSM), see Section 3.4.2.

Finally, the parameters resulting from the optimization scheme are the ones we input into the model for the final calculations, Table 4.3.

Model	Parameter	Symbol	Value in MPa
Probabilistic model for elements of reinforced concrete	Tensile strength	σ_t^{cri}	
	Mean	$\mu_{\sigma_t^{cri}}$	3.4
	Standard deviation	$\sigma_{\sigma_t^{cri}}$	0.5
	Residual stiffness	E_1'	
	Mean	$\mu_{E_1'}$	5300.
	Standard deviation	$\sigma_{E_1'}$	200.

TABLE 4.3: Macroscopic model parameters

$\mu_{\sigma_t^{cri}}$ and $\sigma_{\sigma_t^{cri}}$ are the parameters of the *log-normal* distribution function of the tensile strength of the macro-element. $\mu_{E_1'}$ and $\sigma_{E_1'}$ are the parameters of the *log-normal* distribution function of the residual stiffness after cracking.

4.1.6 Rundown of the Strategy

The parameters involved in the process of creating the complete mechanical model for the probabilistic model of reinforced concrete are:

- The parameters of the probabilistic explicit cracking model of the concrete, section 2.1.2.1.
- The values of C and δ_t^{cri} for the interface elements (steel-concrete bond model) which allows us to perform the correct numerical simulations of the tie-beam test(s). The results from these numerical simulations constitute the starting point for fitting the values of the parameters of the macro-element, section 4.1.3.
- The elastic orthotropic stiffness matrix of the macro-element, assembled with the help of some intuitive hypotheses and the rule of mixtures, section 4.1.4.
- The parameters of the *log-normal* distribution function for the tensile strength of the chosen macro-element (in the direction of rebars). Note that the average value of the tensile strength of a given macro-element is necessarily smaller than that of the same volume of plain concrete; the presence of rebars introduces an extra level of heterogeneity (concentration of stresses around the rebars) that promotes fracture initiation.

- The parameters of the *log-normal* distribution function for the shear strength of the macro-element (note that it is not a major player in our case, thus could be assigned a deterministic value). Its mean value is equal to half of that of the average compression strength of the considered concrete. Its deviation is considered identical to that of the macro-element tensile strength.
- The parameters of the *log-normal* distribution function of the residual stiffness of the macro-element after cracking.

The steps concerning the numerical strategy for the design and characterization of a probabilistic model for the reinforced concrete element in the slab-beam problem are summarized in Figure 4.10

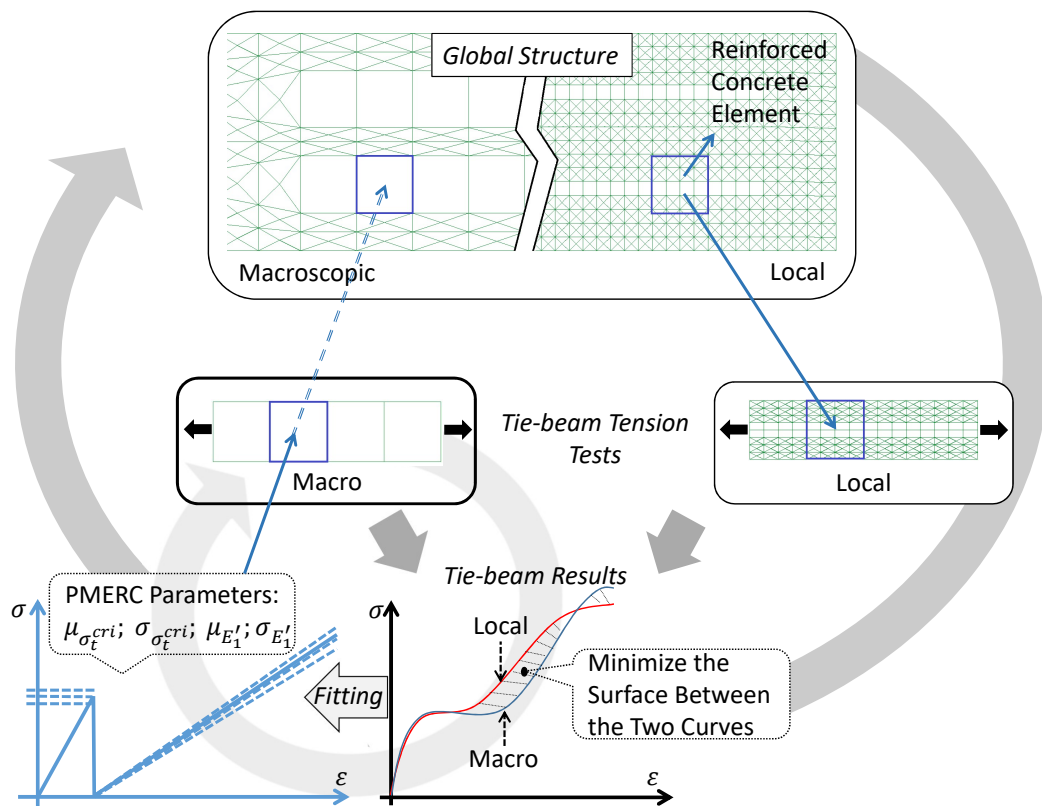


FIGURE 4.10: Multi-scale modeling strategy.

4.1.7 Results

In the frame of the Monte Carlo method, 10 randomly sampled results from every type of numerical test mentioned hereafter are treated.

4.1.7.1 Numerical Tie-Beams

Numerical experimentation on the tie-beams yielded the load-displacement curves shown in Figure 4.11. The results shown here of the macroscopic approach are the best fit to the results from the local approach. The parameters of the probabilistic macro-model for reinforced concrete are dynamically fitted to minimize the area between the two load-displacement curves, Section 3.4. The parameters resulting from the optimization scheme can be found in Table 4.3.

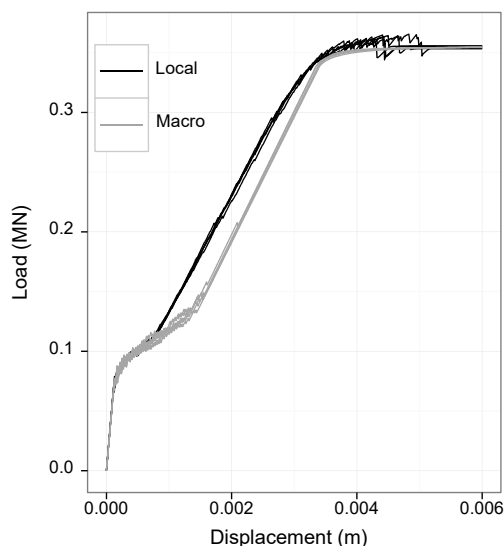


FIGURE 4.11: Numerical tie-beam: Load-displacement curves

As mentioned back in Section 4.1.4.2, the macro-model is “rigid” by design, and is therefore not able to reproduce the exact same global behavior of the tie-beam numerical experimentation using the local approach. The design behind the macro-element constitutive law is driven by the fact that it is supposed to simulate a structural element. So even though we are fitting the macro-model parameters, we cant expect it to yield a perfect result on a structural element such as the tie-beam numerical test when it is actually designed for a larger structural element in a different setting: that of the slab beam under three-point bending.

Nonetheless, the global results as well as the cracking process in both local and macro tie-beam tests seem to be in fair agreement. Figures 4.11, 4.12 and 4.13 are the result of the post analysis done on one random tie-beam of each kind (local and macro). The crack in a macro

element is considered as a straight band which width is given indirectly by the macro model by taking the actual element elongation minus the initial elastic elongation.

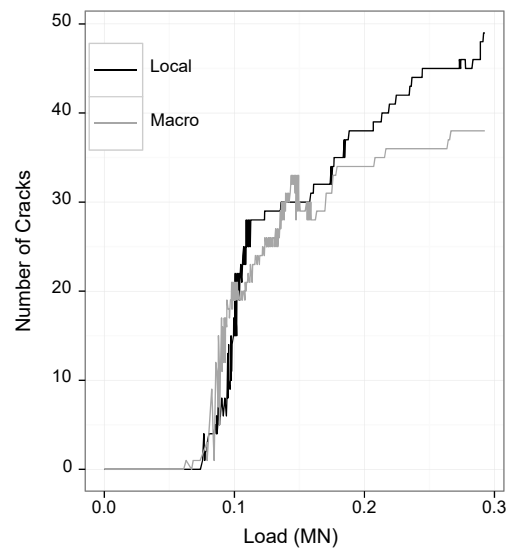


FIGURE 4.12: Numerical tie-beam: Total number of cracks

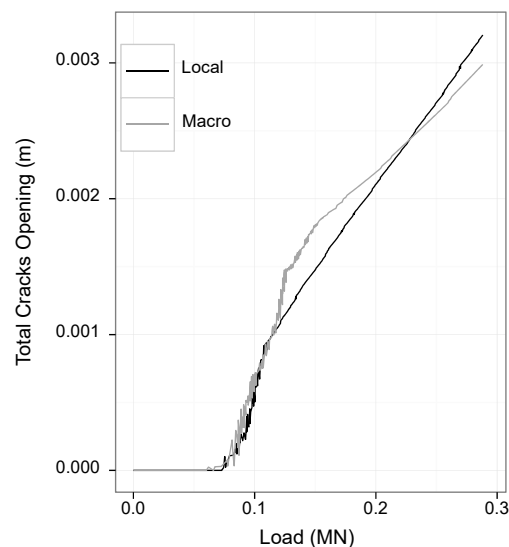


FIGURE 4.13: Numerical tie-beam: Total cracks opening

Due to the nature of the macroscopic approach, some information about the number of cracks becomes more and more unreliable under increasing forces. Since the limit is one macro-crack per macro-element (instead of potentially many micro-cracks), the recount is only viable when looking at cracks with somewhat large openings.

The information about the total cracks opening on the other hand is comparable as expected. We will demonstrate next that this holds in the case of the slab-beam structural element.

In reality, our learning algorithm does not take into account any information about the cracking process in the tie-beams (the training data). We simply cannot afford to invest the time needed to extrude useful information from the local scale. The idea is simply to use the results on the global scale to try and tap into information about the cracking process on the local scale. In the process, we expect to lose only some information about the cracking process in exchange for a substantial gain in calculation costs.

4.1.7.2 Numerical Slab-Beam

At this point of the strategy, all that is left is to implement the resulting parameters, Table 4.3, into the macro-models in the structure for the final calculation.

The problem at hand is a three point bending test of a slab-beam structural element, see Sections 4.1.1 and 4.1.2.

Load-deflection curves obtained with both the local and the macroscopic approach are represented in Figure 4.14.

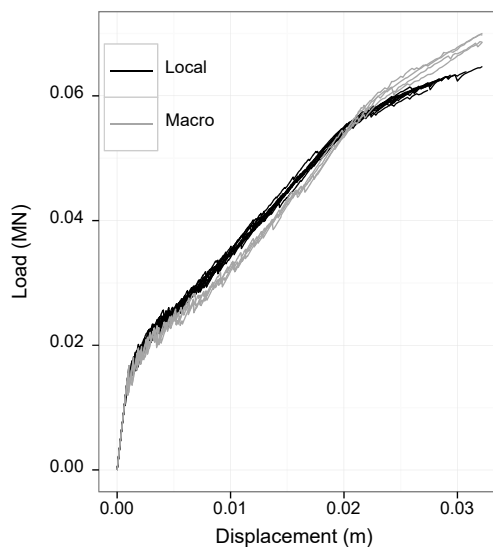


FIGURE 4.14: Numerical slab-beam: Load-deflection curves

We can see that the global results are in agreement. Which means that our reasoning was valid from the beginning. Even though we learned our model on a simple tie-beam tension test, the fact that the main factor in the cracking of a reinforced concrete in a certain direction is the tension stresses in that direction, make it so that a tension test is a good predictor of the cracking of that same element even under a different setting, like that of bending in the case of the slab-beam.

However, some might point out the divergence observed in the results towards the later stage of

the test. This is when the reinforcements on the lower side of the beam have entered their plastic phase, and cracks are deep enough that the top half of the beam is in its own state of bending with a top side under compression and a bottom side under tension. This is a difficult mode to represent with only one macro element across the thickness in the top half of the beam, and this is why the macroscopic approach shows a more rigid beam in that stage of the calculation.

A post-analysis of the data was performed in order to retrieve information about the cracking process in both the local and macro structures. We can visualize the cracking pattern in Figure 4.15, in which we can see a clear resemblance in both cases.

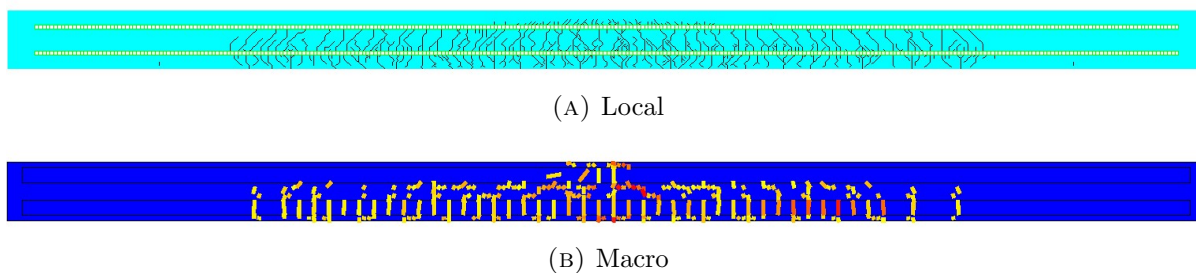


FIGURE 4.15: Numerical slab-beam: Cracking pattern

The information drawn from the macroscopic approach about the total number of cracks on the bottom side of the beam is inaccurate, Figure 4.16. This was expected; the macro-element can represent only one crack across its width, but the structure and the type of loading prompt the creation of numerous thinner cracks. This leads to an underestimation of the actual number of cracks. Although, if we look at a range of cracks with larger opening width (for example $> 200 \mu\text{m}$, Figure 4.17) we find that the results are in coherence (less than 10% in difference).

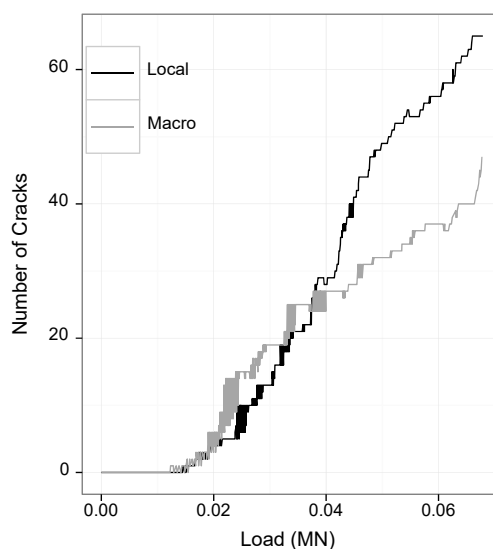


FIGURE 4.16: Numerical slab-beam: Total number of cracks (for cracks with width $> 20 \mu\text{m}$)

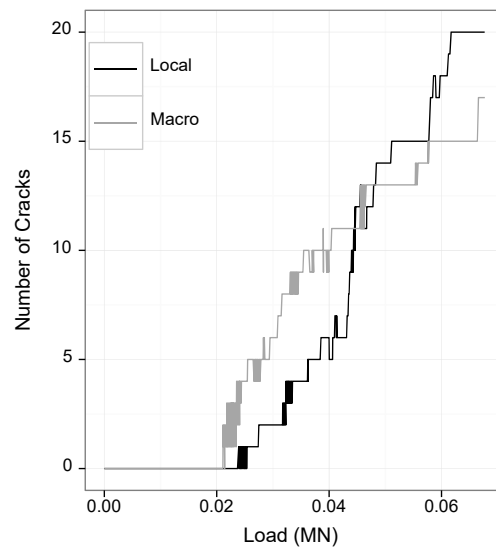


FIGURE 4.17: Numerical slab-beam: Total number of cracks (for cracks with width $> 200 \mu\text{m}$)

On the other hand, we managed to predict the total opening of cracks on the lower side of the beam to an exceptional degree of accuracy, Figure 4.18.

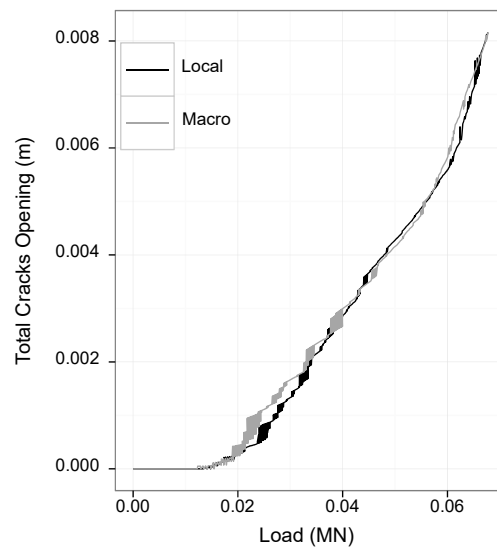


FIGURE 4.18: Numerical slab-beam: Total crack openings

Additionally, if we follow the width opening of the largest crack in each case we get very close results, Figure 4.19.

We can even go further in exploiting the data form post-analysis. For instance, we can find out individual crack openings with respect to their position in the beam. We can also check for

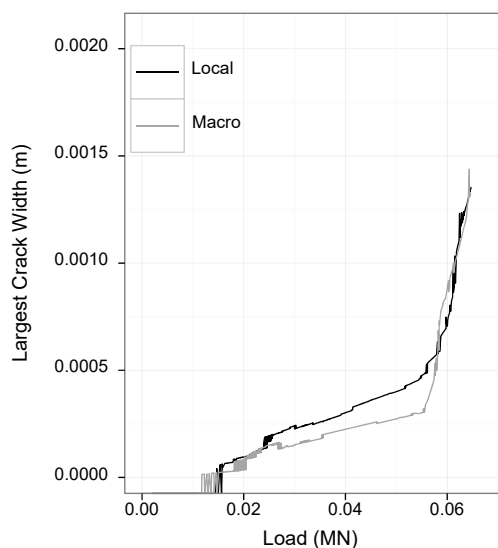


FIGURE 4.19: Numerical slab-beam: Largest crack width

the cracking profile at different thickness levels in the beam (0 cm being the bottom side, and 16 cm the top side), as well as at different levels of applied force, Figure 4.20.

From the results we got out of the macroscopic approach we can note the following:

1. We got similar results on the average load-deflection curves from the two approaches.
2. The total number of cracks measured when applying the macroscopic approach is less than the total number of cracks measured with the local model. This is rather an expected result due to the nature of the macro-element. The idea behind the multi-Scale modeling strategy is to endure small loss in information in order to gain substantially in calculation time.
3. Identical results are obtained concerning the total cracks opening with both approaches. It is consistent with the fact that the load-deflection curves are also close to identical.
4. The number and crack width of large cracks is accurately predicted.

Finally, aside from satisfying results on the global scale and the cracking process, we cannot forget the gain in computational time when using the macro model, Table 4.4.

Structure	Approach	Calculation time (sec)
Slab-beam	Local	~ 54360
	Macro	~ 960

TABLE 4.4: Numerical slab-beam: Computation time

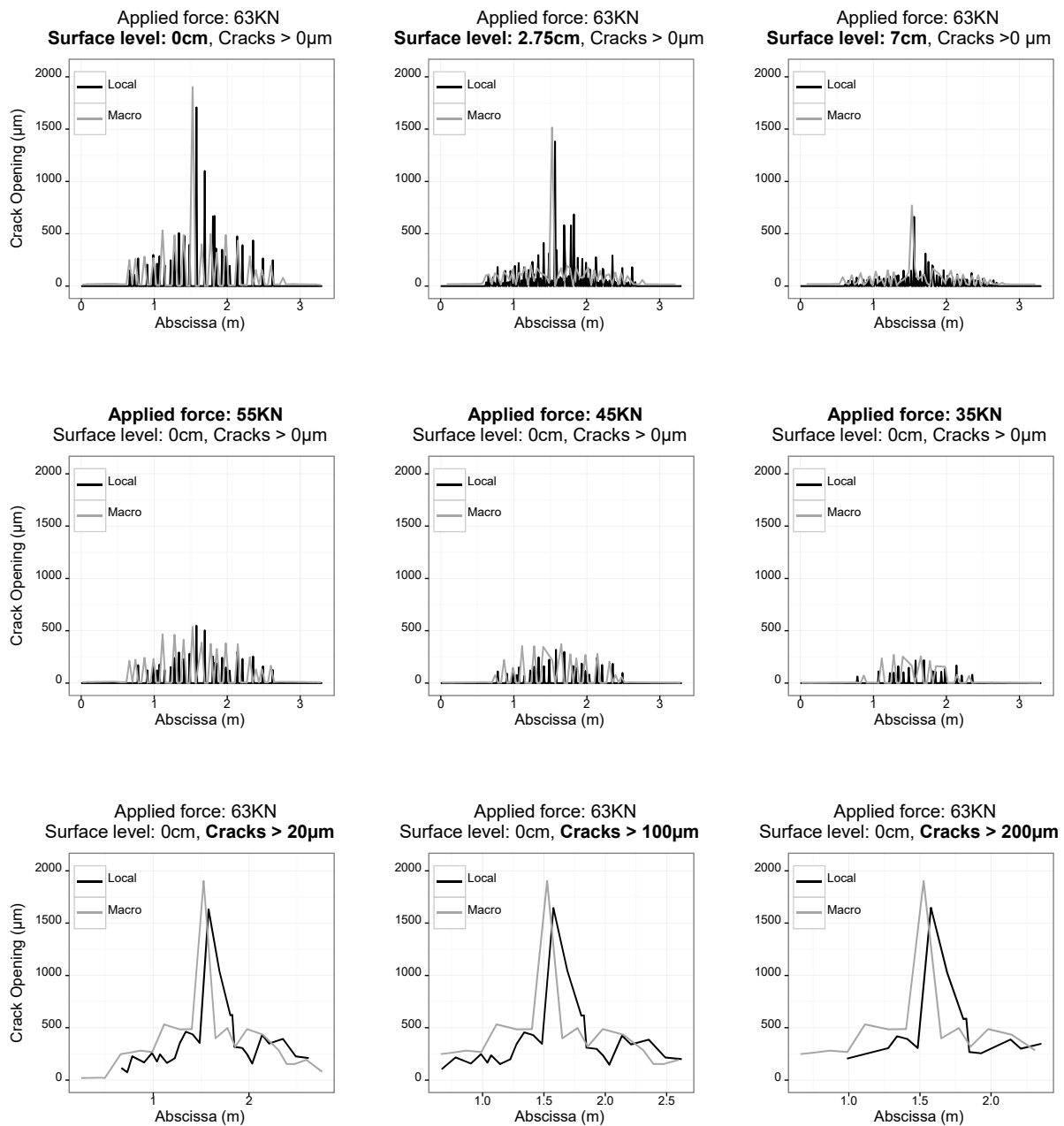


FIGURE 4.20: Numerical slab-beam: Cracking profile

Therefore the **Multi-scale Modeling Strategy** produces reliable information about the macro-cracking process in the structure with less than 2% of the required calculation time using a local approach.

Remark: to give a more precise and honest idea of the computational time saved by using the Multi-Scale Modeling Strategy, it is necessary to take into account the calculation time of the whole optimization scheme to get the parameters for the macro-element model. The relative

weight of this preliminary numerical study on the total computational time of the structure will depend on the size and the complexity of said structure. It is a kind of *incompressible time*. In the present example, this preliminary study consumed **10000 seconds**, which when added, makes for 18% of the calculation time using a local approach. It is equally worth noting that the larger and more complex the structure gets, the less is the weight of this *incompressible time* on the whole computational cost.

4.1.8 Discussion

This section served as a direct application of the multi-scale strategy to develop a probabilistic model for reinforced concrete elements. This strategy consists in building a macro model from numerical experimentation using validated local ones: the *probabilistic explicit cracking model* for concrete, and the *steel-concrete interface model* with a Mohr-Coulomb law for the steel-concrete bond. As a first validation of this Multi-Scale Modeling Strategy, a previously studied case of a slab-beam structural element is proposed. The numerical simulations (in $2D$, plane stresses) have shown that the scientific approach proposed is promising: the global behavior of the structure is correctly predicted, and the macro-cracking pattern is consistent with results given by the local approach. In the process, some information on the total number of cracks is lost (which was expected), but the information about the larger cracks is accurately predicted. The main objective of the strategy was to reduce the massive computational time required to get reliable information about the cracking process in large structures. We can affirm that this objective was reached at least in this example. These results could still be improved, and the gain in calculation time would be even more acute for larger structures and/or problems necessitating $3D$ simulations.

The work in this section aimed at validating the multi-scale strategy in the frame of $2D$ calculations under plane stresses condition, where the evolution of the structure is mainly piloted by fracture creation.

In the next section, we will generalize the strategy in the frame of $3D$ numerical simulations, and we will be addressing the case of fracture propagation.

4.2 Reinforced D.C.B. (3D)

This next validation example is of a reinforced D.C.B. (Double Cantilever Beam). The initial study on this particular type of beam was conceived with the intention to closely examine the phenomenon of fracture propagation in concrete, reinforced concrete and fiber reinforced concrete. An experimental campaign was conducted on such beams and was part of the work done by Rossi [1986]. Our interest will be focused on one particular D.C.B. reinforced with steel bars.

The case of the D.C.B. is interesting for many reasons:

- A numerical study using local models is yet to be conducted on such a beam. The only results at hand are global displacement measurements from the experimental study which will be used only to validate the numerical calculations. So it is as if we are completely blind going in, trying to solve this problem. This is as close as it gets to a real world application of our multi-scale strategy, and correctly predicting the response of the structure would greatly increase the confidence in the approach.
- In order to guide the crack and to maintain it in the median plane, it was deemed necessary to introduce a longitudinal prestressing (by post tension) using several cables. Hence we will get to show how would the strategy take prestressing into account.
- In Section 4.1, we validated the strategy on a reinforced slab-beam submitted to three point bending. This type of structure and boundary conditions prompt the creation of numerous thin macro-cracks, but wont allow for the localization and propagation of a fracture (actually the beam is not thick enough for the process of fracture propagation to take place). So this brings an opportunity to test the strategy in a setting specially devised to study fracture propagation.

In this section, just like in Section 4.1, we will go through a full implementation of the multi-scale strategy summarized in 3.5, this time in a 3D framework, and we will compare the accuracy of our results and calculation costs with that of existing numerical simulations.

4.2.1 Dimensions and Loading Conditions

A crack propagation test was developed since 1976 on very large D.C.B.s (Double Cantilever Beam). After a whole period of experimental development and theoretical interpretation of the test [Benkirane, 1982], we have in our disposition the final results obtained from the experimental campaign and the methodology for exploiting them [Rossi, 1986].

The body of the test is a large D.C.B. 3.5 m long and 1.1 m wide, Figure 4.21. In order to guide the crack and keep it in the median plane, a thinning of the section proved insufficient, it was necessary to introduce a longitudinal post-tension prestressing using several cables. The advantage of using such a setting is twofold, since both the behavior of the material and that of a representative structure of civil engineering are acquired.

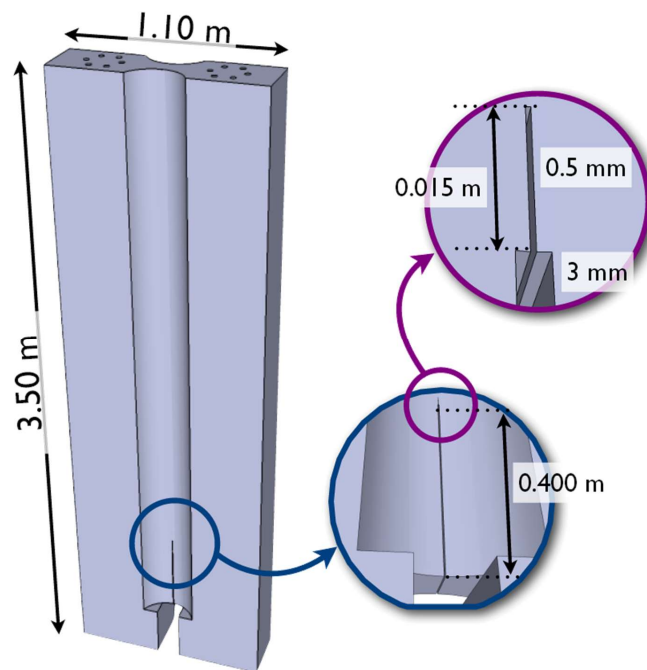


FIGURE 4.21: Double Cantilever Beam: Geometrical characteristics

The beam is placed vertically, the notch at the bottom, the propagation of crack happens from bottom to top. In order to obtain a stable propagation of the crack, the tests were carried out at an imposed displacement speed of $25 \mu\text{m min}^{-1}$. The high adhesion reinforcements HAΦ6 are placed on the path of the crack perpendicularly to the latter. 9 rebars, 10 cm apart, constitute 0.1% of the volume of the beam, Figure 4.22.

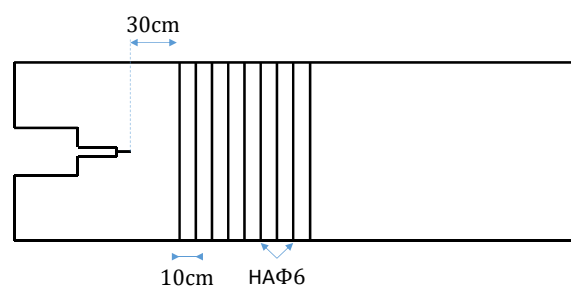


FIGURE 4.22: Double Cantilever Beam: Position of the reinforcements

The crack opening at the point of application of the load P (located at 0.175 m from the lower side of the beam) is measured by averaging the results of two extensometers, one on each side, Figure 4.23. The load P is applied by means of an annular flat cylinder with a maximum capacity of 10 tons. The value of the total load applied as prestress is 709 kN.

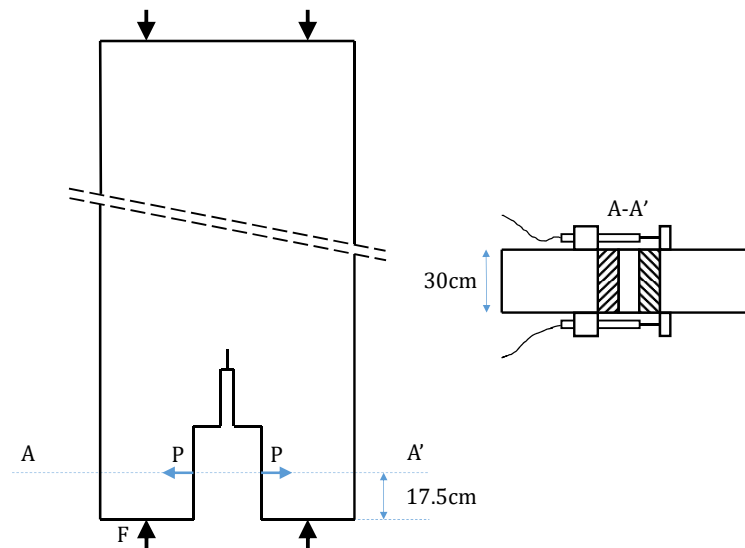


FIGURE 4.23: Double Cantilever Beam: Application of load P , prestress F , and measurement of displacement

4.2.1.1 Materials Characteristics

- **Concrete**

The composition used in these tests is detailed in Table 4.5. Conventional tests for mechanical characterization (compression, splitting) yield the following average values:

- Average compression strength: $f_c = 55$ MPa
- Average tensile strength: $f_t = 3.7$ MPa
- Young modulus: $E_c = 35\,000$ MPa

- **Steel**

The mechanical characteristics of the steel used are:

- Round HA Φ 6: $R_e = 382$ MPa, $R_u = 401$ MPa, $E_s = 191\,000$ MPa

Components	Weight in kg
Sand 0/5	700
Gravel 4/12	1108
Cement HP la FRETTE (LAFARGE, CORMEILLES)	400
Superplasticizer	6
Water	179
Total	2393

TABLE 4.5: Composition of concrete used (per m^3), D.C.B. case study

4.2.1.2 Experimental Results

Figure 4.24 shows the resulting load-displacement curve of the reinforced D.C.B. test. These curves reflect the overall behavior of the beam and are not characteristic of the material in the sense that they do not exclusively depend on the latter.

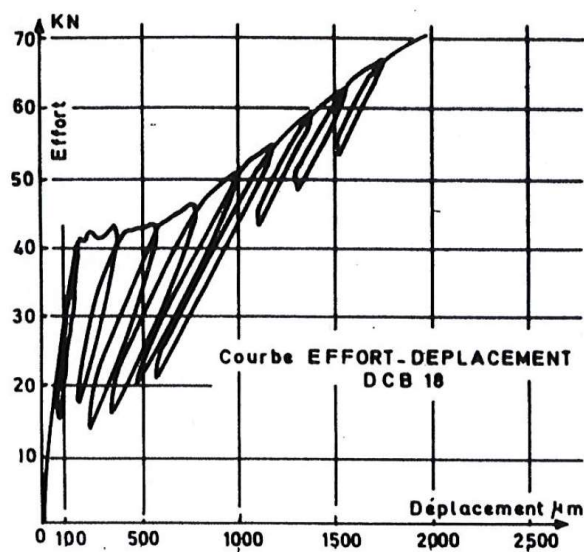


FIGURE 4.24: Double Cantilever Beam: Experimental load-displacement curve [Rossi, 1986]

Other types of experimental data are also available, like measurements of rebar deformation with the help of local extensometers, and information about the crack profile using acoustic emission [Rossi, 1986]. But we will not directly use these results especially since we will have direct access to easily exploitable data on the cracking process from numerical simulations using a local scale approach. Having faith in the results of previous studies, the results of the numerical simulations using local models are reliable regarding the cracking processes.

4.2.2 Numerical Simulation Using Local Models

In this section we will layout the numerical simulation of the D.C.B. test introduced above. A local approach on such a large beam might be considered a bit of an extreme solution, but it is necessary in order to get reliable information on the cracking process. Since this part of the study is not our main object of interest, and because of the high calculation costs that are brought about by local simulations, we decided to perform the numerical simulation using local models in a $2D$ plane stresses framework.

Remark: This numerical simulation of the D.C.B. using a local approach is in no way related to the multi-scale strategy. Its sole purpose is to provide a basis for comparing post analysis results of the global behavior and the cracking profile in the beam, as part of the validation process of the proposed multi-scale strategy, otherwise pointless in a real-life application of the strategy.

The local models used in these calculations are: the *semi-explicit cracking model for concrete*, Section 2.1.2.2, and the *steel-concrete bond model*, Section 2.3.1.1. The steel bars are modeled by a Von-Mises elastoplastic model with isotropic hardening. Like we have stated earlier, this study does not cover a numerical simulation with the mentioned local modeling techniques, so the parameters of the local models are unknown.

The *semi-explicit cracking model for concrete* deals with the crack creation and propagation and the energy dissipation of elementary bodies of concrete. It is “semi-explicit” in the sense that it does not explicitly represent the crack. Instead, “cracked” volume elements in which the crack direction and opening are calculated, would form elementary holes, and link together to coalesce into a crack. This type of approach is far less demanding in calculation costs compared to the *probabilistic explicit cracking model* used in the slab-beam problem, Section 4.1.

The model unknowns are:

- The tensile strength f_t , which will be randomly distributed using a Weibull distribution function with parameters b_f and c_f , both are functions of the concrete used and the volume of the element [Rastiello, 2013].
- The volumetric density of dissipated energy, which has a *log-normal* probability density function with mean G_c and deviation d_G . G_c is considered an intrinsic material property and was determined experimentally by Rossi [1986]:

$$G_c = \frac{K_{Ic}^2}{E} = 1.3141 \times 10^{-4} \text{MN m m}^{-2} \quad (4.13)$$

Where, in the context of fracture mechanics [Irwin, 1968], G_c is the critical rate of energy restitution and K_{Ic} is the stress intensity factor in mode I.

Due to the heterogeneity of the material (the impact of which is seen on the scale of the finite element) the dissipated energy can undergo variations (deviation in statistical terms) around the mean value. This deviation can be considered to be directly related to the size of the material volume involved. The deviation should increase as the size of the volume decreases, due to the heterogeneity of the material which increases when the volume of material in question gets smaller.

According to the model hypotheses, three parameters are to be determined as a function of the size of the finite element: the parameters b_f and c_f of the distribution function for the resistance of the uncracked element, and the dispersion d_G of the cracking energy. It is clear that the inverse analysis procedure, which is essential in order to determine for each finite element size the appropriate distribution laws, will be very costly from a numerical point of view. Therefore, when considering the finite element mesh of the D.C.B. problem, we tried to limit the size range of the finite elements that represent plain concrete (see Figure 4.26). The mesh of the D.C.B. will finally contain elements in the range of $r_e \approx 10^{-2}$, $r_e \approx 10^{-3}$ and $r_e \approx 10^{-4}$ for the elements closest to the notch tip (corresponding to the mesh refinement near the tip). $r_e = \frac{V_e}{V_g}$, is the ratio of the volume of the finite element over the volume of the largest aggregate.. The model parameters corresponding to $r_e \approx 10^{-2}$ and $r_e \approx 10^{-3}$ can be found in Rastiello [2013].

A simple numerical procedure was devised in order to figure out the parameters for elements in the range $r_e \approx 10^{-4}$. The parameters are calibrated to the global response of a block of concrete under tension, Figure 4.25.

The reference will be the numerical results obtained with the same semi-explicit model, on

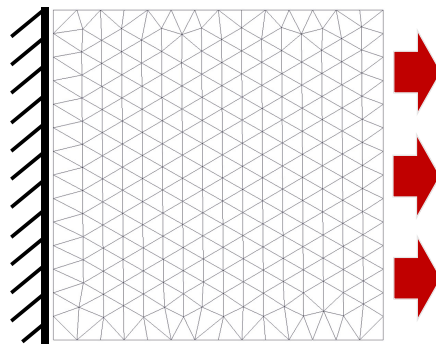


FIGURE 4.25: Concrete block under tension. Elements in the mesh are in the same size range of those used in the D.C.B. local approach calculations

the same test, using the same concrete as in Rastiello [2013] with $r_e \approx 10^{-3}$, the parameters of which are known. The resulting parameters, Table 4.6, will be used to model the concrete in the D.C.B. 2D local calculation.

The *steel-concrete bond model* is an interface model that ensures the displacement continuity between steel and concrete, replaces the ribs in the mesh while representing their mechanical effect, and simulates the loss of adhesion and the subsequent friction between steel and concrete. The unknown model parameters are the maximum shear stress C , and the tangential critical relative displacement δ_t^{cri} . The identification of these parameters is done via numerical inverse analysis. The reference is a tie-beam tensile test modeled using a microscopic approach in a 2D framework, where the steel ribs are explicitly modeled, Figure 4.26.

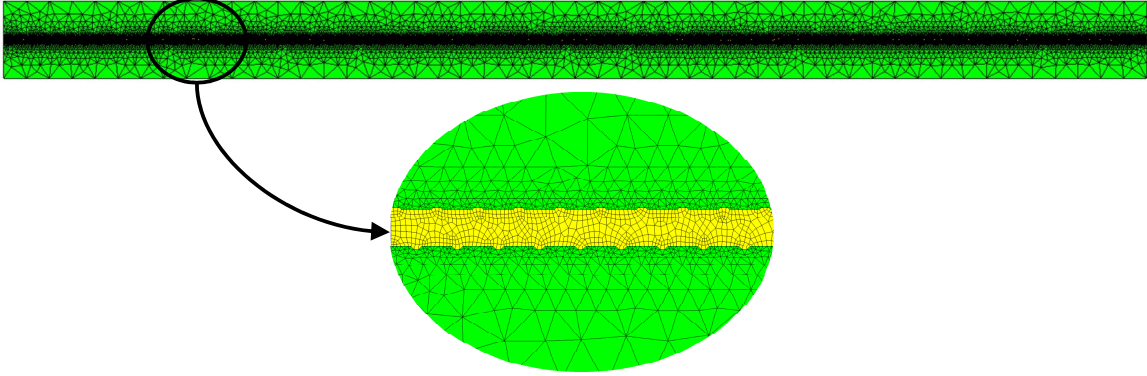


FIGURE 4.26: Numerical tie-beam: Microscopic approach, 2D mesh

This type of local approach is extremely costly in calculation time/memory, but it is a valid way to get reliable global and local results necessary for identifying the parameters of the interface model, especially in case we lack experimental data.

The Material characteristics and model parameters of both local models used in the calculation of the 2D D.C.B. can be found in Table 4.6.

Model/Material	Parameters	Symbol	Values	Unit
Semi-explicit cracking model (for $r_e \approx 10^{-4}$)	Compressive strength	f_c	55	MPa
	Young modulus	E_c	35000	MPa
	Aggregate diameter	D_g	0.012	m
	Tensile strength	f_t		MPa
	Scale parameter	b_f	8.0	
	Shape parameter	c_f	1.0	
	Dissipated energy			
	Mean value	G_c	1.3141×10^{-4}	MN m m^{-2}
	Deviation	d_G	8.4×10^{-4}	MN m m^{-2}
Steel-concrete bond	Cohesion	C	10	MPa
	Critical tangent displacement	δ_t^{cri}	4	10^{-6}m
Steel bar	Young modulus	E_s	191000	MPa
	Elastic limit	R_e	382	MPa
	Ultimate limit	R_u	401	MPa
	Nonlinear hardening modulus	H_s	$\frac{1815}{\log(\sigma)+322}$	MPa

TABLE 4.6: Local models parameters, D.C.B. case study

The 2D mesh of the D.C.B., Figure 4.27, shows the layout of the steel bars in the beam and the mesh refinement around the notch. Since the *semi-explicit cracking model for concrete* describes well the crack initiation and propagation independently of the size of the finite element, we do not really need a refined meshing at the tip of the notch.

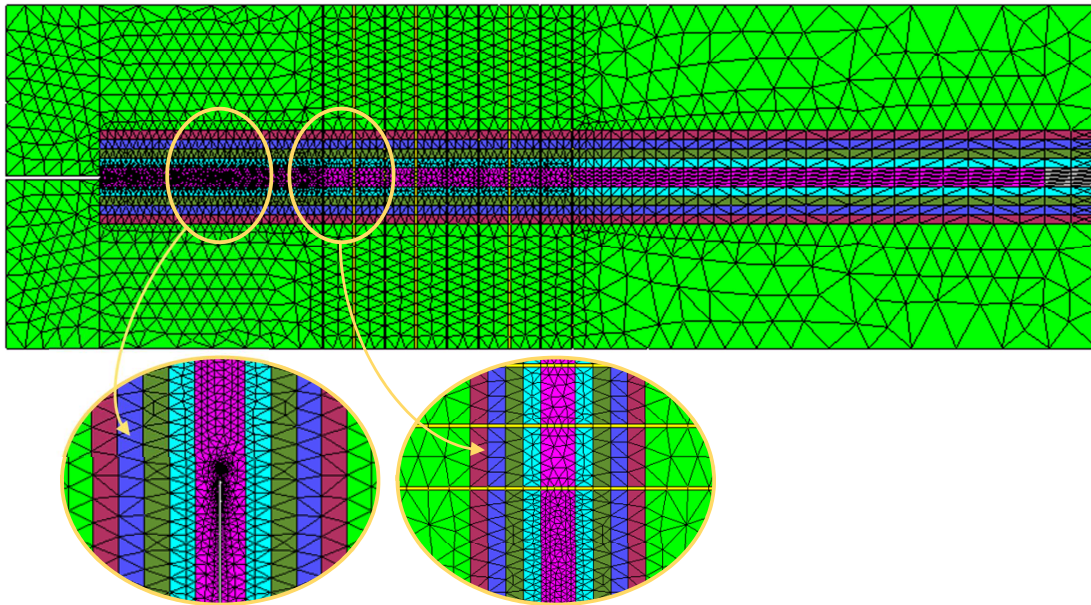


FIGURE 4.27: Double Cantilever Beam: Local approach, 2D mesh

The D.C.B. test, as represented in Section 4.2.1, yields the expected global response, Figure 4.28. Data on the local scale, relating to the cracking process, is also gathered for later comparison with results from the macroscopic approach.

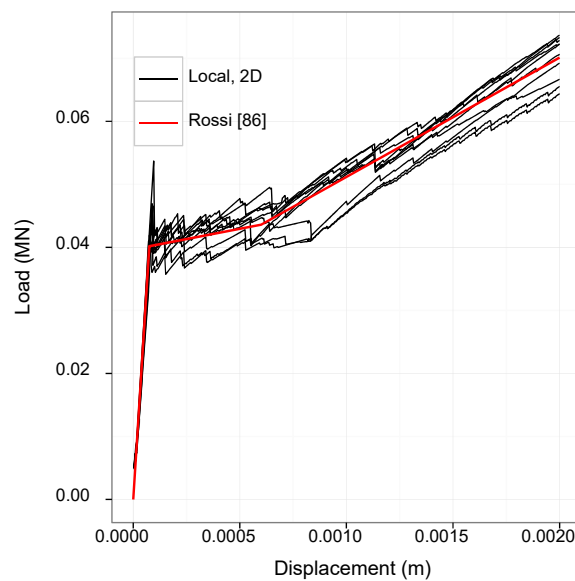


FIGURE 4.28: Double Cantilever Beam: Local approach, load displacement curves

4.2.3 D.C.B. Macro Mesh: Three Types of Macro-Elements

The generic D.C.B. 3D macro mesh is shown in Figure 4.29. The *Green* elements represent concrete that is not supposed to crack (isotropic linear elastic material model). The *Yellow* elements represent concrete that is on the fracture path and/or might be subjected to important stress fields that would lead to elementary cracking (semi-explicit cracking model). The *Blue* elements are cubic macro elements of reinforced concrete on the fracture path (probabilistic reinforced concrete macroscopic model). The *Purple* elements are cubic elements of reinforced concrete that are not on the fracture path (orthotropic linear elastic model taking into account the presence of steel bar(s) in the concrete volume).

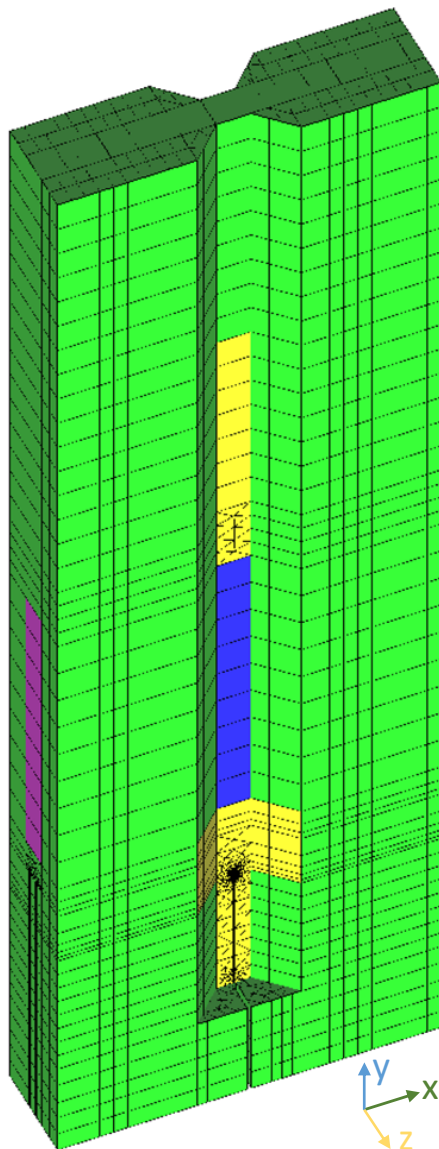


FIGURE 4.29: Double Cantilever Beam: 3D macroscopic mesh

The concrete on the fracture path is meshed with prismatic elements, and numerically modeled with the *semi-explicit cracking model for concrete*, Section 2.1.2.2. The reinforced

concrete band is replaced with cubic/cuboid macro elements that will be the subject of this study.

Given the geometry of the D.C.B. we thought it interesting to test the probabilistic multi-scale strategy with different types of macro-elements. Notably elements with different thicknesses (concrete coating) and with different amount of steel bars represented in the element, Figure 4.30. This will allow us to see how well the strategy fares with different element geometries and constitutions.

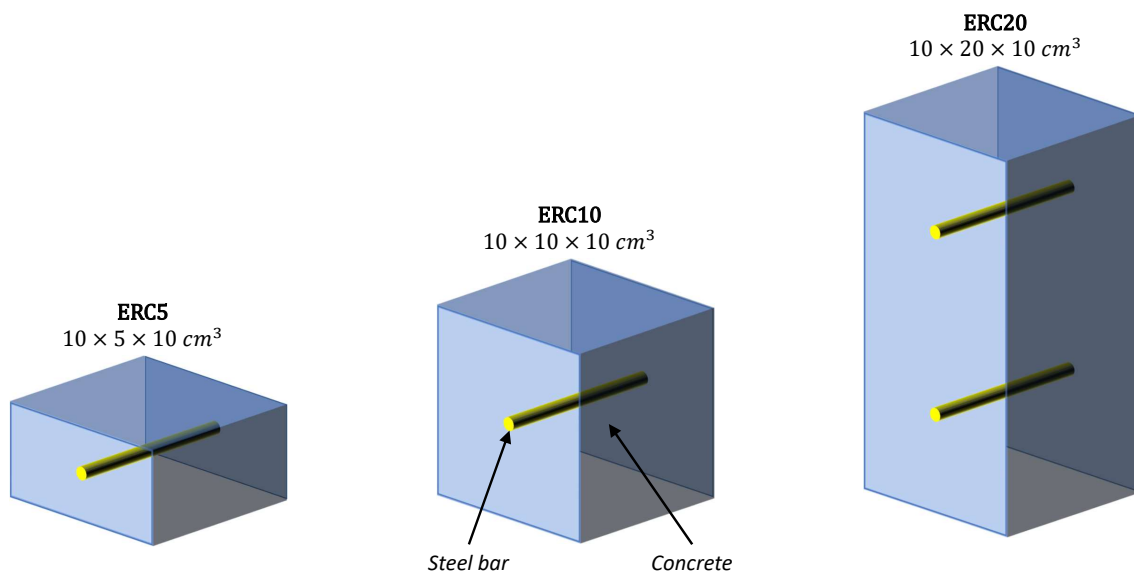


FIGURE 4.30: Three representations of the macroscopic element of reinforced concrete in the D.C.B.

We chose three different types of macroscopic elements to represent reinforced concrete blocks in the D.C.B. tests. Figure 4.31 shows the XY plane of the three macroscopic D.C.B.s meshes depending on the type of macro element used.

For more clarity and ease of use, we will, from here on out, refer to the different types of macro elements by the term **ERC** (element of reinforced concrete) followed by its characteristic thickness in centimeters:

- **ERC5**: $10 \times 5 \times 10 \text{ cm}^3$ cuboid concrete element with 1 reinforcing steel bar.
- **ERC10**: $10 \times 10 \times 10 \text{ cm}^3$ cubic concrete element with 1 reinforcing steel bar.
- **ERC20**: $10 \times 20 \times 10 \text{ cm}^3$ cuboid concrete element with 2 reinforcing steel bars.

Each type of ERC is an interesting case to study in itself. Overall, this will allow us to test the impartiality of the multi-scale strategy with regard to element thickness.

More specifically, the ERC5 study pushes the lower bound limit on the concrete coating thickness

required for a valid macroscopic reinforced concrete element. And since the influence of the steel bar is that much more important than in the other two cases, it would be interesting to see how the macro model would cope to describe the cracking process of such an element.

The ERC10 is the typical element to be used in the D.C.B. study. It has enough thickness and concrete coating to allow the coalition of microcracks into one macrocrack. And at the same time, the element is not too thick and so it does not obstruct the crack propagation.

The ERC20 on the other hand is too thick that the finite element itself might be too rigid for this sort of calculation. Furthermore, we get to observe the changes when having 2 reinforcing steel bars in the element thickness instead of 1. This element is not suited for modeling crack propagation on the scale of the D.C.B. (might be viable for a much larger structure) but looking into this case is necessary for us to draw the limitation on how adaptable are statistical models under extreme scenarios.

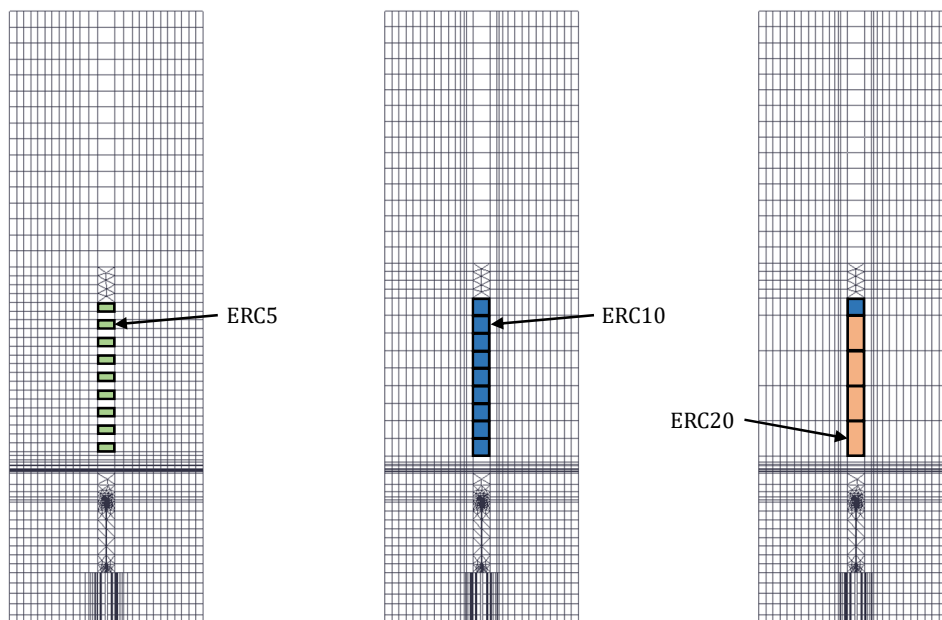


FIGURE 4.31: 2D look at the three macroscopic D.C.B.s in the XY plane

4.2.4 Tie-Beam Numerical Tests

The dimensions and compositions of the macro-elements are now at our disposition, so we are able to design the numerical tie-beam tests according to Section 3.3.2. The tie-beam consists of a succession of macro-elements, long enough to get the complete cracking pattern for such an element; since in this study we plan to implement 3 different types on macro-elements (see the previous Section 4.2.3) we will then have to design a numerical tie-beam test for each. A planar cut of the 3D macro tie-beams meshes and what they represent in terms of reinforced concrete, the equivalent 2D micro meshed tie-beams, are shown in Figure 4.32.

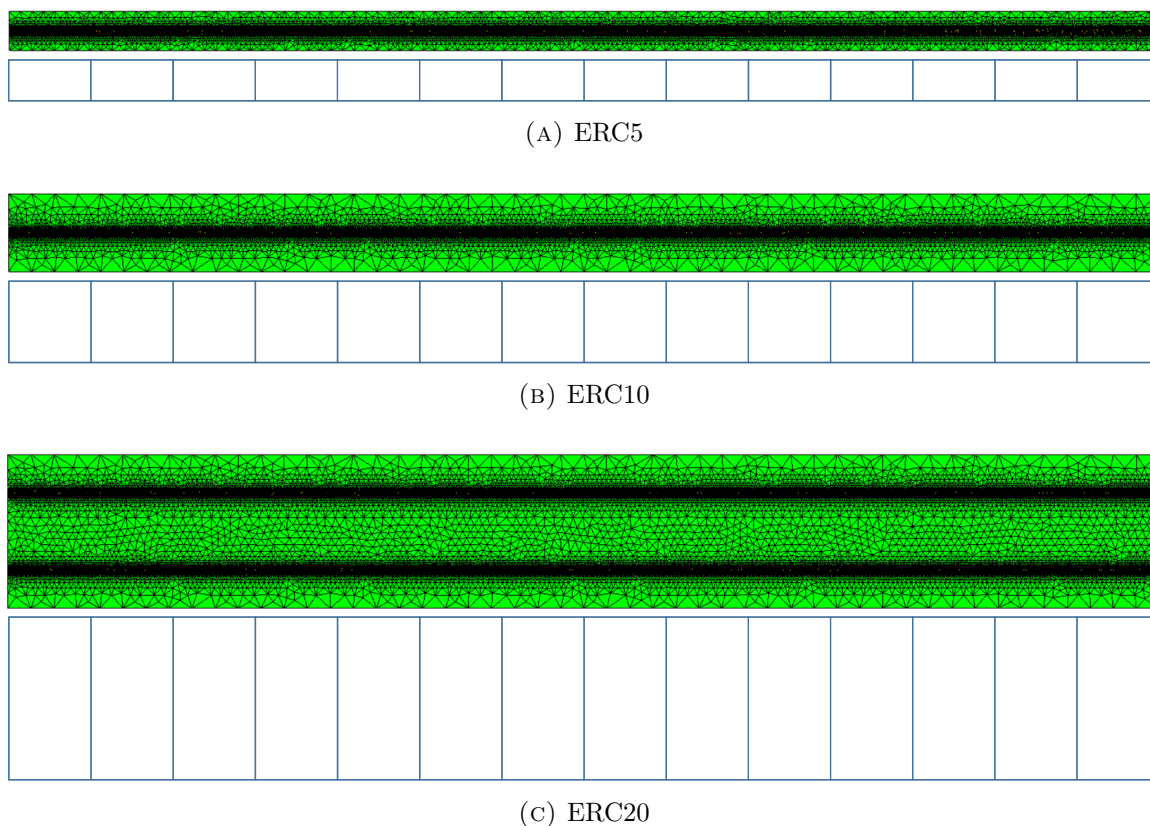


FIGURE 4.32: Tie-beam numerical experiments: micro/macro meshes

The use of a microscopic approach (steel ribs are explicitly modeled, see Figure 4.27) is very costly in terms of calculation time, and would cause the *incompressible time* associated with this study that much more significant. Regardless, where there is lack of experimental data, and the use of a local scale approach to model reinforced concrete is no longer an option, the micro scale approach becomes unavoidable. So in a sense, the micro scale calculations would render obsolete the experimental data needed for the parameter identification of the local models typically used in such a situation. Therefore, we consider the calculation cost associated with the micro scale calculations justified.

In the frame of the Monte Carlo method, 10 randomly sampled results of the micro tie-beam numerical simulations are gathered. The global force/displacement results from the micro tie-beam tensile tests will act as our training data (see Section 3.3.1).

4.2.5 3D Macroscopic Model

Like in the case of the 2D slab-beam (Section 4.1.4), the 3D macro model is required to describe the cracking behavior of the macro-element in the structure, and thus it must present the following features:

- Access to information on macro-cracks openings.
- A probabilistic modeling to allow for a statistical analysis of the structural behavior via a Monte Carlo approach (reliability analysis of the structure).

In this section, we will design a macro model suited for the D.C.B. problem in a $3D$ framework. No experimental or numerical data is yet assumed to be at our disposition.

4.2.5.1 Philosophy

Similarly to what we have seen before (see Section 4.1.4.1), some strong assumptions regarding the behavior of the macro-element in the structural setting are made:

1. In the direction of the reinforcements, the composite element is assumed to have an elastic perfectly brittle behavior. Failure criteria in tension (Rankine) and in shear (Tresca, significant only when dealing with compressive stress fields) are applied and verified at the center of gravity of the macro-element.
2. Once the matrix is broken, we have a sharp drop of the stresses in the element. But unlike the $2D$ macro-element of the slab-beam validation example (see Section 4.1.4.2), this $3D$ macro-element is relatively narrow (depth wise, it is only 10cm) and with a lower steel to concrete ratio. Therefore, it would be wise to refine the immediate post failure behavior. Notably, the stresses no longer drop to zero, but to a value of stress that will be introduced as a new model parameter. By doing this, we are numerically acknowledging the continuous intervention of the steel bar during the cracking event.
3. Immediately after the crack, marked by the drop in stresses, the rebars intervene mechanically. This requires a new evaluation of the coefficients of the stiffness matrix of the macro-element in the direction parallel to the rebars. The new values of these coefficients are associated with the stiffness of the rebars and the phenomenon of tension stiffening.
4. The model will account for the plastic behavior of the rebars in the studied direction: when the linear elastic strain limit of the steel is reached at the center of gravity of the macro-element, its behavior would be represented by an elasto-perfectly-plastic model. We chose, for simplicity, to simulate this behavior with a damage model (with disregard to permanent deformations due to the yield of the rebars). This simplification is only possible because the structures are under monotonically increasing loading.

The mathematical relations describing the mechanical aspects of the model are proposed here in the $3D$ framework.

4.2.5.2 Constitutive Law

Orthotropic elasticity:

In the case of the D.C.B., the macro-element is reinforced in only one direction, it can therefore be considered as an orthotropic material. A fixed orthogonal reference frame is locally placed with its direction $\mathbf{1}$ collinear with the reinforcing steel. Next, in agreement with homogenization techniques, we consider that the element consists of a smeared orthotropic material. Thus the elastic 3D constitutive law is:

$$\boldsymbol{\sigma} = \mathbf{H} \times \boldsymbol{\varepsilon} \quad (4.14)$$

$$\begin{bmatrix} \sigma_{11} \\ \sigma_{22} \\ \sigma_{33} \\ \sigma_{12} \\ \sigma_{13} \\ \sigma_{23} \end{bmatrix} = \frac{1}{\Delta} \begin{bmatrix} \frac{1-\nu_{23}\nu_{32}}{E_2 E_3} & \frac{\nu_{21}-\nu_{31}\nu_{23}}{E_2 E_3} & \frac{\nu_{31}-\nu_{21}\nu_{32}}{E_2 E_3} & 0 & 0 & 0 \\ \frac{\nu_{12}-\nu_{13}\nu_{32}}{E_1 E_3} & \frac{1-\nu_{31}\nu_{13}}{E_1 E_3} & \frac{\nu_{32}-\nu_{31}\nu_{12}}{E_1 E_3} & 0 & 0 & 0 \\ \frac{\nu_{13}-\nu_{12}\nu_{23}}{E_1 E_2} & \frac{\nu_{23}-\nu_{13}\nu_{21}}{E_1 E_2} & \frac{1-\nu_{12}\nu_{21}}{E_1 E_2} & 0 & 0 & 0 \\ & & & G_{12}\Delta & 0 & 0 \\ & \text{SYM} & & 0 & G_{13}\Delta & 0 \\ & & & 0 & 0 & G_{23}\Delta \end{bmatrix} \times \begin{bmatrix} \varepsilon_{11} \\ \varepsilon_{22} \\ \varepsilon_{33} \\ 2\varepsilon_{12} \\ 2\varepsilon_{13} \\ 2\varepsilon_{23} \end{bmatrix} \quad (4.15)$$

Where,

$$\Delta = \frac{E_1 E_2 E_3}{1 - \nu_{23}\nu_{32} - \nu_{31}\nu_{13} - \nu_{12}\nu_{21} - 2\nu_{23}\nu_{31}\nu_{12}} \quad (4.16)$$

Some assumptions are made concerning the coefficients of the elastic orthotropic stiffness matrix \mathbf{H} :

- \mathbf{E}_1 : Young modulus in the direction of the rebars; calculated as a result of the average Young modulus of both the concrete and the rebars according to the rule of mixtures.
- $\mathbf{E}_2 = \mathbf{E}_3$: Young modulus of the concrete (an approximation).
- $\nu_{12} = \nu_{13} = \nu_{23} = \nu_{32}$: Poisson ratio of the concrete.
- $\frac{\nu_{21}}{\mathbf{E}_2} = \frac{\nu_{12}}{\mathbf{E}_1}$; $\frac{\nu_{31}}{\mathbf{E}_3} = \frac{\nu_{13}}{\mathbf{E}_1}$ (to ensure that \mathbf{H} is symmetric)
- \mathbf{G}_{23} : Shear modulus of plain concrete (an approximation).
- $\mathbf{G}_{12} = \mathbf{G}_{13}$: Shear modulus that takes into consideration the presence of the rebars in the volume of the element with respect to the rule of mixtures.

The values of the coefficients of the orthotropic stiffness matrix are calculated for each ERC.

Cracking and post-cracking behavior:

Failure criteria are applied in tension (Rankine) or in shear (Tresca) when the corresponding strengths are reached. Reaching the failure limit results in a sharp drop in the stresses to

a certain value that will depend on the size and constitution of the macro element and will therefore be treated like a model parameter. Stresses are then immediately picked up by a reduced elastic matrix representing the remaining contribution of the steel bars with some residual action from the surrounding concrete (in the form of friction). Some terms of the initial elastic constitutive relation (4.14, 4.15) are then affected by a reduction coefficient β :

$$\boldsymbol{\sigma} = \mathbf{H}' \times \boldsymbol{\varepsilon} \quad (4.17)$$

$$\begin{bmatrix} \sigma_{11} \\ \sigma_{22} \\ \sigma_{33} \\ \sigma_{12} \\ \sigma_{13} \\ \sigma_{23} \end{bmatrix} = \frac{1}{\Delta} \begin{bmatrix} \beta \frac{1-\nu_{23}\nu_{32}}{E_2 E_3} & \beta \frac{\nu_{21}-\nu_{31}\nu_{23}}{E_2 E_3} & \beta \frac{\nu_{31}-\nu_{21}\nu_{32}}{E_2 E_3} & 0 & 0 & 0 \\ \beta \frac{\nu_{12}-\nu_{13}\nu_{32}}{E_1 E_3} & \frac{1-\nu_{31}\nu_{13}}{E_1 E_3} & \frac{\nu_{32}-\nu_{31}\nu_{12}}{E_1 E_3} & 0 & 0 & 0 \\ \beta \frac{\nu_{13}-\nu_{12}\nu_{23}}{E_1 E_2} & \frac{\nu_{23}-\nu_{13}\nu_{21}}{E_1 E_2} & \frac{1-\nu_{12}\nu_{21}}{E_1 E_2} & 0 & 0 & 0 \\ & & & G_{12}\Delta & 0 & 0 \\ & \text{SYM} & & 0 & G_{13}\Delta & 0 \\ & & & 0 & 0 & G_{23}\Delta \end{bmatrix} \times \begin{bmatrix} \varepsilon_{11} \\ \varepsilon_{22} \\ \varepsilon_{33} \\ 2\varepsilon_{12} \\ 2\varepsilon_{13} \\ 2\varepsilon_{23} \end{bmatrix} \quad (4.18)$$

β could also be viewed as an anisotropic damage variable. Actually, the whole process involving the drop in stresses, and the contribution of steel until yielding, can be numerically represented via a damage model type of formulation with:

$$\beta \sim (1 - D) \quad (4.19)$$

Let σ_r be the variable representing the constraint value in direction $\mathbf{1}$ (that of the reinforcement) right after the drop in stresses resulting from the failure criterion being reached. Let E'_1 be the residual stiffness in direction $\mathbf{1}$. σ_r and E'_1 , along with σ_t^{cri} (the tensile strength of the uncracked element) are the unknown model parameters. The drop from σ_t^{cri} to σ_r can be the result of an initial anisotropic damage suffered by the element in the direction $\mathbf{1}$, represented by the constant D_{ini} , where:

$$D_{ini} = 1 - \frac{\sigma_r}{\varepsilon_{0_1} E_1} \quad (4.20)$$

$\varepsilon_{0_1} = \frac{\sigma_t^{cri}}{E_1}$ is the state of strain in direction $\mathbf{1}$ the moment of the brittle failure of the element. So we assume that the cracking of the element has damaged it and we now have established a damage variable D with a lower bound D_{ini} .

The stresses are then picked up by the reduced elastic matrix, E'_1 , which is a probabilistic model parameter. The physical interpretation of E'_1 is the action of the steel bars with some residual friction from the surrounding concrete.

The evolution of stresses will be described by a damage model type of formulation. Similarly to the damage model for the concrete-rebar bond, Section 2.3.1.1, D is considered a state variable,

thus its evolution has to verify the following conditions:

$$\begin{cases} \dot{D} \geq 0 \\ D = \max(D_0, D) \end{cases} \quad (4.21)$$

Where D_0 is the initial damage state, and D is the actual damage state. The initial damage threshold (D_{ini} in this case) is established when the failure criterion is reached in the direction of the reinforcements. Once the element is declared as cracked (failure criteria reached) the damage evolution is then given by the following relations:

$$\begin{cases} D(\tilde{\varepsilon}) = D_0, & \tilde{\varepsilon} \leq \varepsilon_{01} \\ D(\tilde{\varepsilon}) = 1 - \frac{\sigma_r + E'_1(\tilde{\varepsilon} - \varepsilon_{01})}{E'_1 \tilde{\varepsilon}}, & \varepsilon_{01} < \tilde{\varepsilon} \leq \frac{\sigma^p - \sigma_r}{E'_1} + \varepsilon_{01} \end{cases} \quad (4.22)$$

Where $\tilde{\varepsilon} = \langle \varepsilon_1 \rangle_+$ ($\langle \cdot \rangle_+$ is the positive part of (\cdot)). This behavior is held until the (predetermined) yield limit of the steel, σ^p is reached.

To represent the plastic behavior of the reinforcements all we need to do is update the damage model. Note that we are not saying that plasticity is the same as damage, we just use the convenience of the damage formulation to represent the plastic behavior of the macro-element. Once the stresses in the element reach the yield limit of the steel, the behavior of the element will be represented as follows:

$$\boldsymbol{\sigma} = (1 - D)\mathbf{H}' \times \boldsymbol{\varepsilon} \quad (4.23)$$

And the damage evolution is now given by:

$$\begin{cases} D(\tilde{\varepsilon}) = 1 - \frac{\sigma^p - \sigma_r + E'_1 \varepsilon_{01}}{E'_1 \tilde{\varepsilon}}, & \tilde{\varepsilon} > \frac{\sigma^p - \sigma_r}{E'_1} + \varepsilon_{01} \end{cases} \quad (4.24)$$

Figure 4.33 summarizes how the model treats pre and post-cracking behavior in the direction parallel to the reinforcement.

Due to the particular formulation of the model, some limitations concerning the parameters arise in order to make sure that the model is mechanically sound.

Some conditions are more subtle than others. For instance, the following condition should be true at any time:

$$\sigma_r \geq E'_1 \varepsilon_{01} \quad (4.25)$$

This is necessary to ensure that in case of discharge, the cracked (but not yet yielding) element does not gain stiffness compared to its current state.

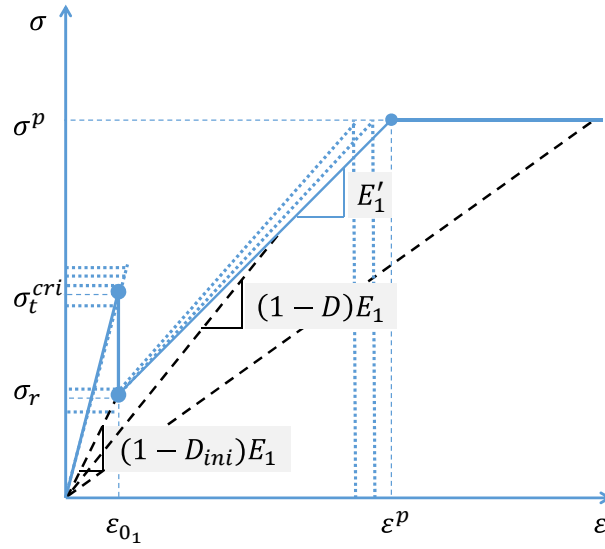


FIGURE 4.33: Probabilistic piece-wise linear model for macro elements of reinforced concrete, D.C.B. case study

Another important condition to validate is:

$$\frac{\sigma^p - \sigma_r + E'_1 \varepsilon_{01}}{E'_1} \leq \varepsilon_s^p \quad (4.26)$$

Where ε_s^p is the theoretical yielding strain of the steel bar(s) taken into account in the macro element. This condition is true because the contribution of the steel bar(s) plus the friction with the surrounding cracked concrete to the stiffness of the element, will always be greater than that of the rebar(s) alone.

4.2.6 Parameters Identification

At this point of the study, each ERC model still carries three unknown variables:

- σ_t^{cri} , the tensile strength of the uncracked element in the reinforcement direction.
- σ_r , the tensile strength in the element right after the drop in stresses resulting from the failure criterion being reached in the reinforcement direction. A sort of *tensile recovery*. For the sake of simplicity, σ_r will be a deterministic parameter, especially since the model is now rich enough by the addition of another parameter. Adding more complexity by implementing all probabilistic parameters is most likely unnecessary.
- E'_1 , the residual stiffness in direction **1**. It represents the stiffness of the elastic steel bars, plus friction with the cracked concrete matrix.

The parameters σ_t^{cri} and E'_1 are continuous and lower bounded by zero. Therefore, just like in the case of the macro model for the slab-beam, they will be represented by a *log-normal* distribution function.

A total of 5 unknown parameters have to be determined for each ERC macro model: the deterministic parameter σ_r , and the parametric model for each of σ_t^{cri} and E'_1 (4.9, 4.12).

The three types of numerical tie-beam calculations are run, with macro elements that behave according to the macro model assigned to each, with a predetermined shape and starting model parameters. The resulting force-displacement curves are then fitted to that of the equivalent micro modeled tie-beam tests (the training data, see Section 4.2.4). The best fit will determine the most suitable parameters to use. This classifies as an optimization problem, which we solve using RSM, Section 3.4.2.

The parameters resulting from the optimization scheme are the ones we input into each model for the final macro D.C.B. calculations, Table 4.7.

ERC type	Parameter	Symbol	Value in MPa
ERC5	Tensile strength	σ_t^{cri}	
	Mean	$\mu_{\sigma_t^{cri}}$	3.2
	Deviation	$\sigma_{\sigma_t^{cri}}$	0.4
	Tensile recovery	σ_r	1.3
	Residual stiffness	E'_1	
	Mean	$\mu_{E'_1}$	1000.
ERC10	Deviation	$\sigma_{E'_1}$	50.
	Tensile strength	σ_t^{cri}	
	Mean	$\mu_{\sigma_t^{cri}}$	3.05
	Deviation	$\sigma_{\sigma_t^{cri}}$	0.4
	Tensile recovery	σ_r	0.75
	Residual stiffness	E'_1	
ERC20	Mean	$\mu_{E'_1}$	390.
	Deviation	$\sigma_{E'_1}$	50.
	Tensile strength	σ_t^{cri}	
	Mean	$\mu_{\sigma_t^{cri}}$	3.4
	Deviation	$\sigma_{\sigma_t^{cri}}$	0.6
	Tensile recovery	σ_r	0.75
ERC20	Residual stiffness	E'_1	
	Mean	$\mu_{E'_1}$	550.
	Deviation	$\sigma_{E'_1}$	100.

TABLE 4.7: Macro model parameters for each type of ERC

4.2.7 Results

In the frame of the Monte Carlo method, 10 randomly sampled results from every type of numerical test mentioned hereafter are treated.

4.2.7.1 Numerical Tie-Beams

Numerical experimentation on the tie-beams yielded the load-displacement curves shown in Figures 4.34, 4.36 and 4.38. The results of the macroscopic approach shown here are the best fit to the results obtained with the micro approach. The parameters of the probabilistic macro-model for reinforced concrete are dynamically fitted to minimize the area between the two load-displacement curves (see Section 3.4).

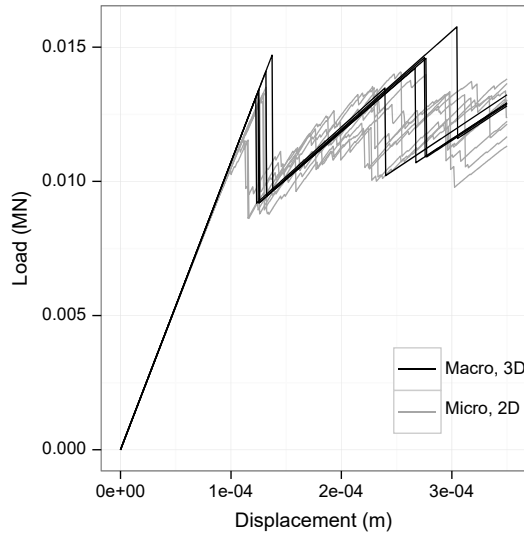


FIGURE 4.34: Numerical tie-beam, **ERC5**: Load-displacement curves

An interesting realization about the global behavior of the macro modeled tie-beams is that it subtly communicates information about the state of macrocracks in the tie-beam. Due to the characteristics of the macro model (Section 4.2.5.2), one can easily realize, only by looking at the global behavior of a macro tie-beam, that each sharp drop in stresses corresponds to the cracking of a macro element in that tie-beam. Which would mean that at the same stage of the calculation, a macro crack either is, or is about to settle in the equivalent micro tie-beam.

This becomes clear when comparing the cracking pattern in the tie-beams at different stages of the calculation. One example of this is the cracking pattern at the last stages of the calculation in the ERC5 tie-beam, Figure 4.35. Here we can see the formation of 2 macro cracks in the ERC5 macro tie-beam, Figure 4.35a, that correctly predicts the cracking profile observed

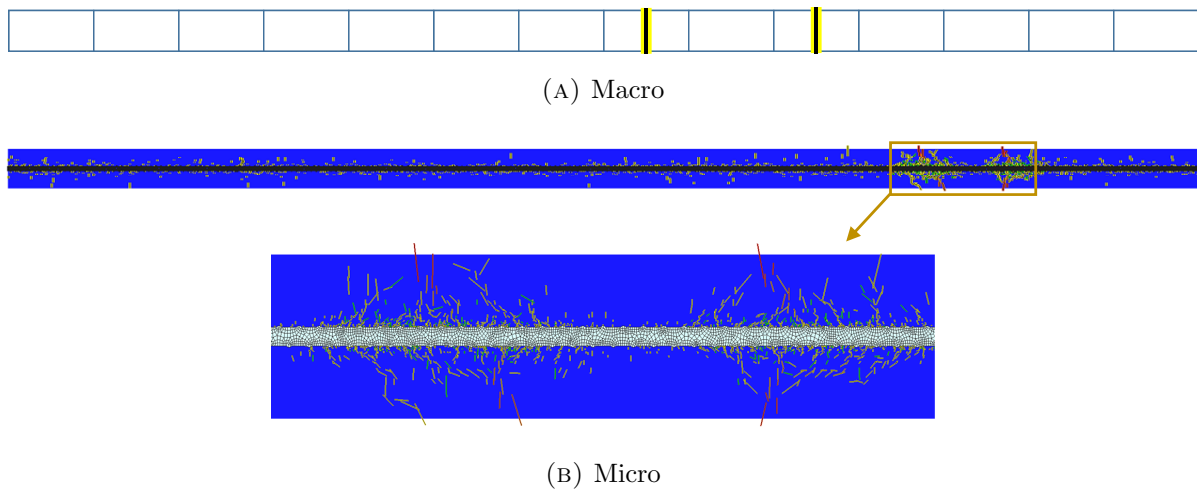


FIGURE 4.35: Numerical tie-beam, **ERC5**: Cracking pattern

in the corresponding micro tie-beam, Figure 4.35b. At the same time, we can draw a similar conclusion only by looking at the global behavior of the ERC5 tie-beam, Figure 4.34.

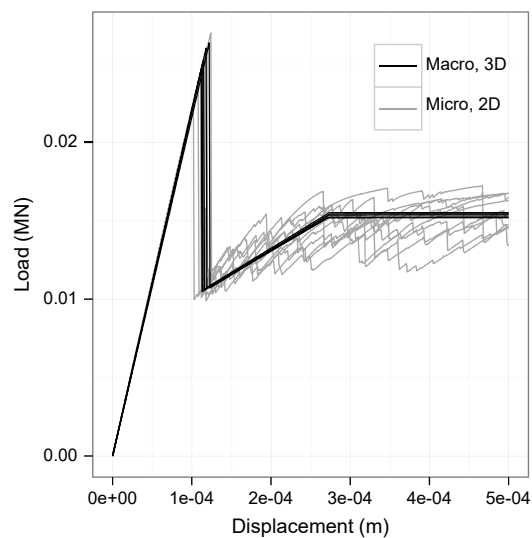


FIGURE 4.36: Numerical tie-beam, **ERC10**: Load-displacement curves

Following the same reasoning, by looking at the global results of the ERC10 macro tie-beam, Figure 4.36, we can predict that towards the later stages of the calculation, only 1 macro crack would have formed in the corresponding micro tie-beam. This again is verified by looking at the cracking pattern in the ERC10 macro tie-beam, Figure 4.37a, that once again correlates with that observed in the corresponding micro tie-beam, Figure 4.37b.

And again, the global behavior of the ERC20 tie-beam Figure 4.38 communicates the correct information about the cracking profile in Figure 4.40.

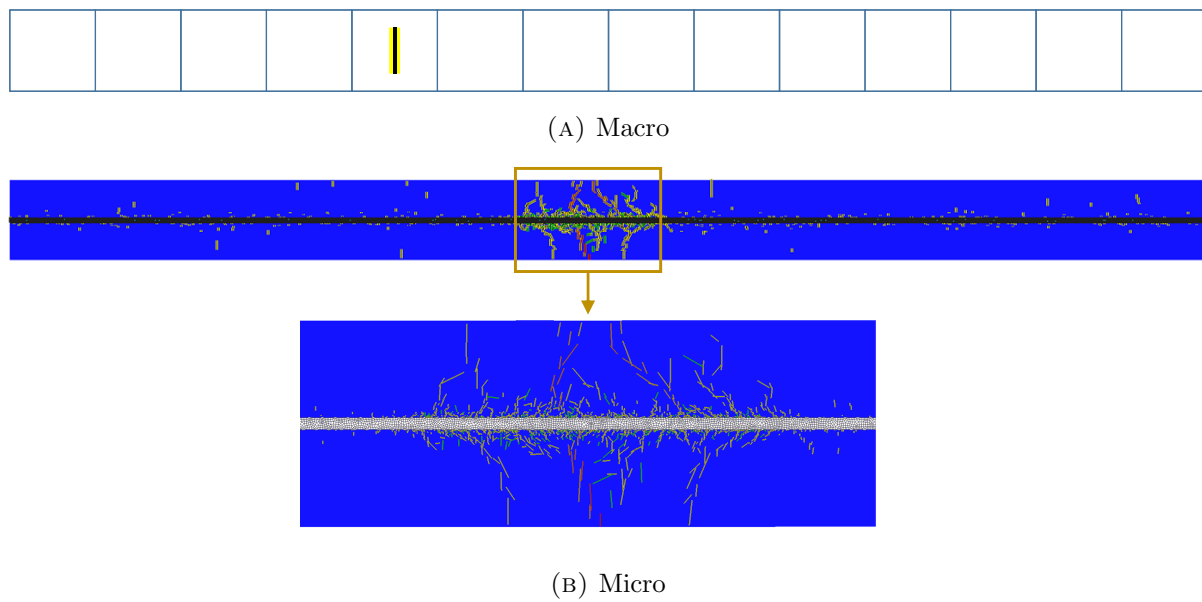


FIGURE 4.37: Numerical tie-beam, **ERC10**: Cracking pattern

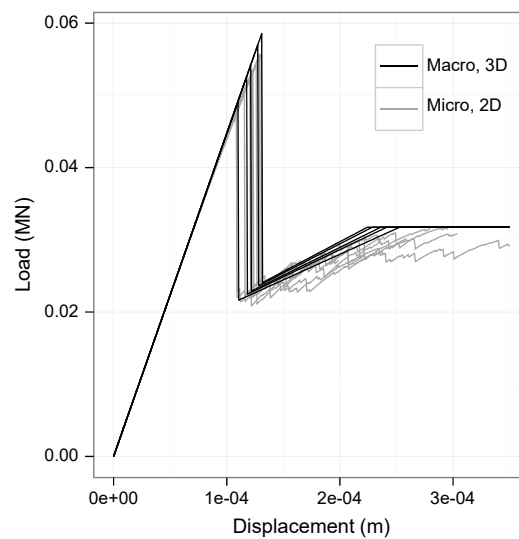


FIGURE 4.38: Numerical tie-beam, **ERC20**: Load-displacement curves

The actual statistical model does not, at any point in the learning process, take into account information about the cracking profile. Nonetheless, the macro model is able to replicate the same cracking profile, in terms of number and opening of macro cracks in the three types of tie-beams, as that of the micro model. This is possible simply by fitting the global response of the macro tie-beam to that of the micro tie-beam. This further justifies our starting hypothesis about the learning data consisting of the global response of a simple tie-beam subjected to tension, and how, when taken in the right context, can represent more complex phenomena like the cracking process in a structure.

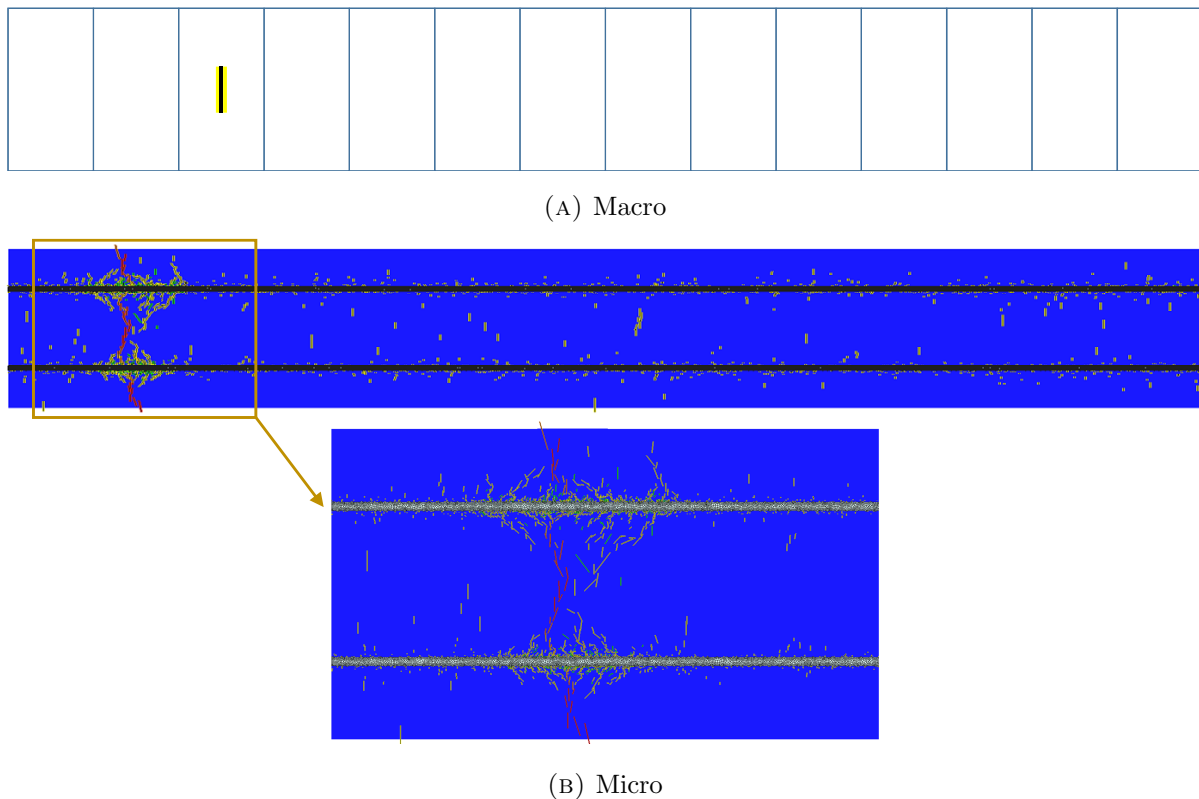


FIGURE 4.39: Numerical tie-beam, **ERC20**: Cracking pattern

In the next section we will implement the $3D$ macro elements in three macro D.C.B. tests and compare global and local results, as well as calculation costs, with results from a similar experimental study on a $2D$ D.C.B. using the local approach (see Section 4.2.2).

4.2.7.2 Numerical D.C.B.

The key macro model parameters resulting from the optimization scheme (Table 4.7) are now implemented into the macro-models in each D.C.B. for the final calculation.

The results from the final $3D$ macro D.C.B. calculations are represented in this section. By comparing the local (cracking) and global results with results from the $2D$ local approach D.C.B., we hope to achieve the same favorable outcome we had with the reinforced slab-beam test (Section 4.1.7.2), this time with the D.C.B., which would prove the effectiveness of the multi-scale strategy in a crack propagation setting.

Figures 4.40, 4.41 and 4.42 show perfect agreement between global results from the macro and local calculations, for all three types of macro D.C.B.s (with different ERCs, see Section 4.2.3). This further confirms our starting hypothesis, that states that a simple tie-beam tension test is a good predictor of the cracking behavior of the macro element even when used in a

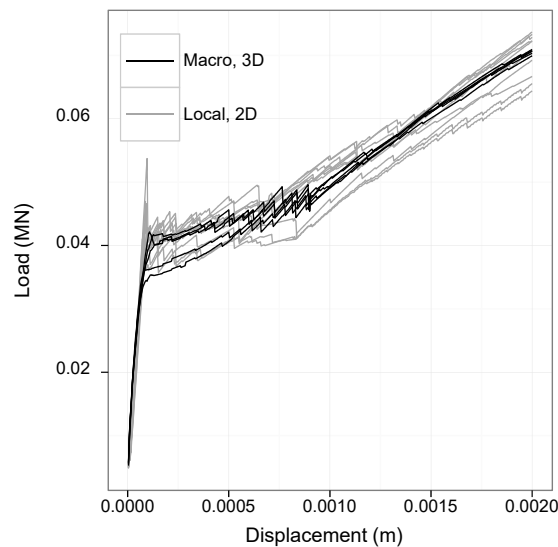


FIGURE 4.40: Numerical D.C.B, **ERC5**: Load-displacement curves

different structure under different boundary conditions. Furthermore, it shows how robust is the model with regard to the dimensions and composition of the macro elements.

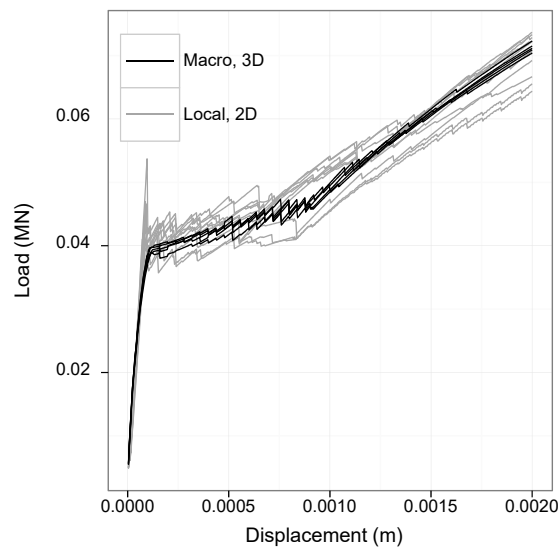


FIGURE 4.41: Numerical D.C.B, **ERC10**: Load-displacement curves

The cracking profile in the micro/macro D.C.B. can be visualized in Figure 4.43. A clear resemblance in the cracking pattern is observed. This is somewhat of an obvious result since the D.C.B. experiment is specially designed to localize the crack in order to study the crack propagation in concrete and reinforced concrete. Therefore only one single crack is observed along the middle part of the beam.

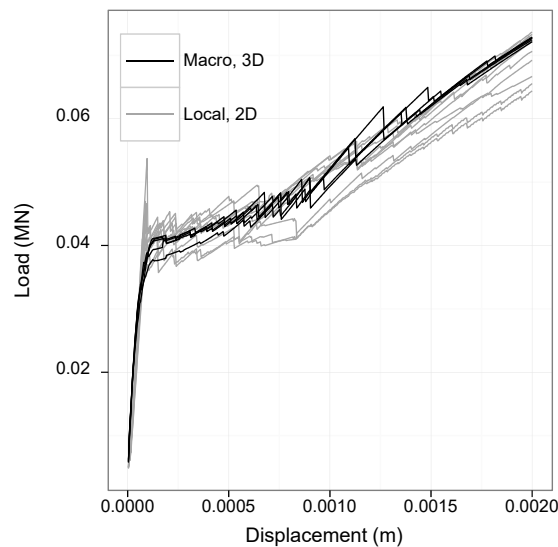


FIGURE 4.42: Numerical D.C.B, **ERC20**: Load-displacement curves

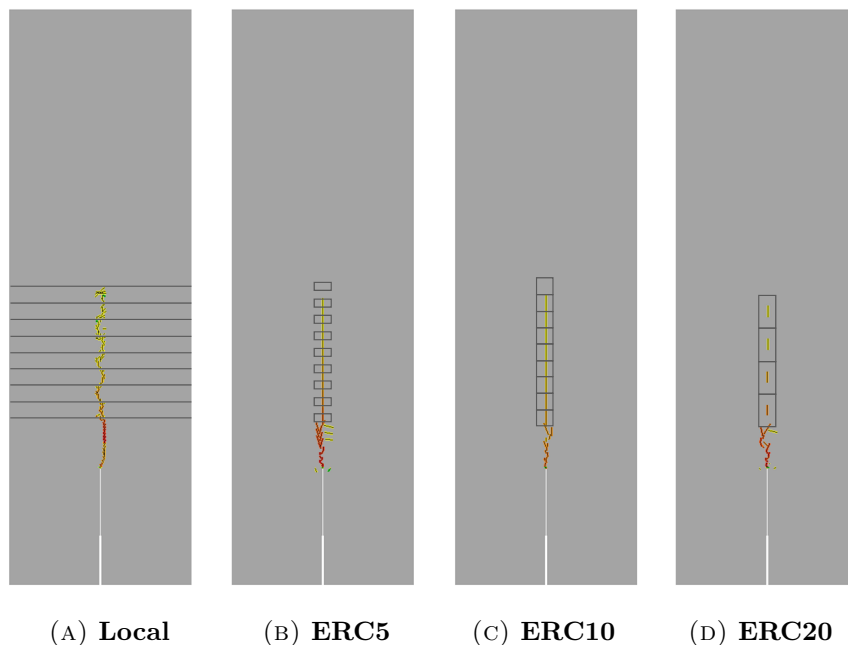


FIGURE 4.43: Numerical D.C.B: Cracking pattern

Data from the post-analysis reveals the following results of the cracking profile in the D.C.B., Figures 4.45, 4.46 and 4.47. Each graph is a plot of the crack opening in one randomly chosen 3D macro D.C.B. against another random 2D local D.C.B., out of a sample of 10; this is done for all three types of macro D.C.B.s and for different heights in the beam, Figure 4.44.

As expected, the macro model has no problem predicting the crack opening. Even the results from the ERC20 D.C.B. are very satisfying considering its unsuitable dimensions for the problem at hand, Figure 4.47.

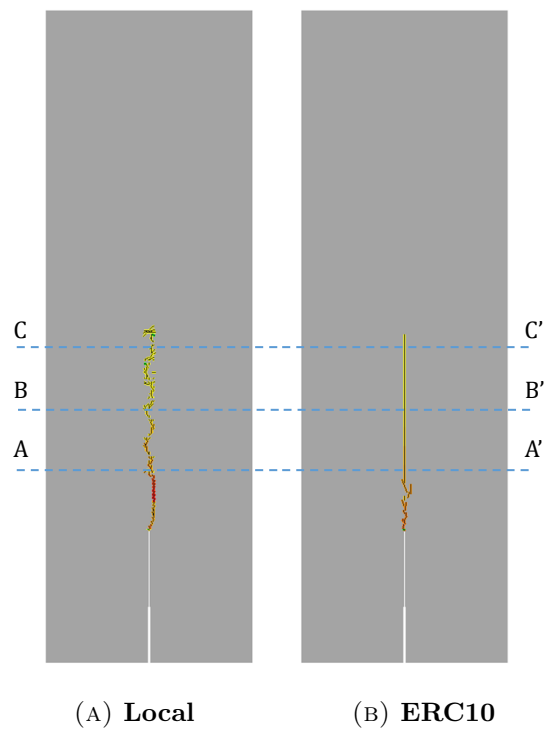


FIGURE 4.44: Numerical D.C.B: Crack width measurements at three different heights in the beam

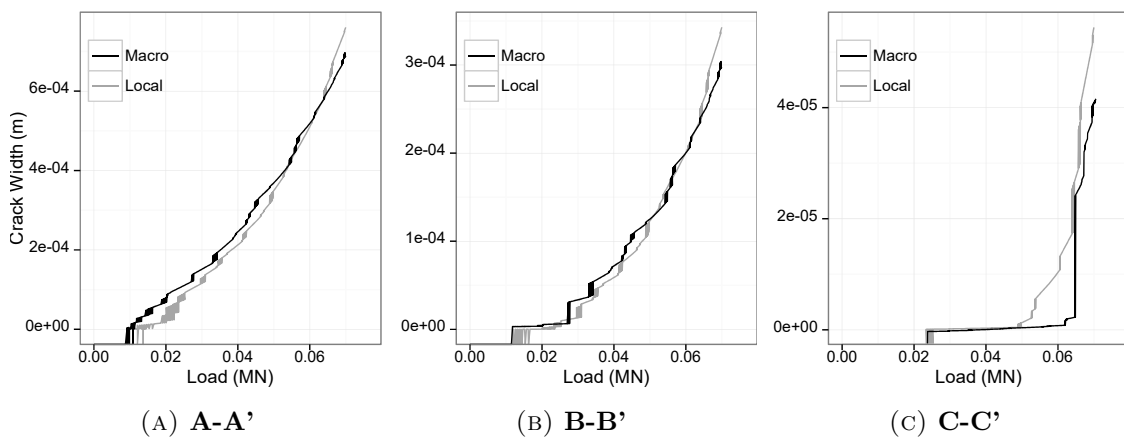
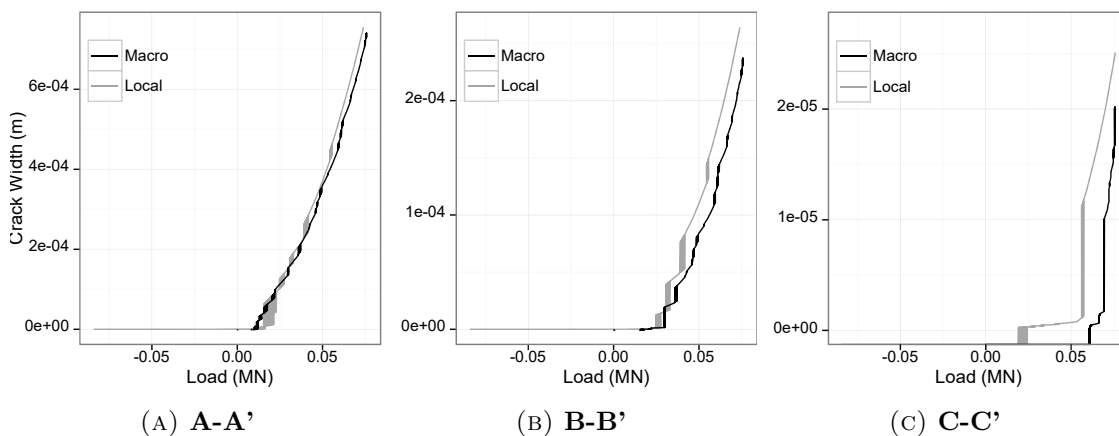
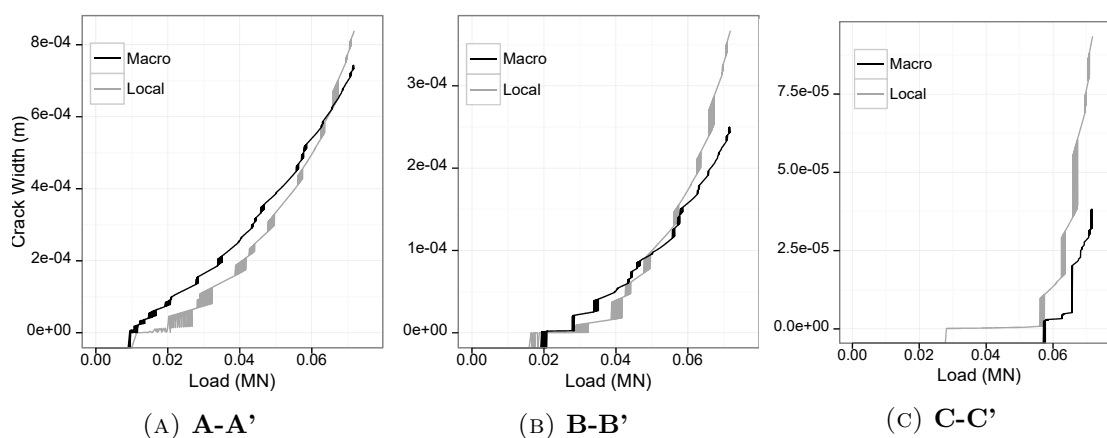


FIGURE 4.45: Numerical D.C.B, **ERC5**: Cracking profile

From the body of data collected from the D.C.B. macro tests, we can note the following:

- We were able to reproduce the global behavior in all three types of D.C.B.s to an impressive degree of accuracy.
- Measurements on the local scale (crack width), and at different heights in the beam, are also closely correlated.

FIGURE 4.46: Numerical D.C.B, **ERC10**: Cracking profileFIGURE 4.47: Numerical D.C.B, **ERC20**: Cracking profile

More importantly is the gain in calculation time that is brought about by the **Multi-scale Modeling Strategy** introduced in this work. In Table 4.8 we directly compare the average calculation time of the $2D$ local approach D.C.B. with that of the $3D$ macro approach.

Structure	Approach	Type	Calculation time (sec)
D.C.B.	$2D$, Local		~ 6400
			~ 3320
	$3D$, Macro	ERC5	~ 2970
		ERC20	~ 2890

TABLE 4.8: $3D$ Numerical D.C.B.: Computation time

This is not a fair criterion to base upon our evaluation of the multi-scale strategy, since a $3D$ calculation is naturally much more demanding in calculation time than a $2D$ one. The design and simulation of a $3D$ local approach D.C.B. is actually possible with the tools we have at hand but at the same time it is an insanely costly way to get the same information about the cracking profile in the D.C.B. that we can get using a much lighter $2D$ approach. So in order to get a more impartial understanding of the computational costs of the D.C.B., we

would have to compare both approaches in a $2D$ plane stresses framework. Parallel tests were run on $2D$ macro D.C.B.s and the average results are shown in Table 4.9.

Structure	Approach	Type	Calculation time (sec)
D.C.B.	2D, Local		~ 6400
	2D, Macro	ERC5	~ 1520
		ERC10	~ 1400
		ERC20	~ 1420

TABLE 4.9: $2D$ Numerical D.C.B.: Computation time

In conclusion, the macroscopic approach yields very reliable information about the global behavior as well as the cracking process in the D.C.B., using only about 23% of the computation time required by the local approach.

Finally, one might bring up the extra *incompressible time* (time consumed in order to evaluate the macro model parameters) that adds to the cost of the multi-scale strategy. Although in this case this does not really apply since a similar but even more expensive numerical experimentation campaign was necessary to determine the parameters of the local models used in the $2D$ local D.C.B. calculation. If all of the “background” numerical experiments for both approaches were to be taken into account, we would have ended up with about 30% for the time used by the multi-scale strategy compared to the local approach.

4.2.8 Discussion

The multi-scale strategy was applied in the special case of the D.C.B., where a probabilistic model for reinforced concrete elements was designed and tested for three different types of macro elements. The macro model design and parameter identification are the result of a learning algorithm with numerical experimentation on tie-beams subjected to tension acting as the learning data. The local models used in the numerical experimentation phase are: the *semi-explicit cracking model* for concrete, Section 2.1.2.2, and the *steel-concrete bond model*, Section 2.3.1.1. This particular study on the D.C.B. structure was chosen for multiple reasons:

- No previous numerical study was done on such a beam. This allowed us to test the multi-scale strategy in a setting that is as close as it gets to real world application.
- It served as a validation of the new generalized $3D$ macro model.
- The previous validation was done on a reinforced slab beam under three point bending, Section 4.1, where the prominent physical phenomenon that is taking place is crack creation. Whereas in the case of the D.C.B., only one macro crack develops and is maintained in the median plane to highlight the crack propagation.

- The 3D macro model is tested on three different types of macro elements, with different dimensions and composition (number of reinforcing steel bars in the element). The idea was to test the adaptive qualities of the model in rendering the numerical approach insensitive to the dimensions and composition of the macro element. This greatly increases the confidence in the multi-scale strategy, as well as its utility range.

The 3D numerical simulations have once more shown that the proposed scientific methodology is viable: the global behavior of the D.C.B. structure was correctly predicted, and the crack pattern and opening is consistent with the results drawn from the local approach.

Furthermore, the reduction in calculation time brought about by the multi-scale strategy is very noticeable, and at no risk whatsoever (no loss in information at the macroscopic level).

4.3 Reflections on the Macro Model Design

We've presented in this chapter, 2 validation examples of the multi-scale modeling strategy: the **Reinforced Slab-Beam**, Section 4.1, and the **Reinforced D.C.B.**, Section 4.2. The different aspects of each case were brought forth individually, but one aspect in particular merits further investigation, and that is the design of the macroscopic model for the reinforced concrete macro element. The macro model is case-specific and specially tailored to the problem at hand.

The macro model designed for the macro elements in the **Reinforced Slab-Beam**, Section 4.1.4.2, is a probabilistic piece-wise linear model with a “switch” behavior at the transition point (from virgin element to cracked element). Once the brittle failure occurs, stresses in the element plunge to zero, then we switch to a behavior that is completely piloted by the steel bars, as the stresses are picked up by a reduced elastic matrix representing the remaining contribution of the rebars with some residual action from the surrounding concrete (in the form of friction), Figure 4.9.

This type of model is well suited for the reinforced concrete macro elements in the slab-beam, Section 4.1.2, for the following reasons:

- The macro element represents a large volume of reinforced concrete ($4.2 \times 80\text{cm}^2$, Figure 4.6) which means that the brittle failure of such an element is very pronounced, thus allowing us to approximate the failure of the macro element to that of a structural element.
- Due to the nature of our problem, many macro elements in the width of the slab-beam will crack, transferring stresses to a reduced elastic matrix representing the elastic steel bars and friction with the surrounding concrete. This de-emphasizes the influence of the concrete volume at the time of failure of the element.

In the **Reinforced D.C.B.** example, the macro model is probabilistic, piece-wise linear, with an extra model parameter representing the “tensile recovery” of the reinforced concrete element right after failure, Figure 4.33. This type of model is more suited for the macro elements in the D.C.B., Section 4.2.3, for the following reasons:

- Here, The macro element represents a relatively small volume of reinforced concrete (**ERC10**: $10 \times 10 \times 10\text{cm}^3$) not large enough to be considered a structural element. In this case, the phenomenon of tension stiffening has much more impact on the cracking process. The macro element that does not crack completely but undergoes progressive microcracking (strain softening).
- The fact that only one macro crack forms in the D.C.B. and is kept in the median plane, means that the macro model needs to provide a fine description of the crack initiation in each macro element lays on the crack path.

From a purely numerical point of view, the D.C.B. macro model is more complex/complete than the slab-beam model, in the sense that it can replace it and still yield the correct results in the slab-beam calculation (given that the correct model parameters were identified).

This was actually verified and found to be true, that when implemented in the case of the *2D* slab-beam, the more complete model is just as accurate as the specially tailored one.

Chapter 5

Conclusions and Prospects

5.1 Conclusions

We introduced in this work a new multi-scale strategy to develop probabilistic models for reinforced concrete structures. This multi-scale strategy consists in building macro models for reinforced concrete macro elements based on numerical experiments using a validated local approach. The strategy is a sort of a multi-steps process that takes over the whole modelization of the structure in the framework of the finite element method. It goes as follows:

1. We start off by meshing, or in our particular case, “partitioning” the global structure. It’s a process for sampling different groups of macro elements of reinforced concrete within a structure with respect to their dimensions and constitution (concrete used and rebars type, number, position and orientation). The most optimal partitioning is defined according to certain rules that depend on characteristics (or measures) of the macro elements like size, complexity, and regularity, Section 3.2.
2. In the framework of supervised learning, we design a set of training data from which we wish to construct prediction rules for a certain complex function. In our case, we wish to predict the cracking behavior of reinforced concrete elements within a certain structural setting. Knowing that cracking is almost always caused by, and perpendicular to, the tension stresses in an element, a strong assumption is made, which states that the macro element’s cracking process is directly linked to the stress field in the element. Therefore, a suitable test to simulate the cracking process in a macro element in the direction of the reinforcement(s) would be a tie-beam under tension. The tie-beam consists of a succession of reinforced concrete macro elements, long enough to get a representative cracking pattern for such an element, Section 3.3.1.

3. Numerical simulations are run to get the global response as well as information about the cracking process in the tie-beam. To achieve that we use validated local models. The models used on the tie-beam tests are usually the same ones we would have had to use to run the structural simulation on the global structure. The local models have no influence on the methodology whatsoever, their sole purpose is to give reliable information about the global behavior and the cracking process in the designed tie-beam. The results from the tie-beam numerical experiments acts as our training data, the means by which we get this data (as long as it's reliable) is of no concern to the unfolding of the multi-scale strategy.

The Local-Macro Multi-Scale Strategy can be applied as long as we have at our disposition validated models that can faithfully represent the behavior at the scale of interest.

4. Choice of the learning algorithm. Now that we've gathered the training set, it's time to determine the input features that are the most representative of the learned function. To that end, we chose a simple parametric model to infer the predictive function. Therefore, the macro model will consist of a simple piece-wise linear model acting on the macro element in the direction of the reinforcement(s). The model parameters will be fitted such that the macro tie-beam yields the same results as the local tie-beam, Section 3.3.2.
5. An optimization scheme using RSM (Response Surface Methodology) is set in place in order to find the correct set of parameters for the macro model, Section 3.4.
6. The final calculation on the global structure can be run using the macro models in the macroscopic discretization of the structure.

We ran 2 validation examples to show how to apply the multi-scale strategy to different structural problems.

As a first validation of this Multi-Scale Modeling Strategy, a previously studied case of a slab-beam structural element subjected to three point bending is proposed. The numerical simulations (in 2D, plane stresses) have shown that the scientific approach proposed is promising: the global behavior of the structure is correctly predicted, and the macro-cracking pattern is consistent with results given by the local approach. In the process, some information on the total number of cracks is lost (which was expected), but the information about the larger crack opening is relevant. The main objective of the multi-scale strategy was to reduce the massive computational time required to get information about the cracking process in large structures. Even after taking into account the incompressible time consumed by the study (which would become negligible when applying the strategy on large structures), the multi-scale modeling strategy produced reliable information about the cracking process in the structure in less than 20% of the calculation time required using the local approach.

Afterwards, we implemented a generalized form of the multi-scale strategy (in $3D$) in the special case of the D.C.B. (Double Cantilever Beam) structure. This study allowed us to test the multi-scale modeling strategy in a setting that can be considered as that of a real world application. The $3D$ macro model was vetted against three types of macro elements to test the adaptive capacity of the strategy regarding the macro element's dimensions and composition. The numerical simulations have shown once more that the proposed multi-scale modeling strategy can correctly predict the global behavior of the structure, and gives similar information about the cracking process (crack opening, path, etc...) as that obtained when applying the local approach, using only about 23% of the computational time required by the latter.

5.2 Prospects

Some perspectives can be proposed concerning studies following the present thesis work:

- Even though we implemented and validated the strategy in its generalized $3D$ form, we still haven't tested the viability of the approach in the case of a complex multi-directionally reinforced concrete element. Theoretically speaking, this shouldn't affect the followed approach, but the fact that the macro element could potentially break and switch to a different state in more than one direction, means that we might need to look into a possible link between the state of the macro element in each direction of the reinforcement. We could say that when the macro element breaks in one direction it should then stay elastic in all other directions. The other option is either to have one unique state for the macro element (which means that when it breaks in one direction, the crack direction is perpendicular to it, but it is considered broken in all other directions as well), or a perfect decoupling of the different states in each direction in the macro element (which means that we could have up to three cracks—one in each of the principal directions—in an element). We were unfortunately unable to test the strategy on multi-directionally reinforced concrete structures mainly because of the lack of reliable data on the cracking process for such structures.
- The validation tests were both performed under monotonically increasing loading and so we disregarded (in the macro model's constitution) the permanent deformations due to the yielding of the rebars. This is another point that we can address, which is the ability of the macro model to take into account cyclic loading.

Finally, concerning the extent of the application of the multi-scale modeling strategy, a future objective would be to consider a cracking-transfer type of coupling that would be able to

solve complex problems of air/liquid diffusion across a volume of reinforced concrete with the efficiency and low calculation cost brought about by the strategy.

Bibliography

- Andrieux Stéphane, Bamberger Yves, and Marigo J-J. Un modèle de matériau microfissuré pour les bétons et les roches. *Journal de mécanique théorique et appliquée*, 5(3):471–513, 1986.
- Andriotis Ch, Gkimousis I, and Koumousis V. Modeling reinforced concrete structures using smooth plasticity and damage models. *Journal of Structural Engineering*, 142(2):04015105, 2015.
- Armero Francisco and Garikipati Krishna. An analysis of strong discontinuities in multiplicative finite strain plasticity and their relation with the numerical simulation of strain localization in solids. *International Journal of Solids and Structures*, 33(20):2863–2885, 1996.
- Babuska I and Melenk JM. The partition of unity finite element method. Technical report, DTIC Document, 1995.
- Bažant Zdenek P and Planas Jaime. *Fracture and size effect in concrete and other quasibrittle materials*, volume 16. CRC press, 1997.
- Bažant Zdeněk P and Raftshol Warren J. Effect of cracking in drying and shrinkage specimens. *Cement and Concrete Research*, 12(2):209–226, 1982.
- Bažant Zdenek P, Bishop Finley C, and Chang Ta-Peng. Confined compression tests of cement paste and concrete up to 300 ksi. In *Journal Proceedings*, volume 83, pages 553–560, 1986.
- Bažant Zdeněk P and Jirásek Milan. Nonlocal integral formulations of plasticity and damage: survey of progress. *Journal of Engineering Mechanics*, 128(11):1119–1149, 2002.
- Bažant Zdeněk P and Oh Byung H. Crack band theory for fracture of concrete. *Matériaux et construction*, 16(3):155–177, 1983.
- Bažant Zdeněk P and Yavari Arash. Is the cause of size effect on structural strength fractal or energetic–statistical? *Engineering Fracture Mechanics*, 72(1):1–31, 2005.
- Bažant Zdeněk P and Yavari Arash. Response to a. carpinteri, b. chiaia, p. cornetti and s. puzzis comments on is the cause of size effect on structural strength fractal or energetic-statistical?. *Engineering Fracture Mechanics*, 74(17):2897–2910, 2007.

- Benkirane ME. *Propagation d'une fissure dans le béton précontraint-interaction avec des armatures passives*. PhD thesis, Université de technologie de Compiègne, 1982.
- Bentley Jon Louis and Ottmann Thomas A. Algorithms for reporting and counting geometric intersections. *IEEE Transactions on computers*, 100(9):643–647, 1979.
- Bornert M, Bretheau Th, and Gilormini P. Homogénéisation en mécanique des matériaux. *Hermes Science Europe, Stanmore, UK*, 2001.
- Bruggi M, Casciati S, and Faravelli L. Cohesive crack propagation in a random elastic medium. *Probabilistic Engineering Mechanics*, 23(1):23–35, 2008.
- BSI British Standards Institution. *Eurocode 2: Design of Concrete Structures: Part 1-1: General Rules and Rules for Buildings*. British Standards Institution, 2004.
- Carpinteri Alberto and Puzzi Simone. The fractal-statistical approach to the size-scale effects on material strength and toughness. *Probabilistic Engineering Mechanics*, 24(1):75–83, 2009.
- Carpinteri Alberto, Chiaia Bernardino, and Ferro Giuseppe. Size effects on nominal tensile strength of concrete structures: multifractality of material ligaments and dimensional transition from order to disorder. *Materials and Structures*, 28(6):311–317, 1995.
- Carpinteri Alberto, Chiaia Bernardino, Cornetti Pietro, and Puzzi Simone. Comments on is the cause of size effect on structural strength fractal or energetic-statistical? by bažant & yavari [engng fract mech 2005; 72: 1–31]. *Engineering Fracture Mechanics*, 74(17):2892–2896, 2007.
- Carpinteri Alberto. Fractal nature of material microstructure and size effects on apparent mechanical properties. *Mechanics of materials*, 18(2):89–101, 1994.
- CEB-FIP Code. Fib model code for concrete structures 2010. *Document Competence Center Siegmur Kästl eK, Germany*, 2010.
- Cedolin Luigi and Bažant Zdeněk P. Effect of finite element choice in blunt crack band analysis. *Computer Methods in Applied Mechanics and Engineering*, 24(3):305–316, 1980.
- Colliat Jean-Baptiste, Hautefeuille Martin, Ibrahimbegovic Adnan, and Matthies Hermann G. Stochastic approach to size effect in quasi-brittle materials. *Comptes Rendus Mécanique*, 335(8):430–435, 2007.
- Combescure Christelle, Dumontet Hélène, and Voltaire François. Homogenised constitutive model coupling damage and debonding for reinforced concrete structures under cyclic solicitations. *International Journal of Solids and Structures*, 50(24):3861–3874, 2013.
- Cope RJ, Rao PV, Clark LA, and Norris P. Modelling of reinforced concrete behaviour for finite element analysis of bridge slabs. *Numerical Methods for Nonlinear Problems, Pineridge Press, Swansea*, 1980:457–470, 1980.

- Cosserat Eugène, Cosserat François, et al. Théorie des corps déformables. 1909.
- Darby AP, Blakeborough A, and Williams MS. Improved control algorithm for real-time sub-structure testing. *Earthquake engineering & structural dynamics*, 30(3):431–448, 2001.
- DE RHJ PEERLINGS R and De Vree JHP. Gradient enhanced damage for quasi-brittle materials. *International Journal for numerical methods in engineering*, 39:3391–3403, 1996.
- De Borst R and Nauta P. Non-orthogonal cracks in a smeared finite element model. *Engineering Computations*, 2(1):35–46, 1985.
- Dolbow JOHN and Belytschko Ted. A finite element method for crack growth without remeshing. *International journal for numerical methods in engineering*, 46(1):131–150, 1999.
- Feenstra Peter H and De Borst René. A plasticity model and algorithm for mode-i cracking in concrete. *International Journal for Numerical Methods in Engineering*, 38(15):2509–2529, 1995.
- Frémond Michel and Nedjar Boumediene. Damage in concrete: the unilateral phenomenon. *Nuclear engineering and design*, 156(1):323–335, 1995.
- Friedman Jerome, Hastie Trevor, and Tibshirani Robert. *The elements of statistical learning*, volume 1. Springer series in statistics Springer, Berlin, 2001.
- Galilei Ferdinando, Galileo. *Dialogo sopra i due massimi sistemi del mondo*. Rizzoli, 1632.
- Giry Cédric, Dufour Frédéric, and Mazars Jacky. Stress-based nonlocal damage model. *International Journal of Solids and Structures*, 48(25):3431–3443, 2011.
- Giusti SM, Blanco PJ, de Souza Neto EA, and Feijóo RA. An assessment of the gurson yield criterion by a computational multi-scale approach. *Engineering Computations*, 26(3):281–301, 2009.
- Guedes JPSCM, Pegon P, and Pinto AV. A fibre timoshenko beam element in castem 2000. *special publication Nr. I*, 94, 1994.
- Häussler-Combe Ulrich. *Computational methods for reinforced concrete structures*. John Wiley & Sons, 2014.
- Hill Rodney. Elastic properties of reinforced solids: some theoretical principles. *Journal of the Mechanics and Physics of Solids*, 11(5):357–372, 1963.
- Huespe Alfredo E and Oliver Javier. Crack models with embedded discontinuities. In *Numerical Modeling of Concrete Cracking*, pages 99–159. Springer, 2011.

- Huguet Miquel, Voldoire François, Kotronis Panagiotis, and Erlicher Silvano. Homogenized global nonlinear constitutive model for rc panels under cyclic loadings. In *11th World Congress on Computational Mechanics (WCCM XI)*. Barcelona, 2014.
- Humbert Pierre, Dubouchet Alain, Fezens Gérard, and Remaud David. Cesar-lcpc: A computation software package dedicated to civil engineering uses. *Bulletin des laboratoires des ponts et chaussées*, 256(257):7–37, 2005.
- Hurlbut Bryan Jackson. *Experimental and computational investigation of strain-softening in concrete*. 1985.
- Ibrahimbegovic Adnan, Colliat Jean-Baptiste, Hautefeuille Martin, Brancherie Delphine, and Melnyk Sergiy. Probability based size effect representation for failure in civil engineering structures built of heterogeneous materials. In *Computational Methods in Stochastic Dynamics*, pages 291–313. Springer, 2011.
- Irwin GR. Linear fracture mechanics, fracture transition, and fracture control. *Engineering Fracture Mechanics*, 1(2):241–257, 1968.
- Khuri André I and Mukhopadhyay Siuli. Response surface methodology. *Wiley Interdisciplinary Reviews: Computational Statistics*, 2(2):128–149, 2010.
- Kouznetsova VG, Geers MGD, and Brekelmans WAM. Multi-scale second-order computational homogenization of multi-phase materials: a nested finite element solution strategy. *Computer Methods in Applied Mechanics and Engineering*, 193(48):5525–5550, 2004.
- Ladevèze Pierre, Passieux J-C, and Néron David. The latin multiscale computational method and the proper generalized decomposition. *Computer Methods in Applied Mechanics and Engineering*, 199(21):1287–1296, 2010.
- Markovic Damijan and Ibrahimbegovic Adnan. On micro–macro interface conditions for micro scale based fem for inelastic behavior of heterogeneous materials. *Computer Methods in Applied Mechanics and Engineering*, 193(48):5503–5523, 2004.
- MATIERE®. Experimental results of rc beam-slabs tests. Technical report, MATIERE®, 2011.
- Matsui Kazumi, Terada Kenjiro, and Yuge Kohei. Two-scale finite element analysis of heterogeneous solids with periodic microstructures. *Computers & Structures*, 82(7):593–606, 2004.
- Mazars Jacky. *Application de la mécanique de l’endommagement au comportement non linéaire et à la rupture du béton de structure*. PhD thesis, 1984.
- Melenk Jens M and Babuška Ivo. The partition of unity finite element method: basic theory and applications. *Computer methods in applied mechanics and engineering*, 139(1):289–314, 1996.

- Michel JC, Moulinec H, and Suquet P. Effective properties of composite materials with periodic microstructure: a computational approach. *Computer methods in applied mechanics and engineering*, 172(1):109–143, 1999.
- Miehe Christian, Schotte Jan, and Schröder Jörg. Computational micro–macro transitions and overall moduli in the analysis of polycrystals at large strains. *Computational Materials Science*, 16(1):372–382, 1999.
- Moës Nicolas and Belytschko Ted. Extended finite element method for cohesive crack growth. *Engineering fracture mechanics*, 69(7):813–833, 2002.
- Myers Raymond H, Montgomery Douglas C, and Anderson-Cook Christine M. *Response surface methodology: process and product optimization using designed experiments*. John Wiley & Sons, 2016.
- Ngo D and Scordelis AC. Finite element analysis of reinforced concrete beams. In *Journal Proceedings*, volume 64, pages 152–163, 1967.
- Nguyen QS, Germain P, and Suquet P. Continuum thermodynamics. *J Appl Sci*, 50:1010–1020, 1983.
- Oliver J. Modelling strong discontinuities in solid mechanics via strain softening constitutive equations. part 1: Fundamentals. *International journal for numerical methods in engineering*, 39(21):3575–3600, 1996.
- Parsons Thomas J, GangaRao Hota VS, and Peterson William C. Macro-element analysis. *Computers & structures*, 20(5):877–883, 1985.
- Peerlings RHJ, De Borst R, Brekelmans WAM, and Geers MGD. Gradient-enhanced damage modelling of concrete fracture. *Mechanics of Cohesive-frictional Materials*, 3(4):323–342, 1998.
- Pellegrino C, Galvanetto U, and Schrefler BA. Numerical homogenization of periodic composite materials with non-linear material components. *International Journal for Numerical Methods in Engineering*, 46(10):1609–1637, 1999.
- Perić D, de Souza Neto EA, Feijóo RA, Partovi M, and Molina AJ. On micro-to-macro transitions for multi-scale analysis of non-linear heterogeneous materials: unified variational basis and finite element implementation. *International Journal for Numerical Methods in Engineering*, 87(1-5):149–170, 2011.
- Phan Thanh Song, Tailhan Jean-Louis, and Rossi Pierre. 3d numerical modelling of concrete structural element reinforced with ribbed flat steel rebars. *Structural Concrete*, 14(4):378–388, 2013.

- Phan TS, Tailhan J-L, Rossi P, Bressolette Ph, and Mezghani F. Numerical modeling of the rebar/concrete interface: case of the flat steel rebars. *Materials and structures*, 46(6):1011–1025, 2013.
- Phan Thanh Song, Rossi Pierre, and Tailhan Jean-Louis. Numerical modelling of the concrete/rebar bond. *Cement and Concrete Composites*, 59:1–9, 2015.
- Phan Thanh Song. *Modélisation numérique de l'interface acier-béton: application au comportement des structures en béton renforcées par des aciers plats crantés*. PhD thesis, UNIVERSITE PARIS EST, 2012.
- Pietruszczak ST and Mroz Z. Finite element analysis of deformation of strain-softening materials. *International Journal for Numerical Methods in Engineering*, 17(3):327–334, 1981.
- Pijaudier-Cabot Gilles and Bažant Zdenek P. Nonlocal damage theory. *Journal of engineering mechanics*, 113(10):1512–1533, 1987.
- Proix JM, Laurent N, Hemon P, and Bertrand G. Code aster, manuel de référence. *Fascicule R*, 8, 2000.
- Ragueneau F, La Borderie Ch, and Mazars J. Damage model for concrete-like materials coupling cracking and friction, contribution towards structural damping: rst uniaxial application. *Mech Cohes Frict Mater*, 5:607625, 2000.
- Rashid YR. Ultimate strength analysis of prestressed concrete pressure vessels. *Nuclear engineering and design*, 7(4):334–344, 1968.
- Rastiello Giuseppe, Tailhan Jean-Louis, Rossi Pierre, and Dal Pont Stefano. Macroscopic probabilistic cracking approach for the numerical modelling of fluid leakage in concrete. *Annals of Solid and Structural Mechanics*, 7(1-2):1–16, 2015.
- Rastiello Giuseppe. *Influence de la fissuration sur le transfert de fluides dans les structures en béton. Stratégies de modélisation probabiliste et étude expérimentale*. PhD thesis, Université Paris-Est, IFSTTAR, 2013.
- Richard Benjamin and Ragueneau Frédéric. Continuum damage mechanics based model for quasi brittle materials subjected to cyclic loadings: Formulation, numerical implementation and applications. *Engineering Fracture Mechanics*, 98:383–406, 2013.
- Rossi P and Richer S. Numerical modelling of concrete cracking based on a stochastic approach. *Materials and Structures*, 20(5):334–337, 1987.
- Rossi P and Wu X. Probabilistic model for material behaviour analysis and appraisalment of concrete structures. *Magazine of concrete research*, 44(161):271–280, 1992.

- Rossi P, Brühwiler E, Chhuy S, Jenq YS, and Shah SP. Fracture properties of concrete as determined by means of wedge splitting tests and tapered double cantilever beam tests. *Fracture mechanics test methods for concrete, Chapman & Hall, London*, pages 87–128, 1991.
- Rossi P, Van Mier JGM, Boulay C, and Le Maou F. The dynamic behaviour of concrete: influence of free water. *Materials and Structures*, 25(9):509–514, 1992.
- Rossi P, Wu X, Le Maou F, and Belloc A. Effet d'échelle sur le comportement du béton en traction. *Bulletin de liaison des Laboratoires des Ponts et Chaussées*, (182), 1992.
- Rossi P, Wu X, Le Maou F, and Belloc A. Experimental study on the scale effect on concrete in tension. In *Probabilities and Materials*, pages 131–139. Springer, 1994.
- Rossi P, Wu X, Le Maou F, and Belloc A. Scale effect on concrete in tension. *Materials and Structures*, 27(8):437–444, 1994.
- Rossi Pierre, Ulm Franz-Josef, and Hachi Fatiha. Compressive behavior of concrete: physical mechanisms and modeling. *Journal of Engineering Mechanics*, 122(11):1038–1043, 1996.
- Rossi Pierre. Fissuration du béton: du matériau à la structure-application de la mécanique linéaire de la rupture. *These présentée pour obtenir le grade de docteur de l'école nationale des ponts et chaussées-spécialité: mécanique et matériaux*, 1986.
- Rossi P. Comportement dynamique des bétons: du matériau à la structure. In *Annales de l'Institut technique du bâtiment et des travaux publics*, number 511, pages 25–39. Institut technique du bâtiment et des travaux publics, 1993.
- Saouma VE and Fava G. On fractals and size effects. *International journal of fracture*, 137(1-4):231–249, 2006.
- Sellier Alain and Millard Alain. Weakest link and localisation w12: a method to conciliate probabilistic and energetic scale effects in numerical models. *European journal of environmental and civil engineering*, 18(10):1177–1191, 2014.
- Simo JC and Oliver J. A new approach to the analysis and simulation of strain softening in solids. *Fracture and damage in quasibrittle structures*, pages 25–39, 1994.
- Smith Shawn H. *On fundamental aspects of concrete behavior*. 1987.
- Spacone Enrico, Filippou Filip C, and Taucer Fabio F. Fibre beam-column model for non-linear analysis of r/c frames: Part i. formulation. *Earthquake engineering and structural dynamics*, 25(7):711–726, 1996.
- Speirs DCD, de Souza Neto EA, and Perić D. An approach to the mechanical constitutive modelling of arterial tissue based on homogenization and optimization. *Journal of biomechanics*, 41(12):2673–2680, 2008.

- Su XT, Yang ZJ, and Liu GH. Monte carlo simulation of complex cohesive fracture in random heterogeneous quasi-brittle materials: A 3d study. *International Journal of Solids and Structures*, 47(17):2336–2345, 2010.
- Sun Bin, Wang Xuan, and Li Zhaoxia. Meso-scale image-based modeling of reinforced concrete and adaptive multi-scale analyses on damage evolution in concrete structures. *Computational Materials Science*, 110:39–53, 2015.
- Suquet PM. Overall potentials and extremal surfaces of power law or ideally plastic composites. *Journal of the Mechanics and Physics of Solids*, 41(6):981–1002, 1993.
- Syroka-Korol E, Tejchman J, and Mróz Z. Fe calculations of a deterministic and statistical size effect in concrete under bending within stochastic elasto-plasticity and non-local softening. *Engineering Structures*, 48:205–219, 2013.
- Tailhan J-L, Dal Pont Stefano, and Rossi Pierre. From local to global probabilistic modeling of concrete cracking. *Annals of Solid and Structural Mechanics*, 1(2):103–115, 2010.
- Tailhan JL, Rossi P, Phan T, and Foulliaron J. Probabilistic modelling of crack creation and propagation in concrete structures: some numerical and mechanical considerations. *SSCS-2012*, 2012.
- Terada Kenjiro and Kikuchi Noboru. A class of general algorithms for multi-scale analyses of heterogeneous media. *Computer methods in applied mechanics and engineering*, 190(40):5427–5464, 2001.
- Terada K, Inugai T, and Hirayama N. A method of numerical material testing in nonlinear multiscale material analyses. *Transactions of the Japan Society of Mechanical Engineering A*, 74:1084–1094, 2008.
- Toutlemond Francois and Rossi Pierre. Free water in concrete pores: an attempt of physical explanation of concrete dynamic behavior. *Special Publication*, 175:261–280, 1998.
- Vořechovský M. Interplay of size effects in concrete specimens under tension studied via computational stochastic fracture mechanics. *International Journal of Solids and Structures*, 44(9):2715–2731, 2007.
- Weibull Waloddi. A statistical distribution function of wide applicability. *Journal of applied mechanics*, 103:293–297, 1951.
- Yang Zhenjun and Xu X Frank. A heterogeneous cohesive model for quasi-brittle materials considering spatially varying random fracture properties. *Computer methods in applied mechanics and engineering*, 197(45):4027–4039, 2008.